DEVELOPMENT OF NEAR-FIELD TEST PROCEDURES FOR COMMUNICATION SATELLITE ANTENNAS
Phase I, Part 1

Allen C. Newell
Andrew G. Repjar

National Bureau of Standards
U.S. Department of Commerce
Boulder, Colorado

September 1985

NBSIR 85-3031

DEVELOPMENT OF NEAR-FIELD TEST PROCEDURES FOR COMMUNICATION SATELLITE ANTENNAS PHASE I, Part 1

Allen C. Newell
Andrew G. Repjar

Electromagnetic Fields Division
Center for Electronics and Electrical Engineering
National Engineering Laboratory
National Bureau of Standards
Boulder, Colorado 80303

September 1985

U.S. DEPARTMENT OF COMMERCE, Malcolm Baldrige, Secretary

NATIONAL BUREAU OF STANDARDS, Ernest Ambler, Director

CONTENTS

DEVELOPMENT OF NEAR-FIELD TEST PROCEDURES FOR COMMUNICATION SATELLITE ANTENNAS PHASE I, PART 1

Allen C. Newell and Andrew G. Repjar

Electromagnetic Fields Division
National Bureau of Standards
Boulder, Colorado 80303

The purpose of this program is to define and further develop the capabilities of near-field antenna test techniques, specifically for the requirements associated with the development and verification testing of reconfigurable, multibeam, frequency reuse, commercial satellite antennas. Phase I, Part 1 gives a general survey, definition, and description of near-field and compact range measurement methods as they apply to satellite antenna systems testing. Each of these methods is evaluated to determine how well they meet the measurement requirements. Included for each technique is a summary of the measurement method, discussions on probe correction and data processing, measurement hardware considerations, a results available section, and measurement accuracy and range certification considerations. The basis for the choice of the best measurement technique is established with the planar near-field measurement method receiving the best score for the directive antennas considered. As a result, further study will focus on this technique and will be reported on subsequently. A detailed presentation of planar near-field measurements theory is presented in Appendix A.

Key words: antennas; antenna measurements; compact range; cylindrical near-field scanning; near-field measurements; near-field testing; planar near-field scanning; satellite antennas; spherical near-field scanning.

1.0 Introduction

The purpose of this program is to define and further develop the capabilities of near-field antenna test techniques, specifically for the requirements associated with the development and verification testing of reconfigurable, multibeam, frequency reuse, commercial satellite antennas. The program includes two phases. Phase I is a study program that will include the following tasks as outlined in the statement of work:

Task I/A & I/I General survey, definition, and description of near-field and compact range configurations including a description of their comparative advantages. These tasks will be discussed in two parts:

1. A clear and concise description of the antenna and satellite systems to be measured, and the associated measurement problems.

2. A description of the three near-field measurement techniques being studied along with the compact range approach. Each of these will be evaluated to determine how well they meet the requirement defined in Part 1 above.

Task I/H Selection of the optimum measurement technique from the above study.

Once the optimum technique has been chosen, the remainder of the study will focus on that technique only. Items to be covered in the remainder of Phase I are:

Task I/B Determination of sampling criteria and scan limits.

Task I/D Development of beam alignment techniques.

Task I/F Specification of hardware requirements for the measurement system.

Task I/C Development of diagnostic and design-assist methods.

Task I/E Development of swept frequency equivalent tests.

Task I/G Outline available computer programs and make them available.

Task I/J Develop the test plan for Phase II.

In the following report, Tasks I/A and I/I will be reported on, covering the research during the first 6 months of the contract.

Phase II is a measurement program that will demonstrate the results of Phase I.

2.0 Definition of the Measurement Problem

The first major goal of this research program, as outlined in Task I/H, is to choose an "optimum" measurement technique for the communication antenna system. To make that choice as objective as possible and to clearly document the reasons for the final choice, we have developed a three-step evaluation process which compares the relative merits of various measurement approaches for a particular application.

The first step in the process, as developed in this section of the report, is a clear description of the antenna system to be measured and the evaluation factors which are determined by the antenna. These evaluation factors are statements of the important measurement results or test requirements that are defined by the antenna rather than the measurement system. For instance, the size of the required test zone, the susceptibility of the antenna to adverse environments, etc., are antenna evaluation factors since the antenna and not the measurement system defines the requirements and their relative importance.

The second step in the evaluation process, to be detailed in Section 3, is a description of the essential features of the measurement techniques under consideration and a definition of the measurement system evaluation factors. Examples of such factors are measurement time for a given result, data processing complexity, diagnostic capability, etc.

In the third step, relative weights ω_i are assigned to each of the factors (the subscript denotes the factor index) representing the relative importance of the factor for the particular application being studied. These weights vary from two for critical requirements to one half for factors with minor importance. In a similar way, each measurement technique denoted by a subscript j is rated by assigning values R_{ij} to represent how well that technique satisfies the requirements of each evaluation factor. The overall score for a given technique is then the sum of the products of the ratings and the weights

$$S_j = \sum_{i=1,n} \omega_i R_{ij}. \qquad (1)$$

In addition to the weighted sum of all factors, the weighted sum of just the critical factors is also important to ensure that the sum of highly rated minor factors does not have undue influence on the final evaluation.

Using the above process, the details and the assumptions leading to a final decision are clearly presented. If there are questions about the final decision, these details and assumptions can be reviewed to verify a correct statement of the problem and justifiable rating of each alternative.

With the evaluation process outlined, let us now turn our attention to the specification of the measurement problem and the identification of the antenna evaluation factors. The type of antenna system being considered is represented by the Intelsat VI satellite shown in figure 1 composed of a number of complex antennas mounted in close proximity to each other on the spacecraft. Because of this close proximity, there will be scattering and interaction between the various feeds, reflectors, and the support structure. The measurement system must accurately account for this interaction so the results will represent the composite antenna/structure effect.

Since the satellite will operate in a zero gravity environment, and total satellite weight is reduced wherever possible, some of the antennas and their support structures are not rigid in Earth's gravity. Because of this, auxiliary support structures are often necessary to hold reflectors in their deployed shape and position. Even with these support structures, it is very difficult to either translate or rotate the satellite in azimuth and elevation and maintain the antenna alignment. It is therefore highly desirable to eliminate or minimize any movement of the antennas during testing.

The size of the antennas affects the measurement system in two ways. First, the large antennas with the large offset distances require a test volume with dimensions of at least 5 meters along each side. The smaller antennas require a measurement technique that is flexible to a wide range in antenna sizes.

Because the satellite is intended for synchronous orbit use, and the Earth subtends an angle of less than 20 degrees at that altitude, all of the antenna beams are relatively narrow. The beamwidths vary from the Earth coverage beams of approximately 20 degrees to the spot beams of approximately 2 degrees. The most difficult requirements are presented by the antennas which are capable of producing a number of different beams, each of which is shaped to match an irregular land mass and steered to a different direction off axis, as shown in figure 2. It has been shown in past studies [1] that far-field measurements on these antennas require ranges on the order of 10 D^2/λ rather than the typical 2 D^2/λ for less complex antennas. This implies that the test zone of a compact range must have more uniform fields than for testing simple antennas. In the case of near-field measurements, the phase will not be constant over the measurement plane as would be the case for a more simple antenna.

Because of the multiple complex beams, the patterns must be measured at closely spaced intervals on the order of 0.25 to 0.5 degree increments over the ±10 degree region in azimuth and elevation. Typically, contour patterns such as figure 3 are required to completely define the pattern shape over the intended coverage region and to ensure noninterference with other beams. The measurement technique must be capable of producing the complete detailed patterns.

Because orthogonal polarizations are used to improve beam isolation, it is important to determine the cross polarized patterns at levels of -30 to -50 dB below the main beam peak and to quantify the accuracy of such measurements.

At present the required measurement frequencies are between 4 and 30 GHz, and the measurement system must have the capability of changing easily from one band to another. The detailed contour patterns shown in figure 3 are obtained at representative fixed frequencies within the operating band of each antenna system. In addition to these fixed frequency patterns, continuous swept frequency measurements are also taken at a few angular positions in the patterns. In a typical requirement, six angular positions are chosen for each hemi-or zone-beam (one at center and five at points along the edge of coverage). At each of these points, swept measurements are made across the operating frequency band for main and cross polarized response. These tests include not only the antenna but the transmission lines and electronic components associated with the satellite transmitter and/or receiver. These tests are important to detect resonant responses which might not show up in fixed frequency pattern measurements.

The pattern measurements are important for diagnostic use as well as verifying specified performance. To do this, measurement technique should have the ability to determine the presence of

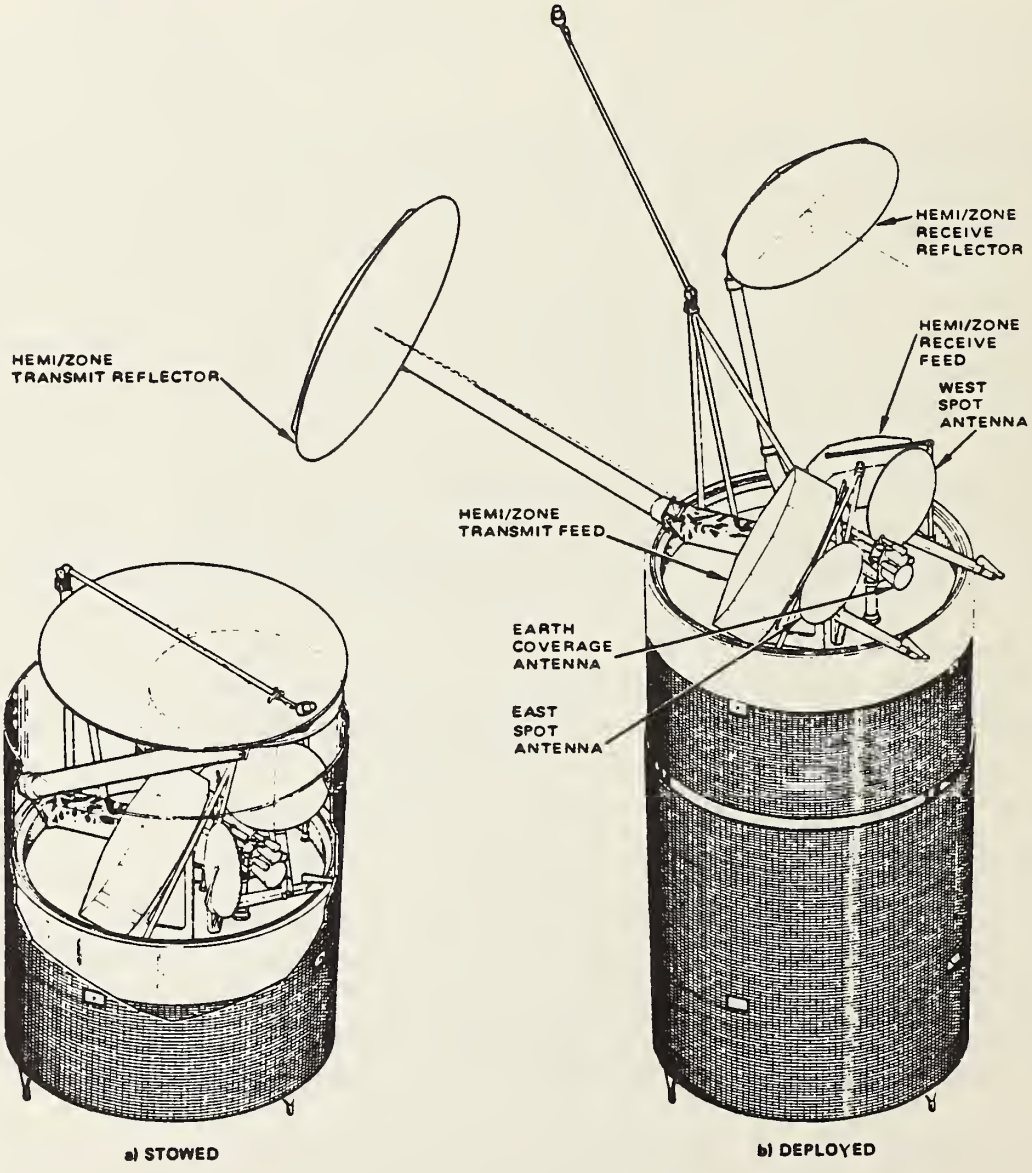

Figure 1. INTELSAT VI satellite illustrating the type of antenna systems under consideration.

Figure 2. Examples of shaped beams achievable from one system using beam switching.

abnormal or undesirable antenna system performance as well as their cause. From either the directly measured data or from some manipulation of the data, such problems as feed element excitation errors, reflector deformations, or alignment problems should be easily identified.

The precise angular location of each beam relative to a coordinate system fixed to the spacecraft must be determined as a routine part of the measurement procedure. Beam alignment accuracies on the order of 0.01 degree are required.

In addition to the antenna parameters of gain, pattern and polarization already discussed, the measurement system must be capable of measuring the total system parameters such as effective isotropic radiated power (EIRP) and the incident flux density required to saturate the receiver.

To summarize the above discussion, table 1 lists the antenna evaluation factors which have been identified along with their assigned weights. (The index refers to the subscript i in eq (1).)

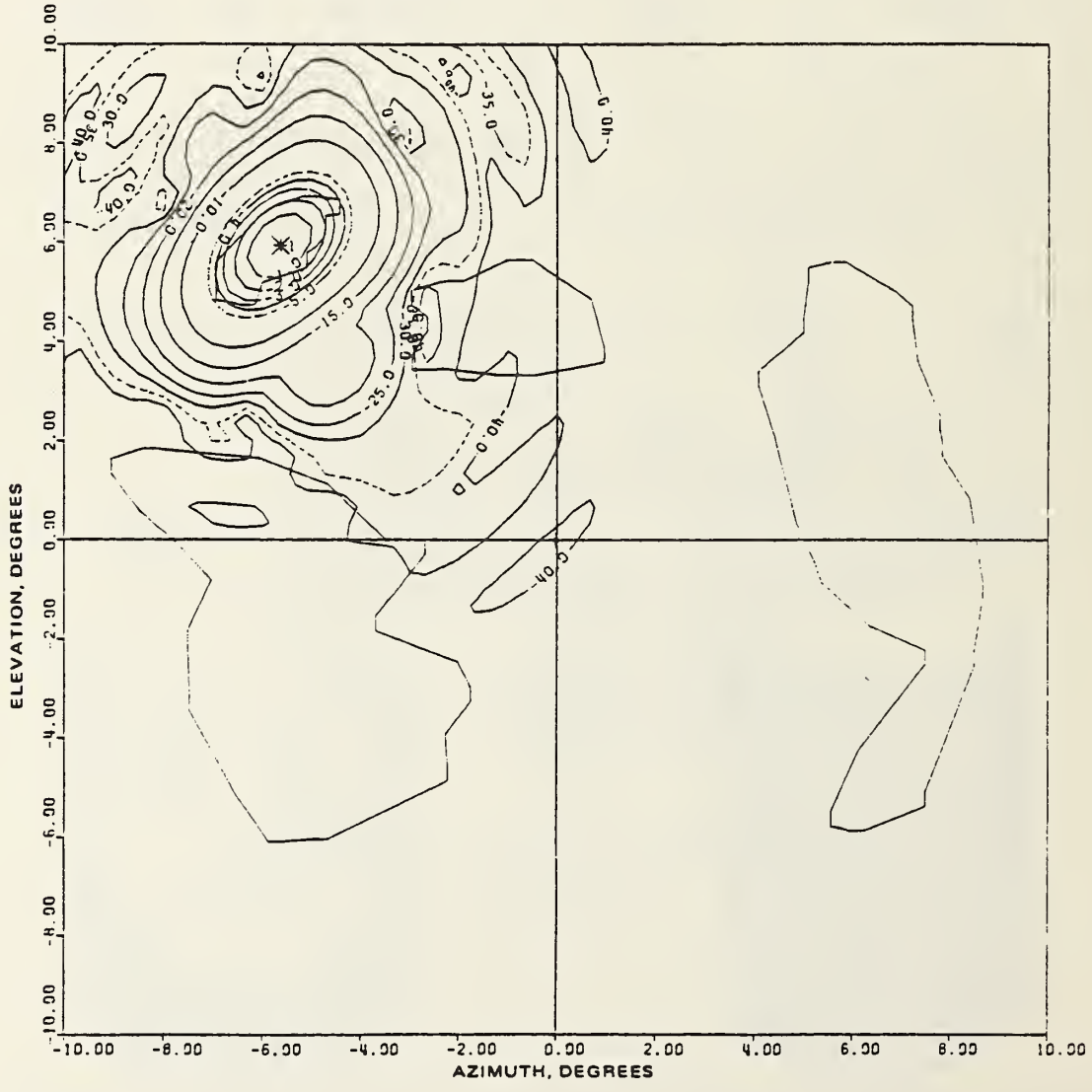

Figure 3. Example of detailed contour patterns required for antenna measurements to ensure noninterference with other beams.

Table 1. Antenna Evaluation Factors

Index	Antenna Evaluation Factors	Weight
1.	Characterize antenna farm interactions	1
2.	Require minimum motion of antenna during measurement	2
3.	Provide required test zone for:	
	a. Individual antennas	2
	b. Antenna and interactions	1
4.	Output detailed patterns for shaped beams	1.5
5.	Give accurate gain, pattern, and cross-polarization results	2
6.	Ease of changing frequency range	0.5
7.	Provide swept frequency results	2
8.	Provide diagnostic information	1.5
9.	Beam alignment accuracies of 0.01 degree	1.5
10.	Provide system parameters of EIRP and saturating flux density	1

3.0 Description of Near-Field and Compact Range Measurement Techniques

Before beginning a discussion of the individual techniques, the measurement system evaluation factors will be identified and listed in table 2. These are largely determined by the measurement system and in some cases are independent of the antenna being measured.

In the following sections, each of the measurement techniques under consideration will be described and the evaluation factors considered. Brief discussions of the theory and basic equations for the planar, cylindrical, and spherical techniques are contained respectively in appendices A, B, and C. These will be referred to as necessary in the following sections which will concentrate on analyzing each measurement technique with respect to the satellite measurement problem. Sufficient information will be presented or referenced to serve as the basis for assigning a rating to each of the evaluation factors for each measurement technique.

Table 2. Measurement System Evaluation Factors

Index	Measurement System Evaluation Factors	Weight
11.	Need for probe correction	0.5
12.	Software is efficient and fast	0.5
13.	Hardware is practical for:	
	a. Antenna size test zone	2
	b. Antenna and interaction size test zone	1
14.	Commercial availability	0.5
15.	Practical implementation	2
16.	Flexibility to antenna size	1
17.	Measurement time	1.5
18.	Demonstrated results and users experience available	1.5
19.	Achievable accuracy and methods of facility certification	1.5

3.1 Planar Near-Field Measurements

3.1.1 Measurement Summary

Before actually making near-field measurements on the antenna under test (AUT), a probe must be chosen and calibrated. Generally, the probe is one whose main polarization is the same as that of the AUT. The calibration involves on-axis measurement of gain and polarization parameters along with far-field pattern measurements. The pattern measurements include both amplitude and phase patterns for the probe's main and cross polarized responses. With these data and the appropriate computer program, the probes' plane wave receiving characteristic, $\underline{s}'_{02}(\underline{K})$ is obtained. (See section A-4 of Appendix A for the definition of the probe, AUT, and data quantities referred to below.) The above process is repeated for a "second" probe whose polarization is nominally orthogonal to the first. The second probe may be a separate antenna, a second output port on a dual polarized probe, or the first probe rotated by 90 degrees in the case of linear polarization. If the latter is used, repeat measurements are not required since the original data may be rotated by the computer. In any case, the second probe characteristic $\underline{s}''_{02}(\underline{K})$ is likewise obtained.

As noted in Appendix A, the AUT and probe coordinate systems are defined with reference mirrors, boresight scopes, or fiducial marks, and the antenna and probe are aligned in a known orientation with respect to the planar measurement surface. The first probe is moved over the measurement plane and relative near-field data $B'_0(\underline{P})$ are obtained at equally spaced points of a rectangular lattice. $B'_0(\underline{P})$ represents the amplitude and phase output of the probe. Similar data are obtained with the second probe and denoted $B''_0(\underline{P})$. In addition to these relative data, insertion loss normalization constants are measured for each set of data (see eq (A53)).

The Fast Fourier Transform algorithm is used to calculate the angular spectra of the two sets of data (see eqs (A54) and (A56)) and the probe correction is applied to obtain the plane wave spectra for the AUT, $\underline{t}_{10}(\underline{K})$. From $\underline{t}_{10}(\underline{K})$ the usual parameters of gain, pattern, and polarization are easily obtained (see eqs (A68) - (A70)).

3.1.2 Probe Correction

As evidenced by eq (A57) and eqs (A60) - (A61), the probes act as both polarization and angular filters on the AUT spectrum producing the measured spectra $D'(\underline{K})$ and $D''(\underline{K})$. The probe correction removes that filtering effect to give the desired result, $\underline{t}_{10}(\underline{K})$. In many cases the effect of the probe correction is small and may be neglected, and by using the basic equations and some knowledge about the probe the necessary conditions are easily defined.

If we assume that the first probe is polarization matched to the AUT, eq (A60) reduces to

$$t_{10m}(\underline{K}) = \frac{D'(\underline{K})}{s'_{02m}(\underline{K})}, \tag{2}$$

where the m subscript denotes the main component of the AUT. Since $|s'_{02m}(\underline{K})|$ is proportional to the relative far-field pattern of the probe, the directivity of the probe and the angular region over which results are desired determine the need for a probe correction. For instance, figure 4 shows a plot of the far-field pattern for two typical probes along the k_x=0 plane. The maximum errors due to neglecting probe correction for these probes and various angles off-axis are shown in table 3.

Table 3. Maximum Errors due to Neglect of Probe Correction

Probe	Off-Axis Angle (deg)	Error in $\lvert t_{10m}(\underline{K})\rvert$ (dB)
Waveguide	18	0.25
Waveguide	54	1.75
Horn	18	4.0
Horn	54	16.5

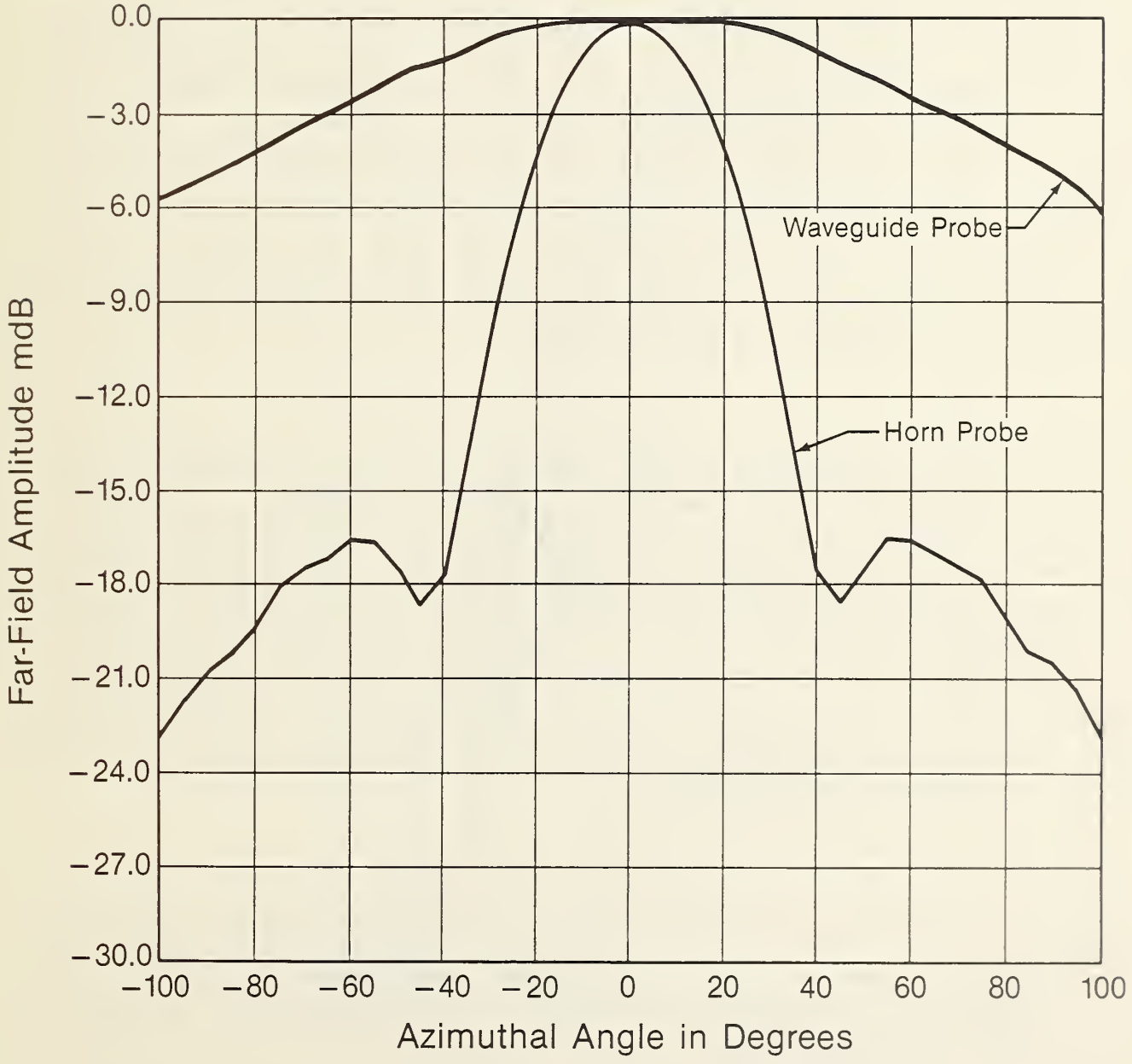

Figure 4. Two typical probe patterns with different directive patterns.

The relative polarization ratios of the AUT and the "second" probe, the one used to measure the cross polarization, also affect the need for a probe correction. If the second probe is better polarized than the AUT, eq (A61) reduces to

$$t_{10c}(\underline{K}) = \frac{D''(\underline{K})}{s''_{02c}(\underline{K})}, \tag{3}$$

where c denotes the cross polarization of the AUT, and only the directivity of the second probe has an influence on the effect or lack of a probe correction. If the second probe is not as well polarized as the AUT, both the patterns and polarization of the second probe must be considered. Every situation cannot be discussed in detail, but given the parameters of a measurement situation, the effect of probe correction can be easily determined.

The probe is usually chosen to enhance/improve the accuracy of the most important information in a given measurement. Very small probes, such as open-ended waveguides, are used when wide angle pattern results are desired. More directive probes such as horns are used when the important information is within a limited angular region centered on the z-axis. The more directive probes filter out the more rapid variations in the near-field data associated with wide-angle sidelobes allowing larger data point spacings. The accuracy in the gain of the AUT is also alightly improved due to better signal-to-noise ratio and better accuracy in both the probe gain and the normalization constant A' (see eq (A53)). The improved value of A' is due to the fact that A' is approximately equal to the ratio of AUT and probe gains (difference of gains in dB). As the gain of the probe increases, the dB value of A' decreases and it can be measured with better accuracy.

3.1.3 Data Processing

The data processing can be divided into three categories: 1) editing and normalization of measured data, 2) calculation of antenna parameters, and 3) graphical representation of results. The times required for categories 1 and 3 are largely independent of the measurement approach, whether it is near-field, far-field, or compact range. In category 2, the planar technique uses the Fast Fourier Transform (FFT) to evaluate the integral in eqs (A52) and (A56) and complex arithmetic for the probe correction and pattern calculations. It is the most efficient of the three near-field techniques in terms of data processing. Figure 5 shows the relative times for planar, cylindrical and spherical for one specific computer. (In the figure, the parameter n indicates the effect of increasing the theoretical data point spacing in ϕ by a factor n. It has been demonstrated that this can be accomplished without loss of accuracy for certain antennas.)

3.1.4 Measurement Systems Hardware Considerations

The hardware for any of the measurement approaches is composed of the electronic system, the antenna positioner, and the scanner, or reflector, in the case of the compact range. The electronic system for all three near-field techniques and also the compact range are basically the same and will not be considered in detail in this section. We will consider the antenna positioner and scanner and point out how they impact the measurement.

In the planar measurements, the scanner is a mechanical structure which moves the probe over a plane area along a rectangular lattice where measurements are obtained. Examples of two types of scanner are shown in figures 6 and 7.

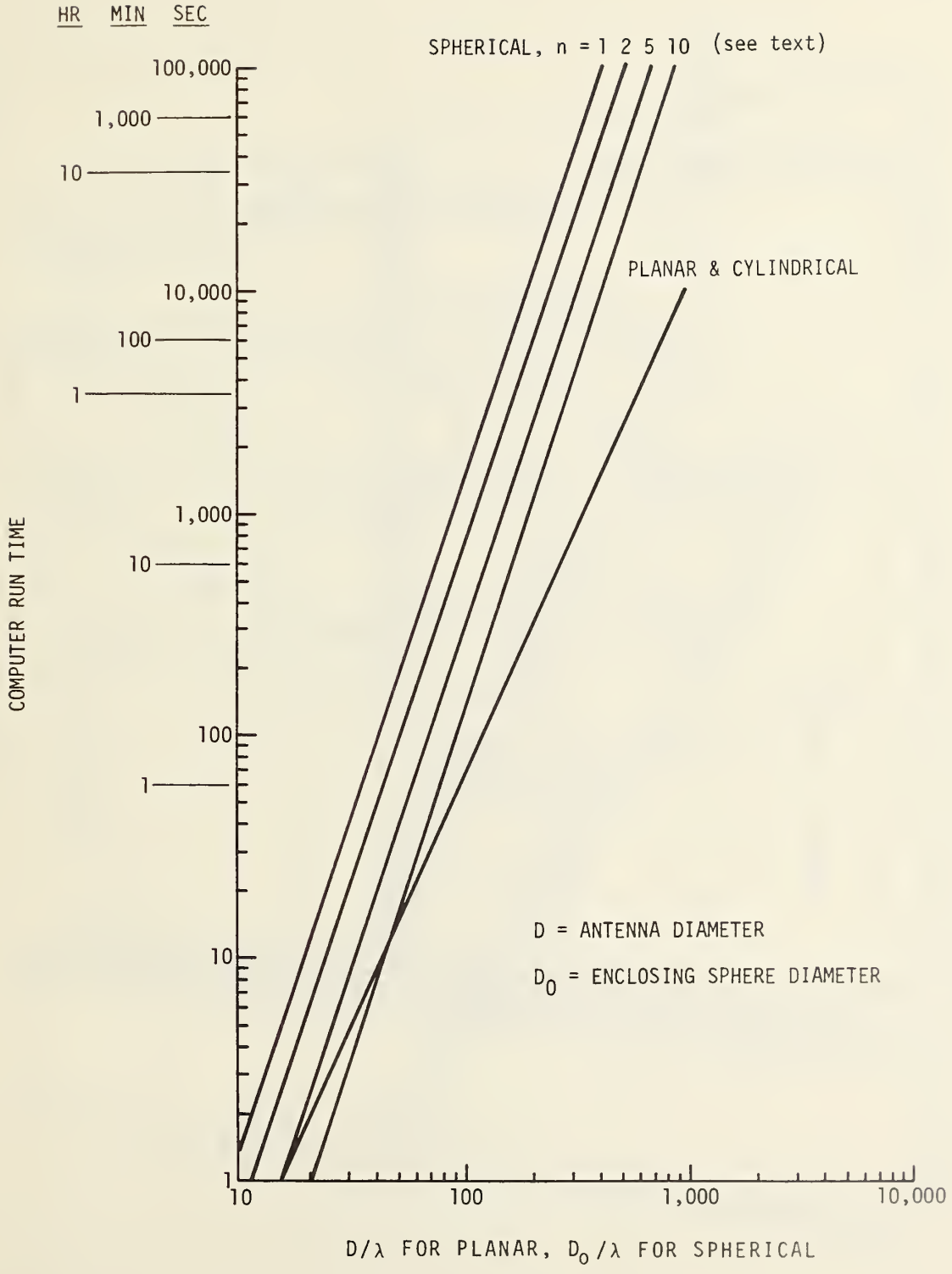

Figure 5. Comparison of computer CPU times for three near-field techniques.

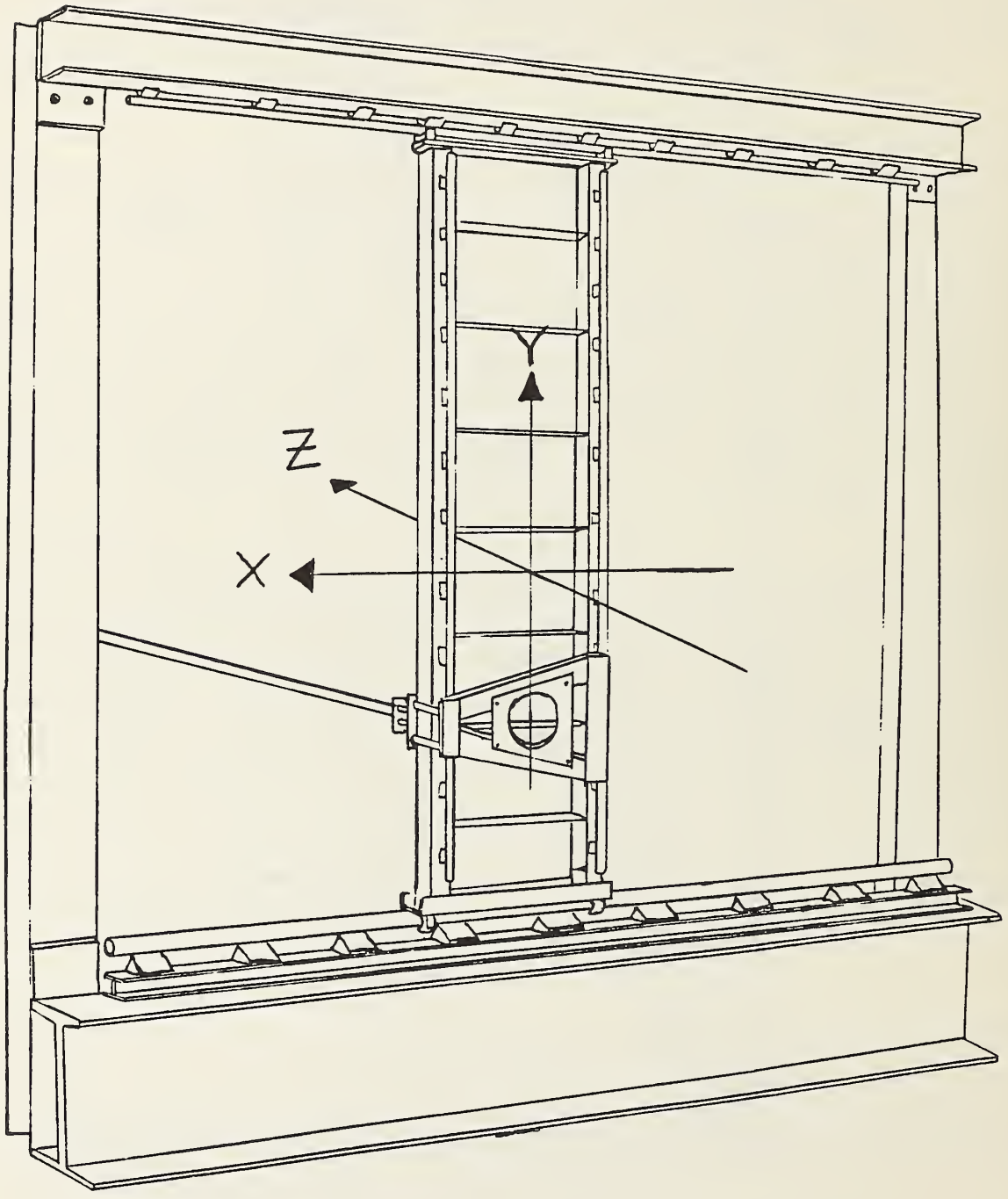

Figure 6. Box frame planar scanner.

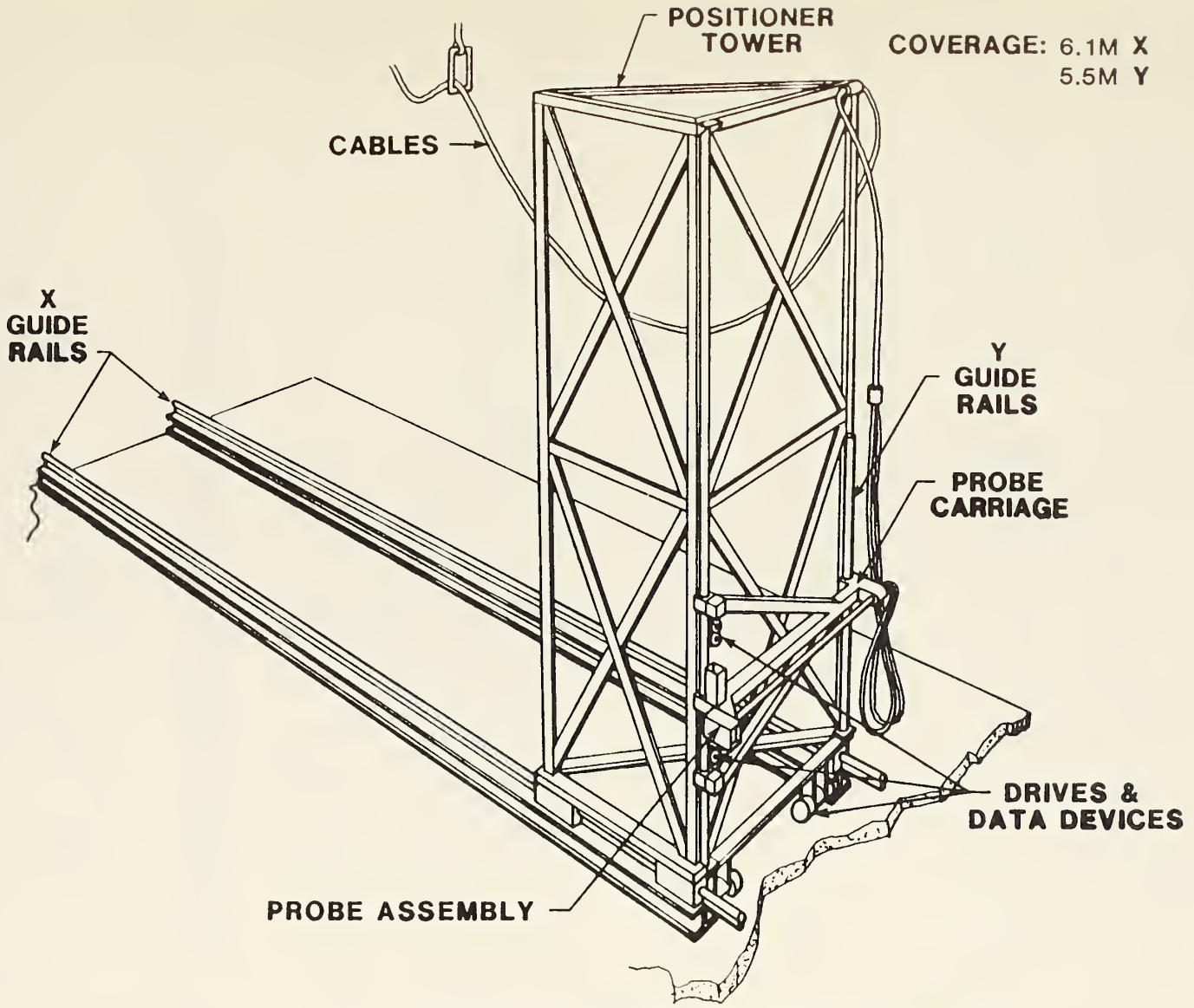

Figure 7. Track/tower planar scanner.

The size of the scanner determines the sizes of antennas that can be measured, the angular region over which results are valid, and the magnitude of errors due to scan area truncation. The theory requires data over an infinite plane, and truncation of the measurement plane produces errors in the measured results. It has been shown [2,3] both theoretically and experimentally that the truncation causes two effects. First, the pattern results of the measurements are valid only for angles smaller than θ_s shown in figure 8. Secondly, the abrupt truncation of the measured data causes a "ringing" on the far-field pattern producing some errors for angles less than θ_s. The characters of the amplitude and phase at the edge of the scan area determine the magnitude of these errors. Generally, if the amplitude at the boundary of the scan area is 30-40 dB below the peak amplitude and the phase varies rapidly around the boundary, the ringing effects are small.

Referring to figure 8, the size of the scanner is chosen to cover the antenna area plus the additional area required to ensure valid results over the specified angle θ_s. In the case of the

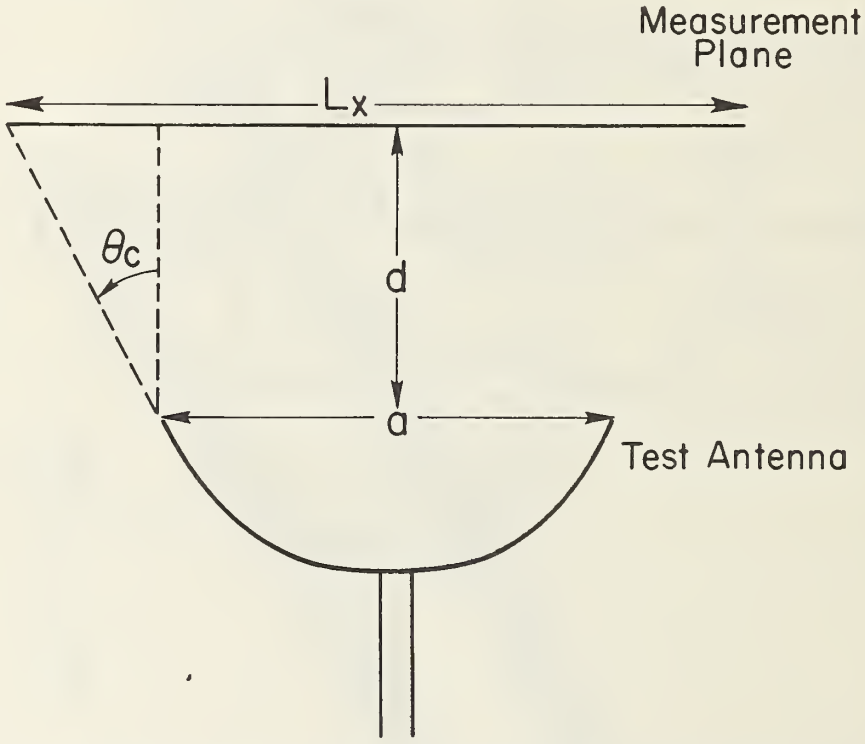

Maximum Angle for Accurate Far Field = θ_c

$$\theta_c \simeq \mathrm{Tan}^{-1}\left(\frac{L_x - a}{2d}\right)$$

TRUNCATION OF MEASUREMENT AREA

Figure 8. Schematic relationship between scan length and maximum angle to which far-field patterns can be accurately computed.

Intelsat satellite shown schematically in figure 9, the offset configuration of the reflectors and the diameter of the satellite body supporting the feeds requires a large separation distance between the reflectors and the scan plane. For the transmit reflector the minimum separation distance is 6.0 m. For the Earth coverage requirement, θ_s is ten degrees and therefore the scan length must be at least 2.12 m longer than the antenna. If the complete antenna farm interactions with all multiple scattering effects are to be included in the measurement, the "antenna" dimension must include all the feeds, reflectors, and supports on the spacecraft. As shown in figure 10, this requires scan lengths of 10.4 m in the x-direction and 6.6 m in the y-direction. Every near-field measurement on the satellite will not require this complete area, however. Preliminary scans may indicate that for a given feed there is negligible scattering or radiation from some parts of the structure, and the scan area may then be limited to the region where there is significant energy contributing to the angular region of interest defined by θ_s. In another case it may be desirable to reduce the scan area to purposely exclude the effects of scattering and concentrate the measurement on one reflector and its feed, as shown in figure 11. This would be the case in diagnostic measurements when checking feed alignment, reflector shape, or feed illumination errors. In these cases, scattering from other objects could tend to obscure the desired results and by limiting the scan area these extraneous effects are excluded. The maximum required scan area of 10.4 m x 6.6 m is feasible with existing technology. Using the design shown in figure 7, x- and y-scan lengths of 6.7 m are currently being achieved. It is relatively easy to increase the scan length in the x-direction by increasing the length of the horizontal rails, and the 10.4 m length should be easily achieved. One of the main advantages of the planar technique for spacecraft testing is that the antennas do not have to move during measurement. The antennas may then be supported in a fixed position to overcome the distorting effects of Earth's gravity.

Currently there are at least 20 planar near-field measurement systems in operation at various commercial and government laboratories around the world. These include a variety of mechanical designs similar to those shown in figures 6 and 7, as well as some which employ horizontal scan planes. Commercial companies do not sell these as standard product items, partly because each user has fairly unique requirements. The experience and expertise does exist, and some companies have expressed an interest in designing and constructing planar scanners to meet user specifications.

With the planar measurements it is relatively easy to change from one frequency band to another since only the probe has to be changed. This will require calibration of the probe or calculation of its gain, pattern, and polarization, depending on the accuracy requirements.

Due to the large scan areas, the planar measurements may require a number of hours to complete. For a scan area with dimensions of L_x and L_y, data point spacing in the x-direction δ_x, and probe scan speed v, the measurement time is approximately

$$T = \frac{L_x L_y}{\delta_x v_y} . \tag{4}$$

Since the probe speed is limited to about 10 cm/sec due to mechanical vibrations, and the scan area and data point spacings are fixed by the antenna being measured, little can be done to reduce the total measurement time. The measurement efficiency can be greatly improved, however, by obtaining multiple patterns during one traverse of the measurement area. This is accomplished by switching between different frequencies, beams, polarizations, etc., between each data point in the y-direction. (It is assumed for this discussion that the probe moves continuously in the y-direction,

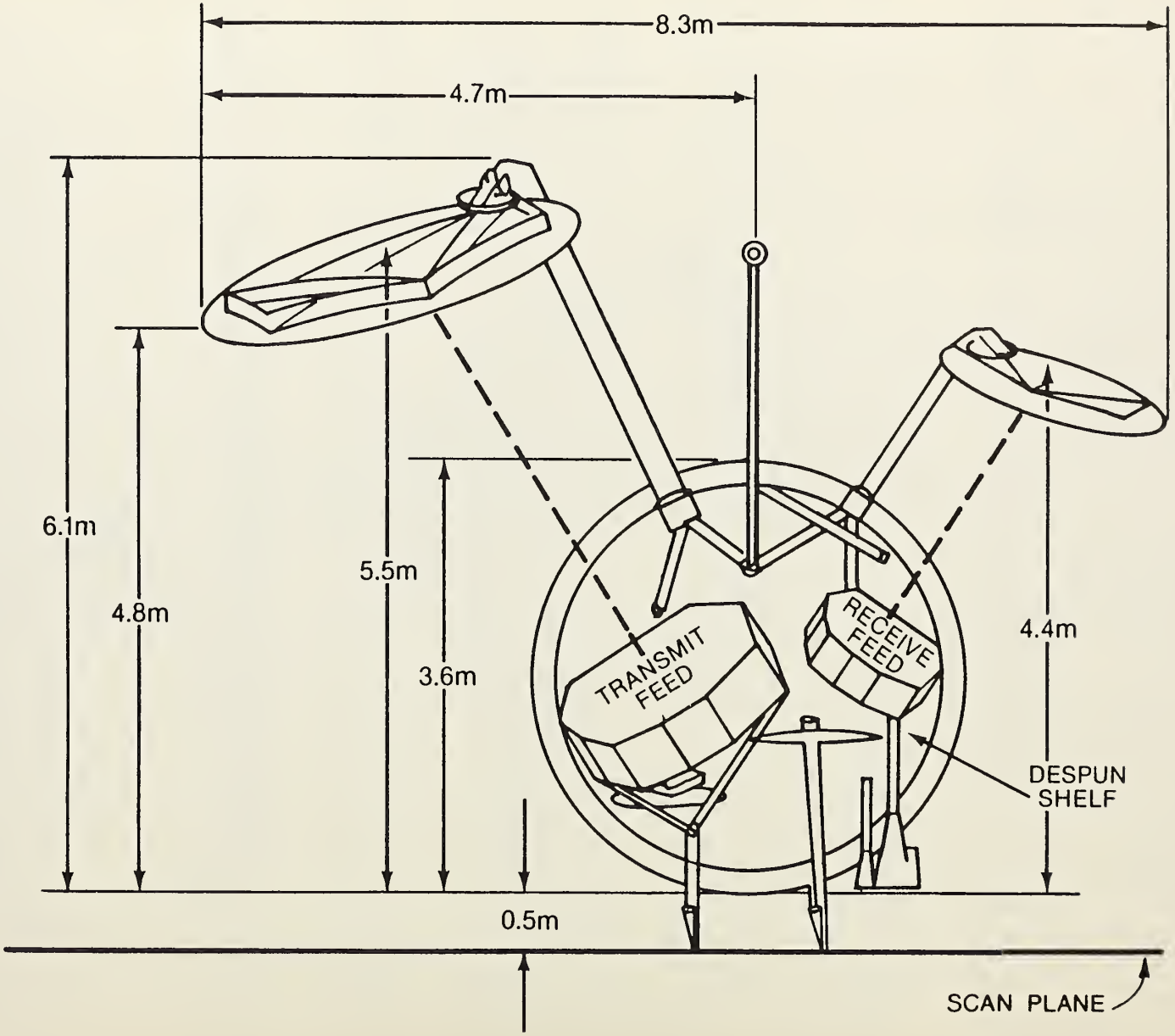

Figure 9. Schematic of satellite with offset antennas and resulting scan plane.

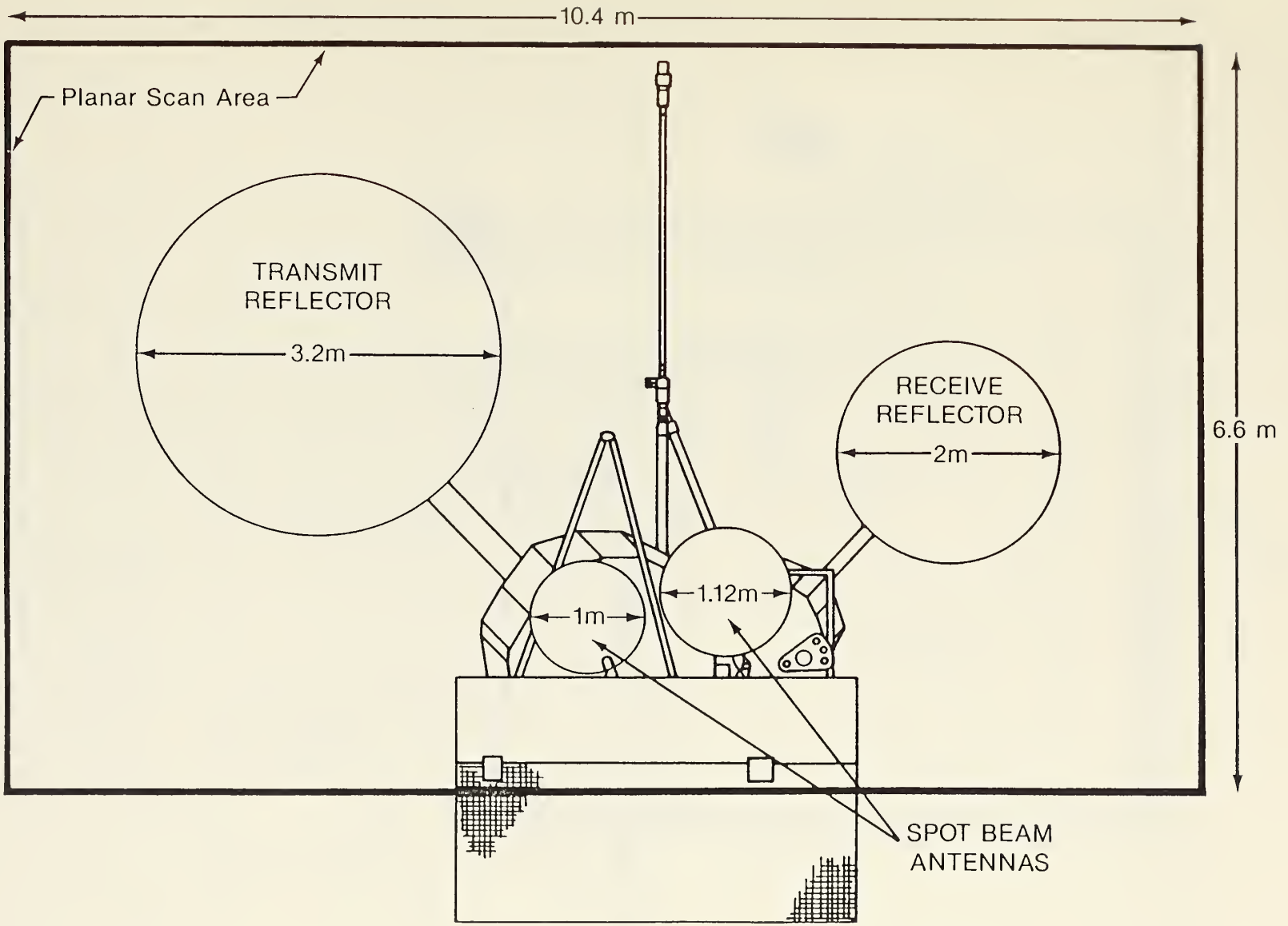

Figure 10. Planar scan area required for full interaction coverage and no movement of satellite to measure all antennas.

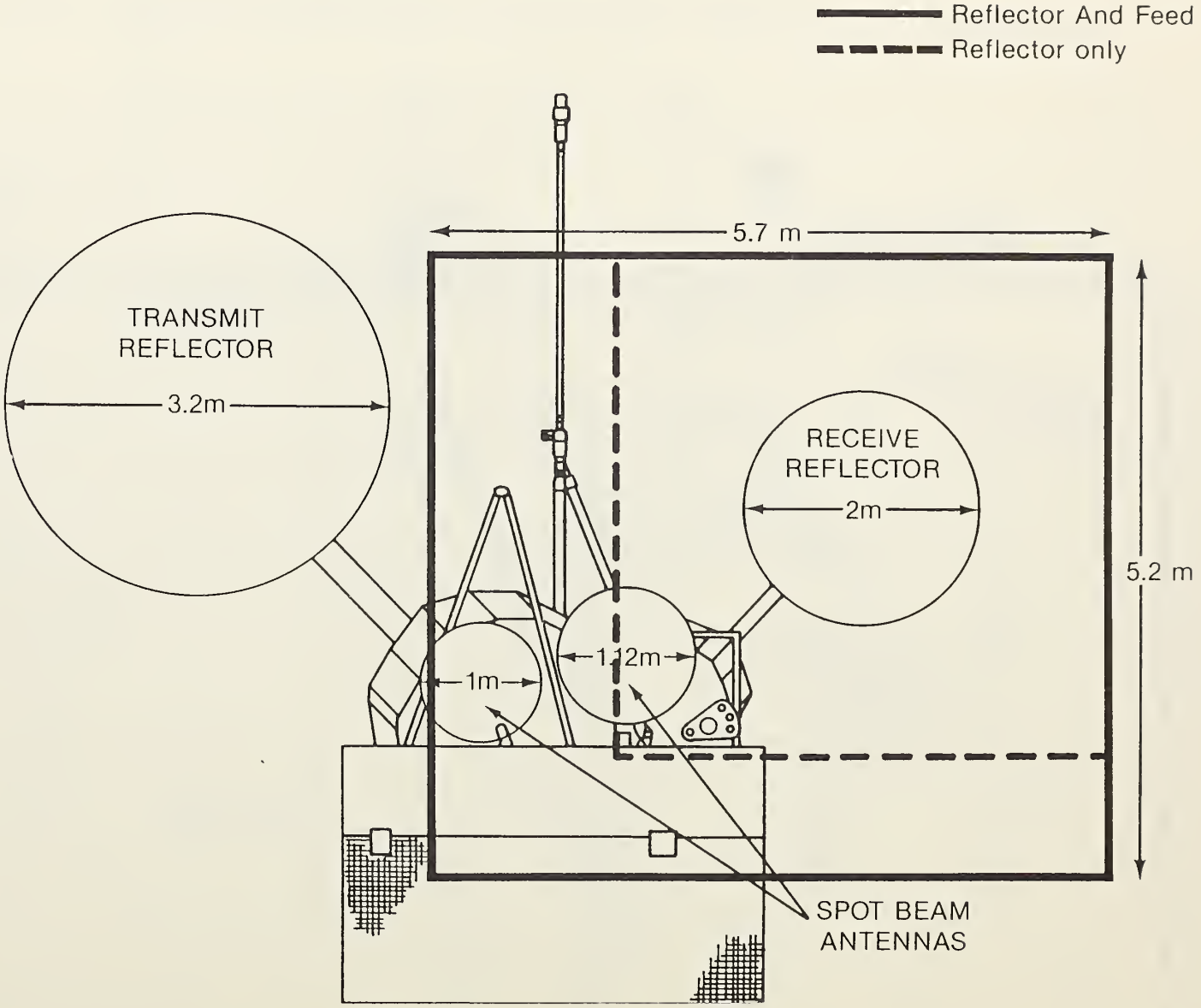

Figure 11. Reduced planar scan areas for coverage of only one antenna at a time without full interaction coverage.

measuring data at intervals of δ_y and stepping in the x-direction at the end of each y-scan.) The total number of patterns obtainable during one scan is

$$N \leq \frac{\delta_y}{v_y \tau} \tag{5}$$

where τ is the time required to accomplish the switching. The various time intervals comprising τ, along with some representative times available with current equipment, are shown in table 4. Using the multiplexing scheme, it is possible to obtain many patterns during one scan of the plane area.

Table 4. Representative Switching Times

Action	Time (msec)
Beam or polarization switch	0.5 - 2.0
Frequency switching	10.0 - 20.0
Receiver settling (after frequency change)	10.0 - 100.0
Receiver analog to digital conversion	0.5 - 10.0
*Computer command time	0.5 - 50.0

*The computer time is dependent on how many different patterns are switched

3.1.5 Results Available

The required detailed far-field patterns for both main and cross polarization are readily available from the planar technique. There is no difficulty in obtaining the high resolution contour patterns, such as shown in figure 3. The accuracies of these results are dependent on the accuracy of the measurement systems, and this will be discussed in more detail in the following section.

Absolute gain values are obtained as a natural result of the data processing. In addition, it is possible to obtain system parameters such as EIRP and saturating flux density, as illustrated in figures 12 and 13. The relative near-field data used to obtain patterns and gain, $B_0'(\underline{P})$, are also employed here. In addition, the probe is placed at the reference point, $\underline{P}_0$, and either the received power (for EIRP) or transmitted power (for saturating flux density) are also measured. These techniques are relatively new developments, and will require some refinement in the measurement details, but they should be straightforward and very reliable.

Beam alignment is a topic which will be covered in more detail in a future report. We assert here that it is possible to achieve beam alignment with errors of $\pm$ 0.01 degrees or less.

The near-field data before transformation can be used very effectively for antenna diagnostics. Figures 14 and 15 show the measured phase data as contour plots superimposed on the reflector geometry being measured. The regions of reflector surface irregularities are easily identified. There are existing techniques for transforming measured data back to a plane closer to the reflector or array. This additional processing can enhance the diagnostic capability of the planar near-field measurements. No other technique offers the present capabilities and future possibilities in the area of diagnostics. This is related to the fact that for the directive antennas being considered here, the desired field on a plane is generally the known quantity and especially the phase data are a very sensitive measure of performance.

Near-Field Measurement of EIRP

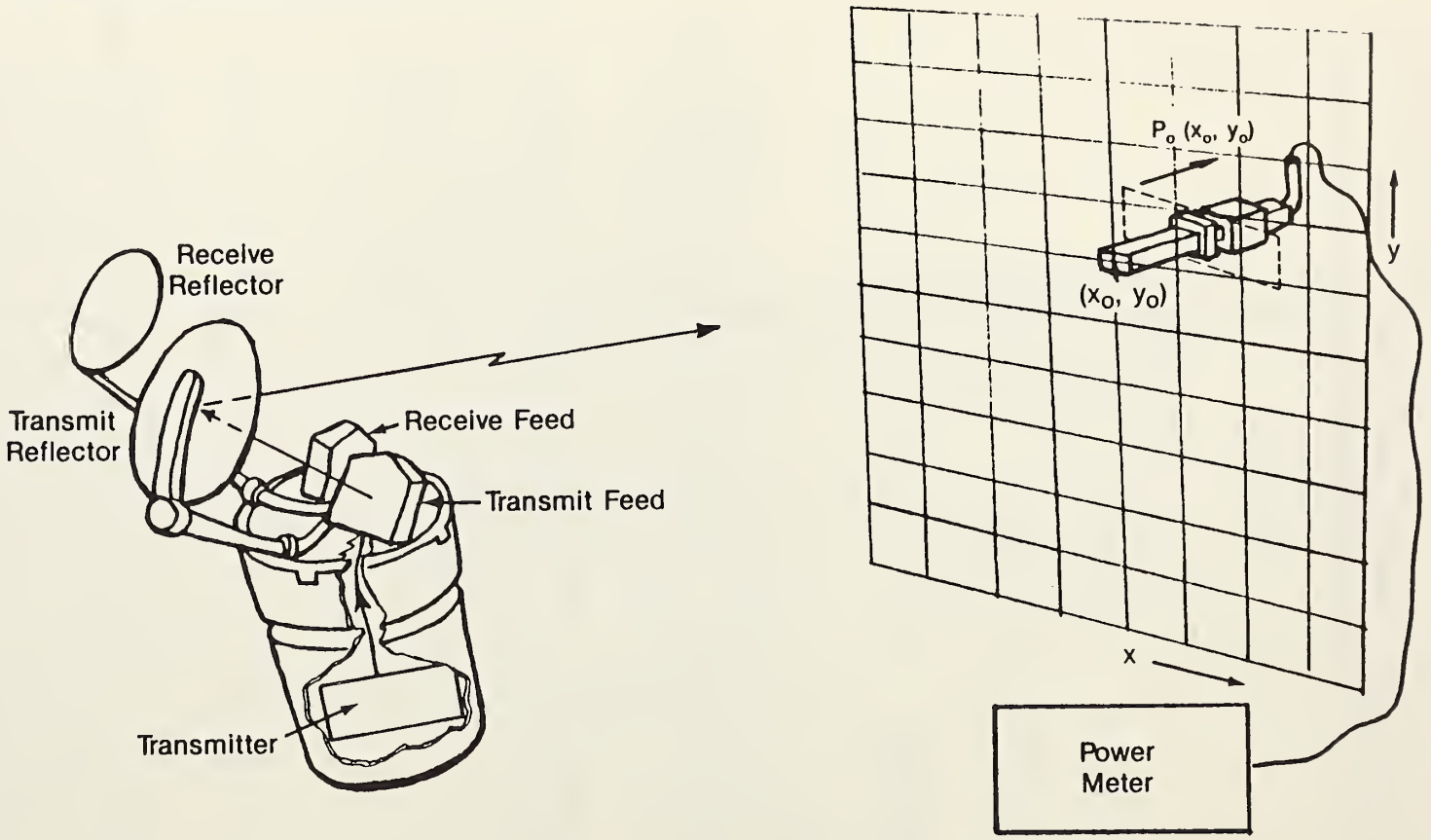

$P_o\ (x_o, y_o)$ = Power Received at Reference Point (x_o, y_o)

$$EIRP = (4\pi)^2 \frac{P_o\ (x_o, y_o)}{\text{Gain of Probe}} \times \left| \int \frac{B(x, y)\ dx\ dy}{\lambda^2} \right|^2$$

Figure 12. Schematic of EIRP planar near-field measurement.

Near-Field Measurement of Saturating Flux Density

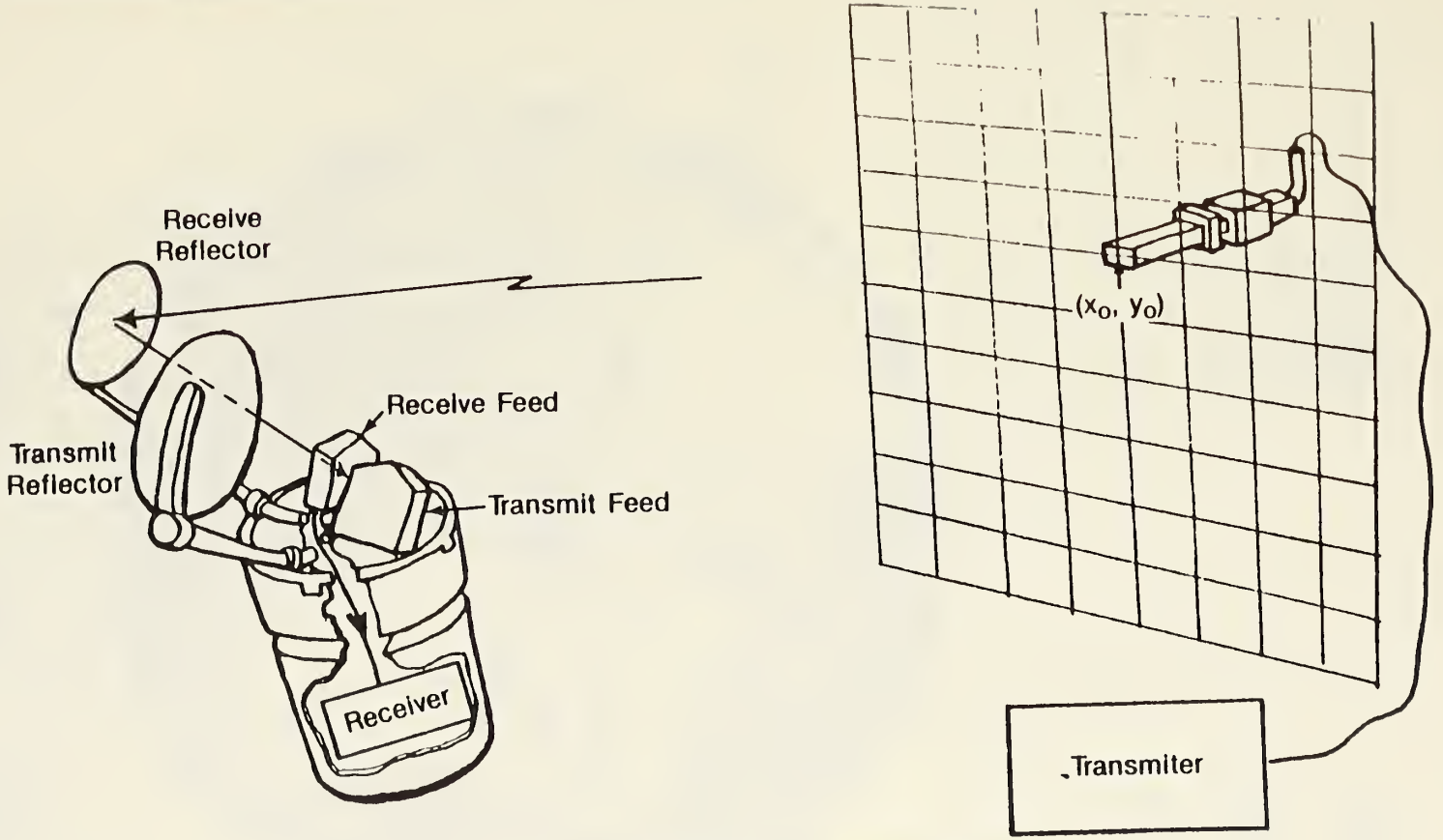

$P_i\,(x_o, y_o)$:= Power Input to Probe at Reference Point

$$S_o = \frac{P_i\,(x_o, y_o) \times \text{Effective Area of Probe}}{|\int B\,(x, y)\,dx\,dy|^2}$$

Figure 13. Schematic of planar near-field saturating flux density measurement.

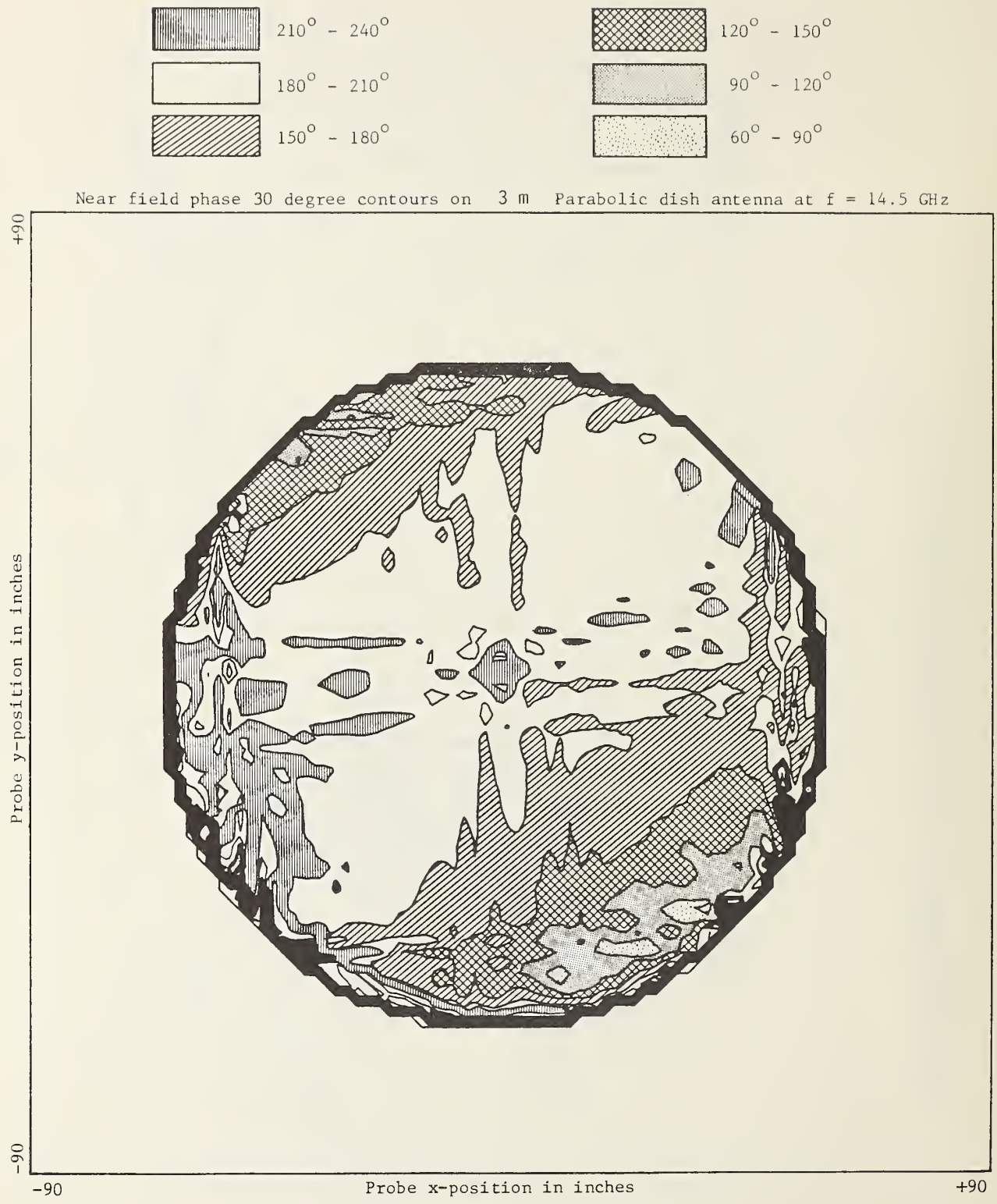

Figure 14. Measured near-field phase contours for 3 m parabolic reflector.

The one area where all three near-field techniques are lacking in development when compared to the measurement requirements is in obtaining swept frequency results. In far-field tests, a few specific directions are chosen, and continuous swept frequency gain, side lobe level, and cross-polarized isolation are measured. The combination of far-field pattern measurements at fixed frequencies combined with the swept data is illustrated graphically in figure 16. The solid cube represents the "volume" describing the complete antenna performance at any azimuthal and elevation angle (horizontal coordinates) and frequency (the vertical coordinate). At any frequency the antenna pattern is represented by a contour plot, and the cube is composed of a continuous layer of these plots, of which three representative ones are shown. The swept frequency measurements are taken at specific fixed azimuthal and elevation coordinates and are represented by the vertical lines.

Currently it is not feasible to obtain continuous results along the vertical lines with near-field techniques in the same way as far-field tests. Fixed frequency measurements could be obtained at a large number of fixed frequencies, but this would be very time consuming. Preliminary research has indicated that it may be possible to develop near-field measurements that would give swept frequency information equivalent to the far-field results. The proposed approach is to place the near-field probe at representative points in the x-y plane and obtain near field swept frequency amplitude

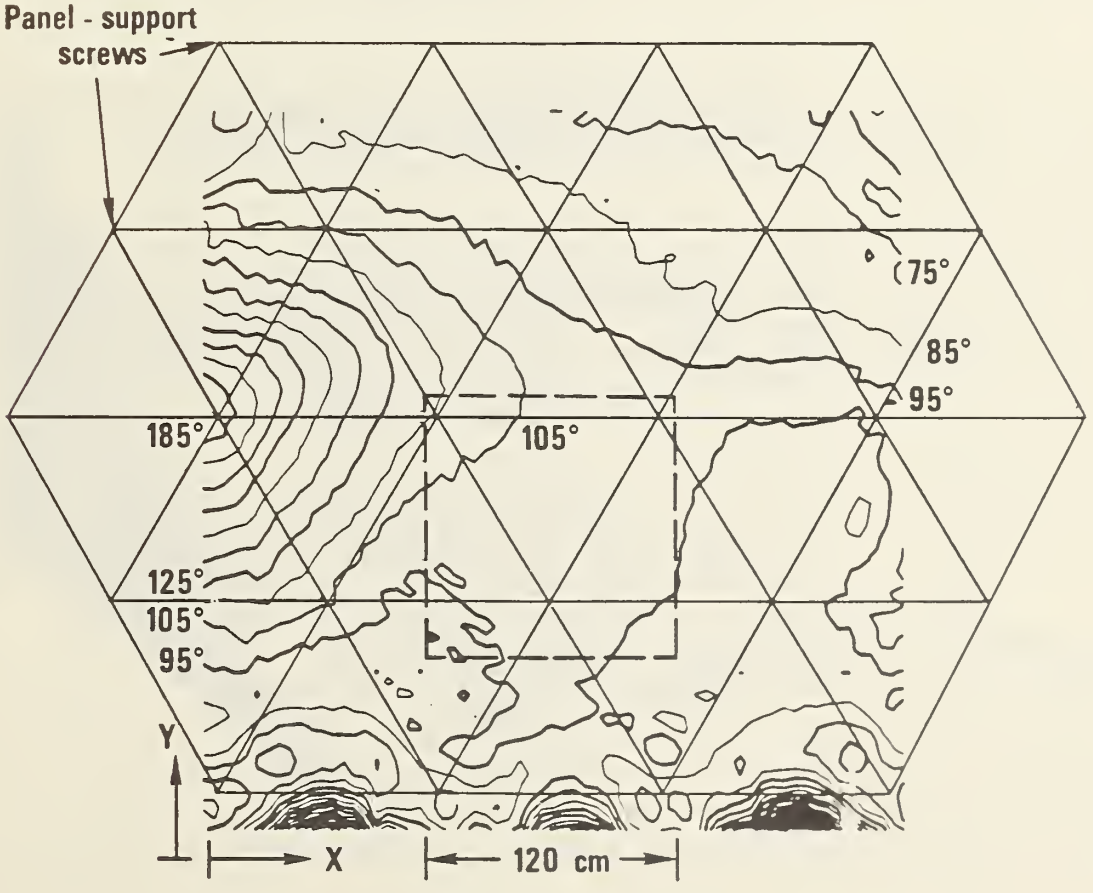

Figure 15. Measured near-field phase contours for hexagonal panel reflector showing effect of one support screw maladjustment.

and phase data. By appropriate analysis, which is currently under development as a part of this contract, the frequency intervals required to completely specify the antenna system frequency response would be determined. This would guarantee that if fixed-frequency near-field measurements were obtained at these intervals, the continuous response could be reliably interpolated. In addition, techniques to reduce the amount of near-field data required to obtain the frequency response patterns are to be investigated. At present these methods are not fully developed. They show promise and, if developed, could provide swept frequency results equivalent to far-field techniques.

3.1.6 Measurement Accuracy and Range Certification

For any measurement technique, accuracy is one of the primary concerns, and this is especially true of a new method involving a significant level of mathematical analysis such as the near-field technique. The determination of error bounds for any given antenna/probe/near-field measurement system combination is a difficult and demanding task, and the mathematical complexity is a major reason for the difficulty. There is a temptation to bypass the mathematics and attempt to establish error bounds for the general measurement technique by a comparison measurement on a specific

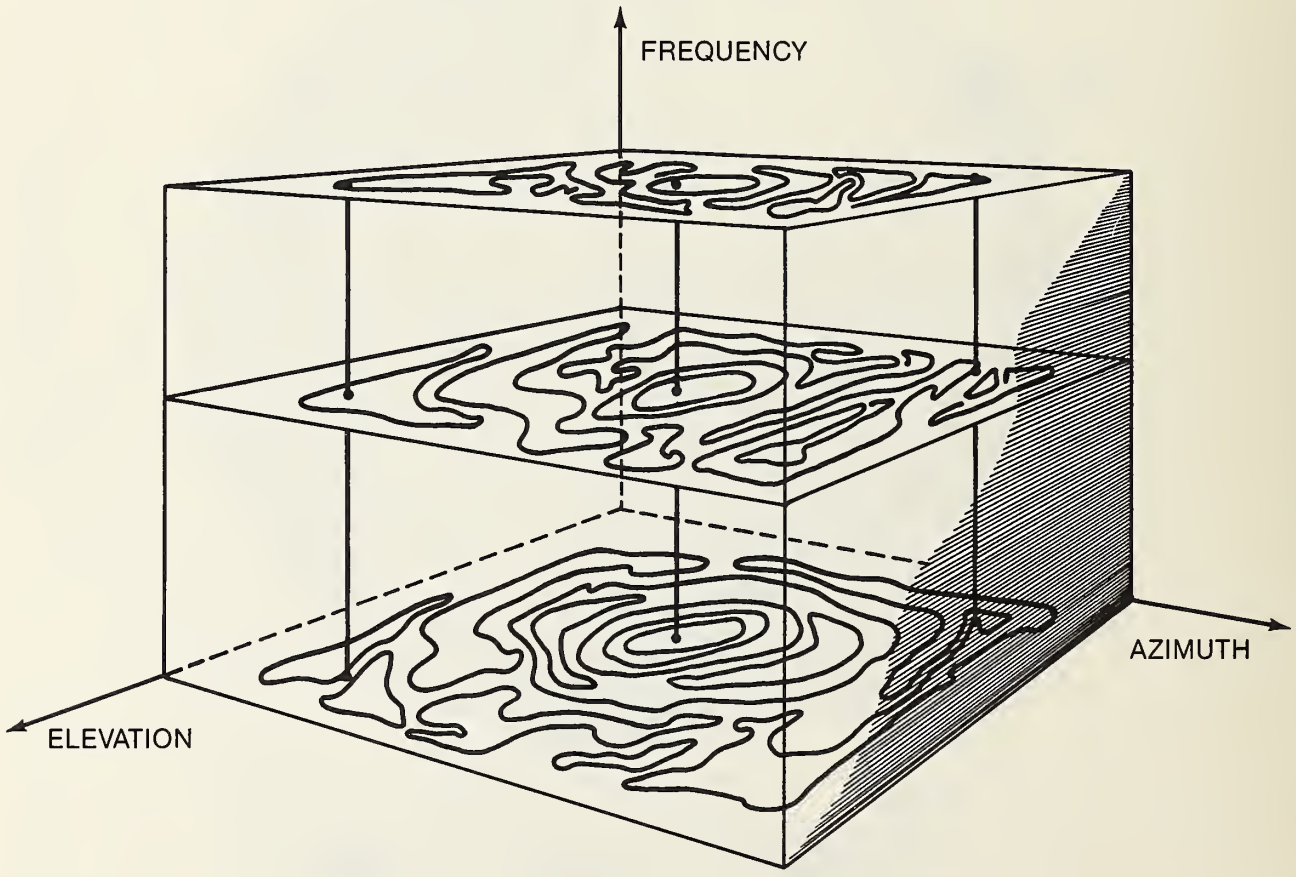

Figure 16. Schematic representation of fixed and swept frequency results as part of data volume.

antenna. In this approach, the results of near-field measurements on a given antenna are compared with far-field measurements, and differences between the two are taken as a measure of the errors in the near-field technique. The limitations of such an approach are obvious. 1) The observed differences are due in part, and could be primarily due, to errors in the far-field measurement. 2) It is difficult to generalize one result to other antennas and measurement systems. 3) There is no indication of which measurement parameters are the most critical or the contribution from each error source.

This does not mean that comparisons are not valuable exercises. They demonstrate reliability, help to establish confidence without detailed mathematical study, and indicate possible areas where more detailed study should be done. They are one piece in the error analysis puzzle, but certainly not the whole picture.

A second useful approach is computer simulation of various types of errors. Either actual or hypothetical near-field data are assumed to represent perfect, error-free measurements. These data are then modified with errors of various types and magnitudes. Differences between far-field parameters computed from the error-free and modified data sets are a direct measure of the effect of each error source. This approach also has limitations. 1) The error types considered (i.e., linear, quadratic, random) may not represent actual or worst-case types of errors. 2) The assumed effect of a given error may not be correct. For instance, assumptions must be made about how probe position errors or multiple reflections effect the data, and those assumptions may not be completely valid. 3) The results may not be general unless the simulation is performed for a wide variety of antenna types.

A third method of error analysis can result in a direct measurement of the effect of some error sources for a specific measurement. This is essentially a self-comparison technique where measurements on a given AUT are repeated after making a specific known change in the system. The change is made to produce a sign reversal in the effect of some particular error, and the difference between two results is then a direct measure of that error. For instance, measurements made at z-separation distances differing by $\lambda/4$ will show the effect of multiple reflections. Other examples include translation of the antenna between measurement sets in x or y to identify probe position error or room scattering effects and sequentially reducing the data area size or data point density to produce changes in the errors due to truncation and aliasing. The combination of all these tests is involved, time consuming, and generally will not be performed on every antenna; but they are valuable in initially certifying a measurement facility or studying the details of a particular error source. Along with the other approaches, they can be used when appropriate, and provide part of a complete method of error analysis.

The fourth method of error analysis is the most detailed and generally the most useful. This method is based on a study of the mathematical relations between near-field data and far-field results. The results of this study are general error equations which define the error in various far-field parameters as a function of essential antenna parameters and the magnitudes of individual near-field errors. The equations are quite general, can easily be applied to different antennas, and can be used either to estimate final error bounds or to design a measurement system capable of achieving a given level of accuracy.

The mathematical error analysis begins from the point of view that the basic equations are exact, without approximation, and, therefore, include no built-in limit on attainable accuracy. These include the transmission integral, eq (A50); the calculation of the angular spectra, eqs (A54) and

(A56); the probe correction, eqs (A60) and (A61); and the evaluation of far-field parameters in eqs (A68) - (A70). The generality and rigor of these equations, although not obvious in the development in Appendix A are established by a more detailed analysis [4]. There are, indeed, some assumptions made in the derivation of these equations concerning ideal measurement conditions (such as a planar surface, rectangular measurement lattice, absence of multiple reflections, etc.), and if these conditions are not realized, errors will result. These errors are simply included with others that arise from the nonideal character of the measurement system. By adopting the above point of view, the focus of the error analysis is on the nonideal character of the measurement system, not the mathematics.

All four of the above approaches have been used extensively to test and verify the accuracy of the planar near-field measurement techniques. Comparisons with far-field measurements were some of the earliest [5] and continue to be used as each new facility is first used. Extensive computer simulations of various errors were done by Joy [6] and were used to verify and assist in the mathematical error analyses [7,8]. The net result of these studies has been the identification of a number of error sources in the near-field measurement system and equations to specify bounds on the magnitude of the resulting far-field error. The details of these equations can be obtained from the supplied references, and the various error sources are listed in Table 5. These error sources can be classified under two categories. Namely, uncertainties in probe parameters $\underline{s}'_{02}(\underline{K})$ and $\underline{s}''_{02}(\underline{K})$ arising from the gain, pattern, and polarization measurements on the probe; and errors in the calculated spectra $D'(\underline{K})$ and $D''(\underline{K})$ arising from the measured data $B'_0(\underline{P})$ and $B''_0(\underline{P})$. All of the error sources in Table 5, except number 15, are systematic errors. That is, the effect of the error is not reduced by repeating the measurement a number of times under the same conditions.

Reliable and realistic error bounds will be predicted if the following assumptions are true: 1) The equations used to calculate the far-field parameters are exact. This can be shown from a careful study of the theory. 2) All known sources of error have been included in the list of Table 5. 3) The magnitudes of the near-field errors have been reliably measured. This requires, for instance, the use of laser optical systems to measure the x-, y-, and z-position errors; calibration techniques to measure receiver linearity; and system tests to determine the effect of reflection, area truncation, and aliasing. 4) The error equations correctly predict the far-field error. This is verified by the mathematical analysis, the computer simulation, and self-comparison tests. 5) The individual error components are correctly combined to give a realistic estimate of total resultant error.

3.2 Cylindrical Near-Field Measurements

3.2.1 Measurement Summary

It should be evident from a comparison of appendices A and B as well as more complete and detailed derivations [4,8] that there are many parallels between the planar and cylindrical theories, basic equations, and, as a result, the measurement techniques. These similarities include: 1) transmission equations written in terms of AUT transmitting coefficients and probe receiving coefficients; 2) the general requirement to measure near-field data with two independent probes; 3) solution of the transmission equation by using the FFT and probe correction; and 4) virtually identical electronic measurement systems.

Because of these similarities, this section will only cover in detail the areas where there are distinct differences that have an impact on the measurement problem under consideration.

Table 5 Error Sources in Planar Near-Field Measurements

Source of Error	Primary Method of Evaluating: Computer Simulation	Test on Meas. System	Error Equations
1. Probe gain measurement			x
2. Probe relative pattern			x
3. Probe polarization ratio			x
4. Normalization constant			x
5. Probe alignment error			x
6. Antenna alignment error		x	x
7. Measurement area truncation	x	x	x
8. Data point spacing (aliasing)		x	x
9. Multiple reflections (probe/AUT)		x	
10. Room scattering		x	
11. Probe x-y position errors	x		x
12. Probe z-position errors	x		x
13. Receiver amplitude nonlinearity		x	x
14. System phase error due to: Receiver, Flexing cables/rotary joints, Temperature effects		x	x
15. Impedance mismatch factor			x
16. Random errors in amplitude/phase		x	x
17. Leakage and crosstalk		x	x

NOTE: The above errors are all associated with the measurement system and do not include such things as changes in the antenna during measurement due to environmental factors.

3.2.2 Probe Correction

In the planar technique there are measurement situations where the probe correction can be ignored completely, and reliable results may still be obtained. In contrast, the probe correction or its equivalent is always required in cylindrical measurements. If the probe is small compared to the measurement wavelength, and/or the diameter of the measurement cylinder is large enough, an "ideal" probe may be assumed. The probe receiving coefficients are then given analytically as proportional to Hankel functions. An alternative point of view is to consider the near-field data as a direct measure of the electric field components. From this point of view, the resulting equations do not involve an explicit probe correction, but they do include the Hankel functions representing the ideal probe effect. If the probe correction is required, the probe calibration process used for the planar method also applies here. Part of the data processing is also employed, but in addition the probe coefficients must be transformed from the probe's coordinates to that of the AUT (see eq (37) in reference [8]).

3.2.3 Data Processing

Since the FFT is used extensively for the planar and cylindrical methods, the computation times for these methods are similar. One additional step is required here in the calculation of the far-field since the AUT coefficients must be summed (see eqs (B1) and (B2)). But since this is a one-dimensional sum, and again the FFT is used, the additional computer time is fairly minor.

3.2.4 Measurement System Hardware Considerations

The usual configuration for a cylindrical near-field scanner is shown in figure 17. The AUT is mounted on an azimuth rotator whose axis of rotation is parallel to the axis of the one-dimensioned probe transport. This generally means that the scanner is less expensive than for planar. More complete pattern coverage is also achieved since results can be obtained over 360 degrees in ϕ (azimuth), even though the size of the probe transport limits the elevation coverage in the same way it did with planar measurements.

The main disadvantage of the cylindrical scanning for the satellite problem is the required satellite rotation during measurement. This produces stability problems for the fragile antennas and support structures. The amount of rotation required depends on the dimensions of the "antenna" being measured, the radius of the "minimum cylinder" and the angular region over which patterns are required. As previously mentioned, the "antenna" dimensions should include the reflector and any other objects which could radiate or scatter energy. The minimum cylinder is defined as one centered on the azimuth axis of rotation which will completely enclose the antenna as above defined. Given a radius of R for the minimum cylinder, an antenna dimension a, and requirement for results over azimuthal angles bounded by ϕ_s, the ϕ-rotation required is as illustrated in figure 18. For the Intelsat satellite dimensions, and including all structures as potential scattering sources, the ϕ-rotation angles required for ±10 degree coverage on the transmit reflector and feed are from -72 degrees to 11.5 degrees as shown in figure 19.

The size of the minimum cylinder also determines the data point spacing in ϕ, and therefore influences the measurement and calculation times. To satisfy the sampling criteria and therefore avoid aliasing errors, the angular data point spacing must satisfy the criteria

$$\Delta\phi \leq \frac{\lambda}{2R} \text{ (radians)}, \tag{6}$$

and the number of data points is

$$N_\phi \geq \frac{4\pi R}{\lambda}, \tag{7}$$

with the additional requirement that

$$N_\phi \, \Delta\phi = 2\pi \equiv 360°. \tag{8}$$

Since all of the antennas are located away from the center of rotation of the satellite, the minimum cylinders in every case are larger than the reflector dimensions and relatively fine spacing are required. Table 6 lists the estimated scan parameters for each of the Intelsat VI antennas, assuming that the minimum cylinders include the reflector and feed for each antenna, but may exclude some potential scatterers.

Table 6. Cylindrical Scan Parameters

Antenna	Frequency (GHz)	R(meters)	$\Delta\phi$ (degrees)	N_ϕ
Transmit	4.0	5.4	0.40	900
Receive	6.0	4.5	0.36	1000
Spot Beam	14.0	2.5	0.25	1440

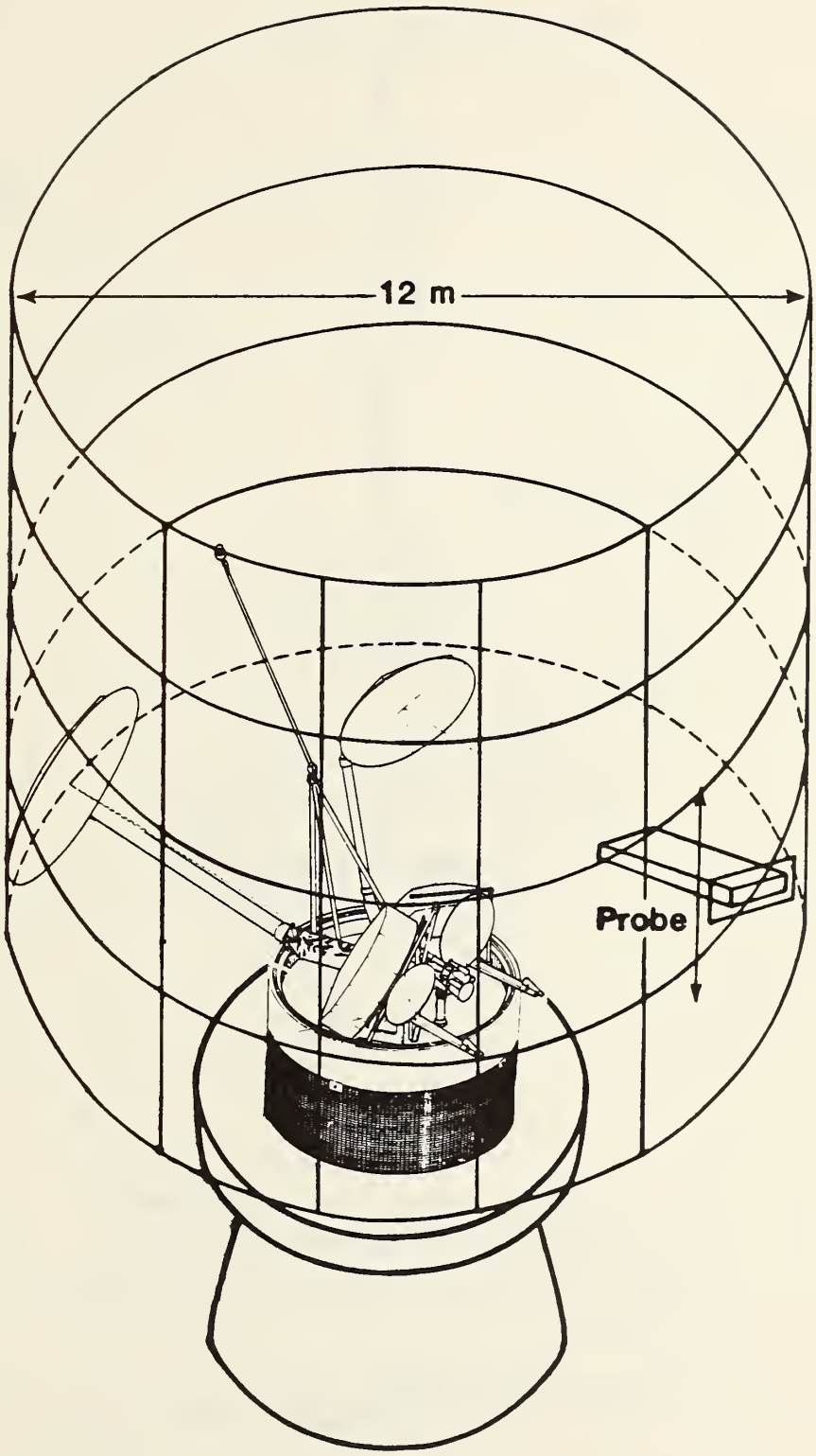

Figure 17. Cylindrical near-field schematic for satellite antennas.

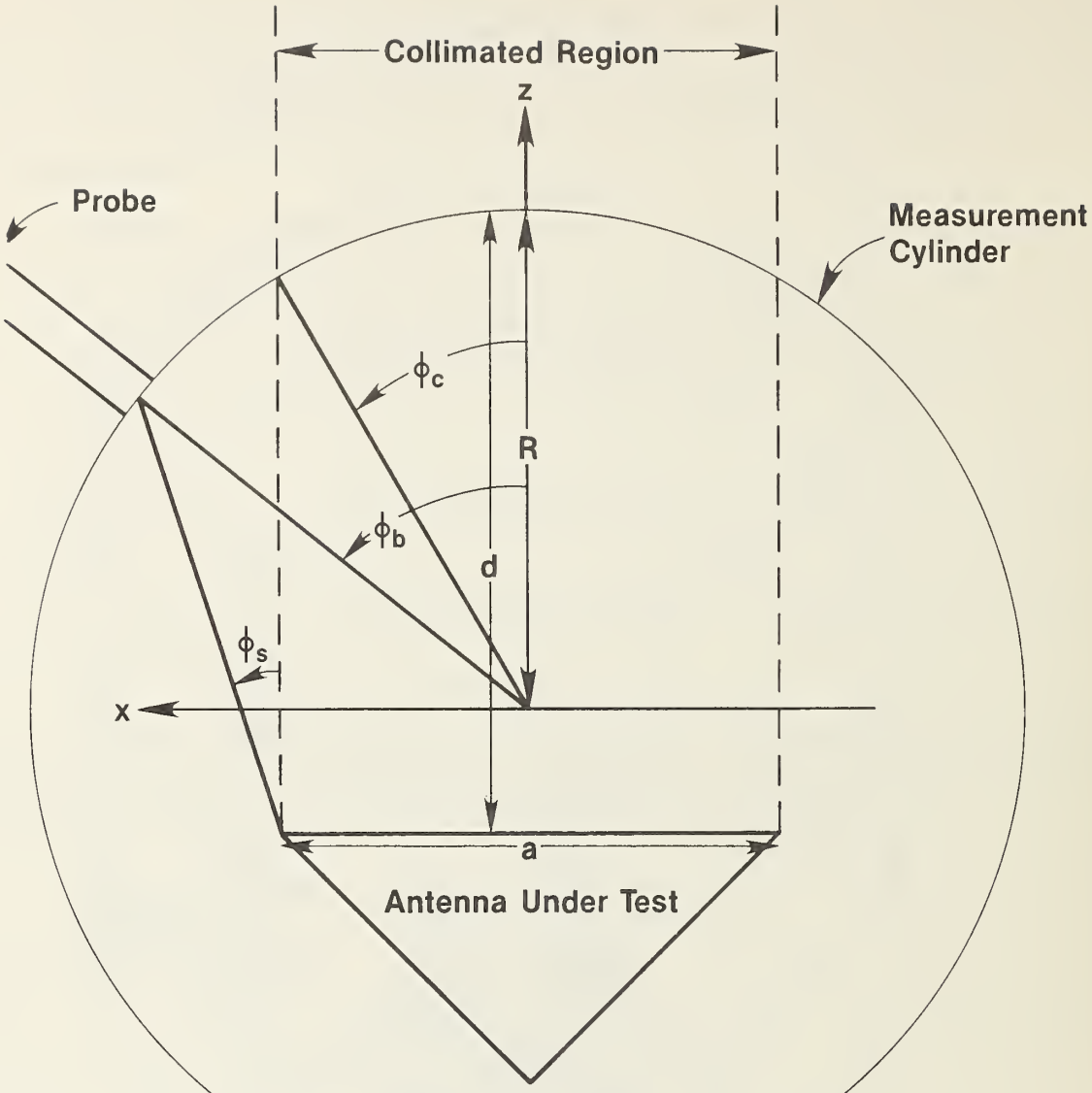

ϕ_c = ANGULAR BOUNDRY OF COLLIMATED REGION

ϕ_b = ANGULAR BOUNDRY OF MEASURED REGION

ϕ_s = ANGULAR BOUNDRY OF RELIABLE RESULTS region

$$\phi_c = \text{ARCSIN } \frac{a}{2R}$$

$$\phi_s = \text{ARCTAN} \left(\frac{\text{Sin } \phi_b - \frac{a}{2R}}{\text{Cos } \phi_b - 1 + d/R} \right)$$

Figure 18. Relationship between antenna dimensions, its location in measurement cylinder, angular coverage, and angular scan region.

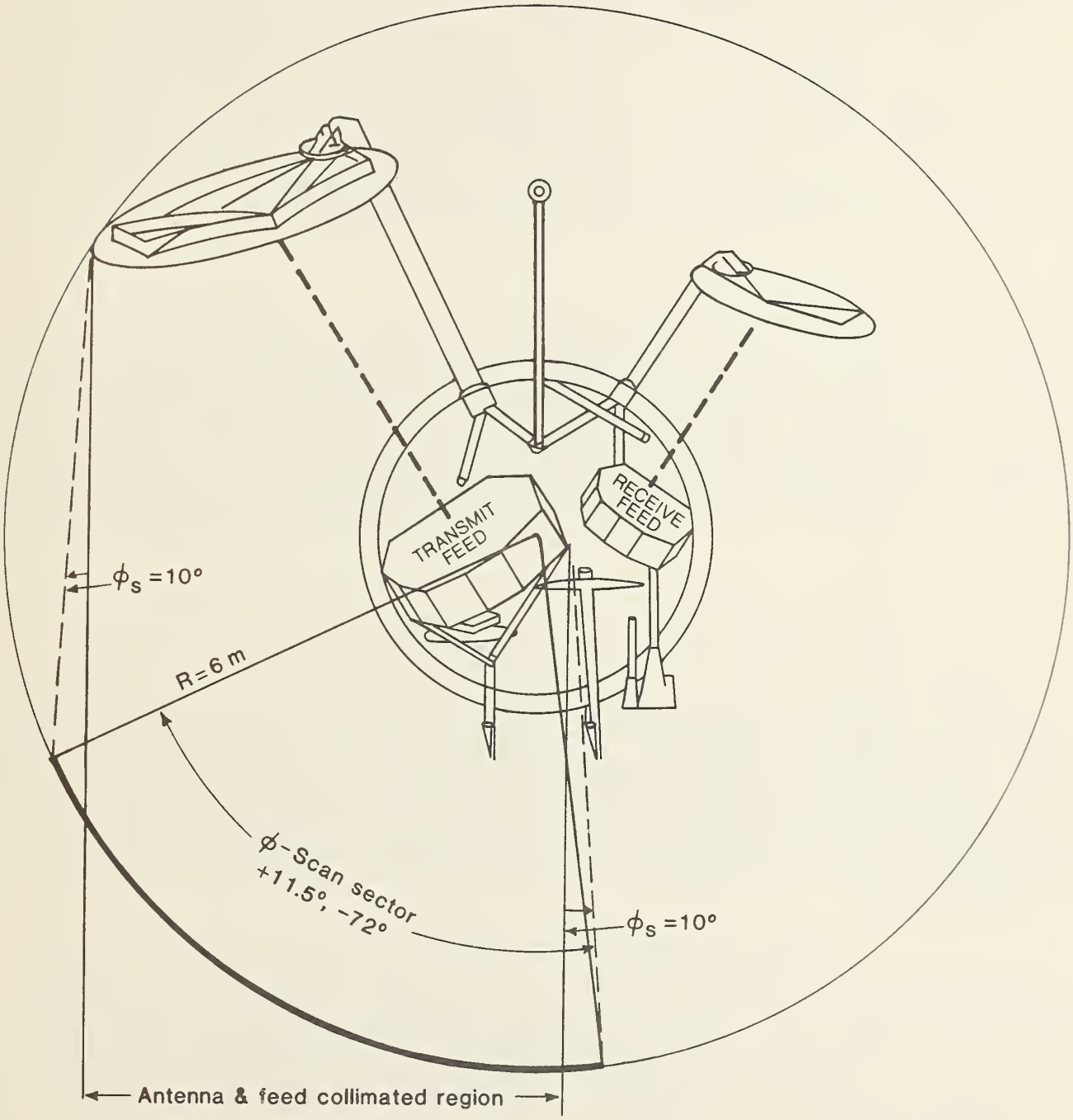

Figure 19. Angular scan sector for transmit antenna and feed giving ±10 degrees coverage in resultant patterns.

3.2.5 Results Available

The pattern, gain, and polarization results obtainable from cylindrical measurements are very similar to those for planar. The measurement details have not been developed to provide the system parameters of EIRP and saturating flux density; however, it should be straightforward and could be achieved with appropriate research. The same is true of beam alignment techniques. Little has been done to develop these techniques, test them on sample antenna systems and document the results, but there is no fundamental reason why they could not be perfected.

The cylindrical approach does not offer either the same current state of development or the potential of the planar method in the area of antenna diagnostics. Very little has been reported in this area. The best possibility appears to be in processing the measured data to obtain far-field amplitude and phase patterns, and then using these results to calculate reflector or feed illumination patterns. This requires more processing than using the planar data directly, but is comparable to the steps required when using planar data to obtain illumination on other planes.

3.2.6 Measurement Accuracy and Range Certification

Of the four methods for evaluating measurement errors discussed in section 3.1.6, only two have been employed to a significant extent for cylindrical near-field measurements. These are comparison with other methods and computer simulation. The comparisons have been encouraging and indicate that the cylindrical method has a potential for accuracy similar to the planar technique. Computer simulation has provided some guidelines for predicting errors, but there is a need for the analytical error analysis to serve as the basis for designing measurement systems and reliably estimating the errors in each measurement.

3.3 Spherical Near-Field Measurements

3.3.1 Measurement Summary

The spherical technique shows the same similarities with the planar and cylindrical techniques that were outlined in section 3.2.1, and again only the differences will be discussed in detail. The theory for this technique is more complex, and this leads to more involved computer programs and some increase in the difficulty of implementing practical measurements. The measurement procedures that have been developed and verified, however, are very similar to those for planar and cylindrical.

3.3.2 Probe Correction

In the two previous near-field techniques, there were no theoretical limitations on the probe characteristics other than requiring the two probes to produce independent data. This requirement meant that the two probes could not have identical polarization ratios for any combination of the independent variables, namely $\underline{K}$ for planar and γ,η for cylindrical (see Appendices A and B for definitions). The patterns could be essentially arbitrary and in principle the two probes could have distinctly different patterns.

The probe used for spherical near-field measurements does have restrictions, however. The pattern of the probe must have rotational symmetry about its z-axis, and therefore the ϕ dependence of the pattern must be given in terms of $\sin\phi$ and $\cos\phi$. This restriction is necessary to allow both an inversion of the coupling equation (eq (C3)) and practical limits on the amount of near-field data

required. If the probe did not have this symmetry, prohibitively large amounts of data would be required as a function of three variables, θ, ϕ and χ, where χ is the rotation of the probe about its axis. In addition to the ϕ-pattern restriction and when the probe is nominally linearly polarized, the "second" probe must be the first probe rotated about its axis by 90 degrees. In principle, two circularly polarized probes with opposite senses of polarization can be used, but they must be perfectly polarized on-axis.

These restrictions are not too difficult to realize, for with careful design and fabrication the required pattern can be achieved to high accuracy. Circular waveguide or conical horns can be machined or electroformed to produce the pattern symmetry.

As with cylindrical measurements, the probe correction or its equivalent is always required. There are many cases where the probe is small or the measurement sphere is fairly large and under these conditions, the probe can be assumed to be an ideal dipole. Some of the details of a general probe correction are then eliminated, but others involving the analytical probe coefficients still remain.

3.3.3 Data Processing

A practical data processing approach was developed by Wacker [9] and is the basis for all spherical near-field programs. It utilizes the special symmetrical probe concept to invert the transmission equation and employs a combination of FFT and matrix multiplication to accomplish the numerical integration. It is a highly efficient method but not as efficient as planar or cylindrical calculations as evidenced by figure 5. The spherical processing time is proportional to N^3 (where N is the number of data points) as compared to N^2 for the others.

3.3.4 Measurement System Hardware

In the usual implementation of spherical measurements, the probe remains fixed and the antenna is rotated about two axes. The rotator/antenna configuration may be as shown in figure A4 where the boresight direction is along the z axis, the main beam is near the pole of the sphere, and the antenna is rotated in ϕ by 180 or 360 degrees during measurements. This is completely impractical for the satellite system due to the nonrigid character of the antennas. Alternatively, the antenna can be mounted on either of the rotators shown in figures A5 and A6 with the beam along the equator. In these situations, reduced angular rotations are possible, but due to the large offset distances, the antenna must still be rotated over much larger angles than the ±10 degree far-field coverage obtained.

From figure 20, and for measurements on the Intelsat VI transmit reflector,

R = measurement sphere radius = 6.0 m,
a/2 = x-distance from rotation center to antenna edge = 4.7 m,
d = z- distance from antenna to sphere surface = 9.7 m, and
θ_s = angular boundary of reliable results region = 10 degrees.

This leads to the requirement that the antenna must be rotated in azimuth by θ_b = 72 degrees, similar to the requirement for cylindrical measurements shown in figure 19. Similar rotations in elevation would also be required for this reflector, and though smaller rotations would be sufficient for the other smaller antennas, this makes the spherical measurements very undesirable for these satellite applications.

Smaller rotation angles could be achieved by increasing the size of the measurement sphere. For instance, if R = 18 m, $\theta_b \simeq 30$ degrees for the above case, but this would require a much larger room with increased amounts of microwave absorber.

3.3.5 & 3.3.6 Results Available and Accuracy

The spherical and cylindrical techniques are essentially the same in the area of results available and predicted accuracy. More work needs to be done in developing system measurement techniques as well as analytical error analyses.

3.4 Compact Ranges

The far-field testing of microwave antennas requires that the test antenna be illuminated by a uniform plane wave. Approximating this condition for adequate far-field range operation requires that the distance between the transmitter and receiver be between 2 D^2/λ to 10 D^2/λ, where D is the diameter of the test antenna including significant scattering/reflecting surfaces, and λ is the wavelength [10]. For electrically large antennas, this distance can be several kilometers, requiring that the test antenna be measured outdoors. In compact ranges, the uniform plane wave can be approximated close to the antenna by illuminating either a single parabolic reflector [11,12] or two parabolic

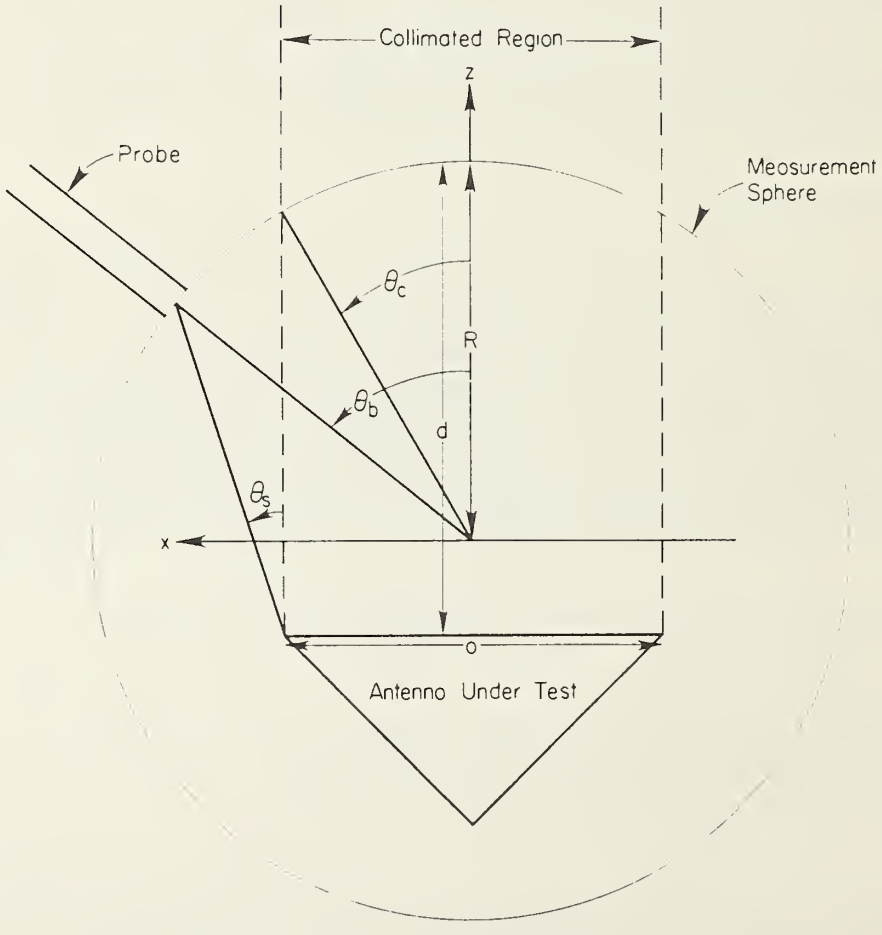

Figure 20. Relationship between antenna dimensions, its location in measurement sphere, angular coverage, and angular scan region.

cylinders that are positioned perpendicular to one another [13] with a spherical source feed. Simply stated, the rays from the feed are collimated by the reflector(s), resulting in an approximate plane wave illumination over a measurement zone where the test antenna is to be placed (figure 21). Such a facility can be placed indoors, thereby avoiding ground reflections, adverse weather conditions, and high towers--features associated with outdoor ranges (figure 22). Compact ranges offer the advantage of the direct measurement of far-field antenna patterns when compared to near-field methods which require the measured near-field data to be processed using FFTs and other mathematics. Hence, there are no software requirements other than those routinely used with far-field ranges. Compact ranges are widely used for both antenna and radar cross section measurements and, as a result, much experience has been obtained in their use.

As with any measurement facility, however, compact ranges have problem areas which must be addressed. Of primary importance is the certification of the measurement zone (also known as test zone, quiet zone, sweet spot, plane wave zone, etc.) where the antenna under test is positioned. Ideally, the measurement zone without antenna is illuminated by a uniform plane wave; that is, the amplitude and phase are constant over any plane transverse to the range axis in the test zone, and the phase progresses linearly along the axis through the test zone. Practically, however, the plane wave illumination is approximate and a typical specification for antennas with $D \leq 1.2$ m requires the measurement zone to be 1.2 m high by 1.2 m wide by 1.2 m deep; to have less than a 0.5 dB amplitude variation, and less than a 10 degree phase variation at any operating frequency that may extend from 1 to 100 GHz (figures 23-25). (This compares to a far-field range where typically a 0.25-0.50 dB amplitude taper and 22.5 degree phase variation is assumed over the test aperture at a range distance of

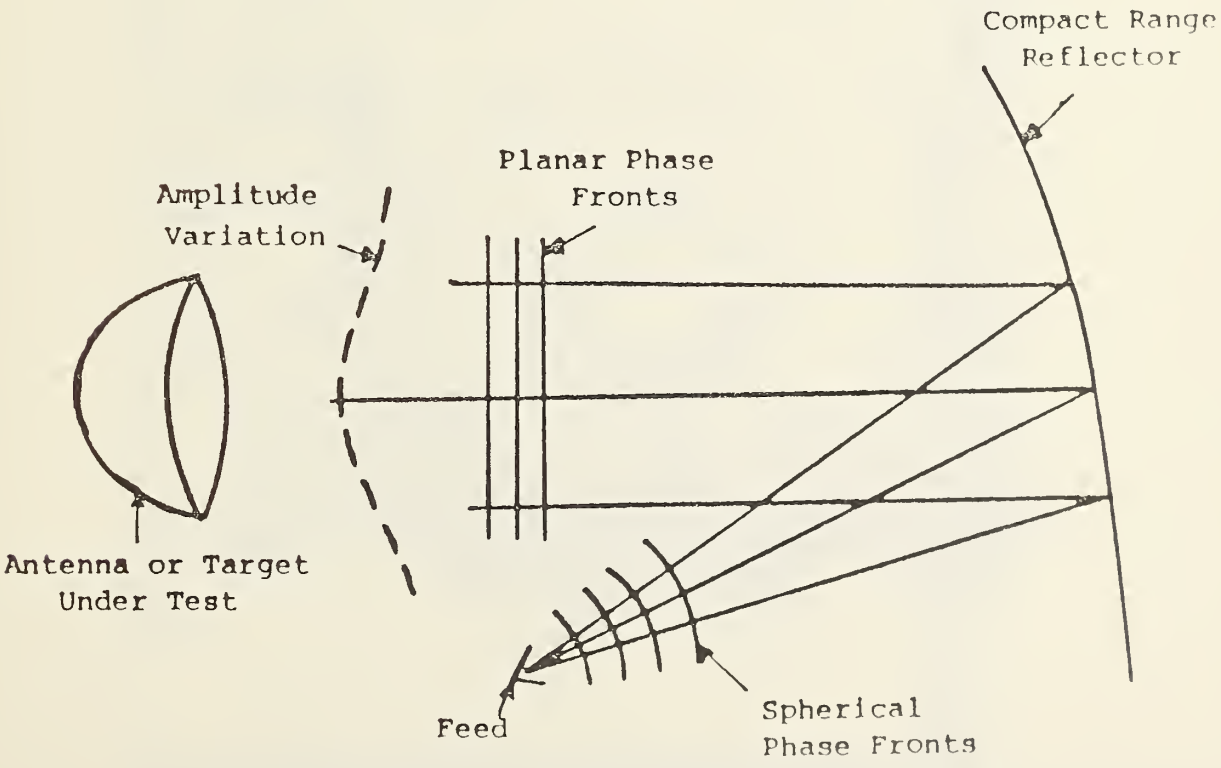

Figure 21. Compact range schematic

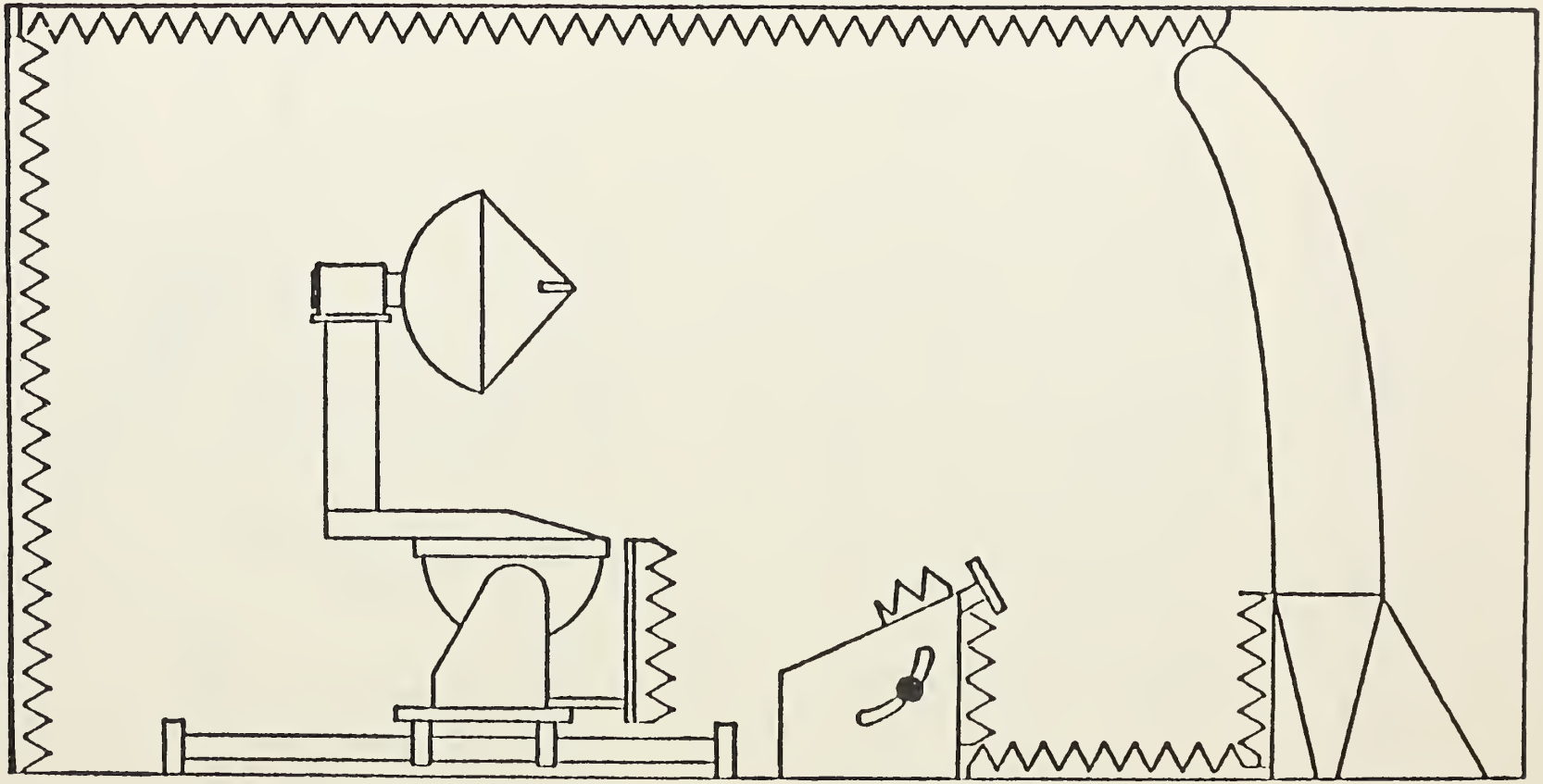

Figure 22. Indoor compact antenna range (15).

$2\ D^2/\lambda$. For a distance of $4\ D^2/\lambda$, one assumes an 11.25 degree phase variation over the test aperture.) To verify the adherence to such specifications at each frequency band requires a planar near-field scanner (figure 26) or at least a field probe mechanism (figure 27).

The sources of error that contribute to the nonuniform plane wave in the test zone must be considered in the design of a compact range. They include space attenuation from the feed, diffraction from the reflector edges, reflector surface tolerances, and depolarizations. Also important are the adverse effects due to the direct radiation from the feed, diffraction from the feed and its supporting structure, stray radiation in the room, and reflections between the test antenna and compact range [11].

In the light of the above discussion, the important question to be resolved is how well the compact range facility applies to spacecraft antenna testing problems. First, where antenna patterns

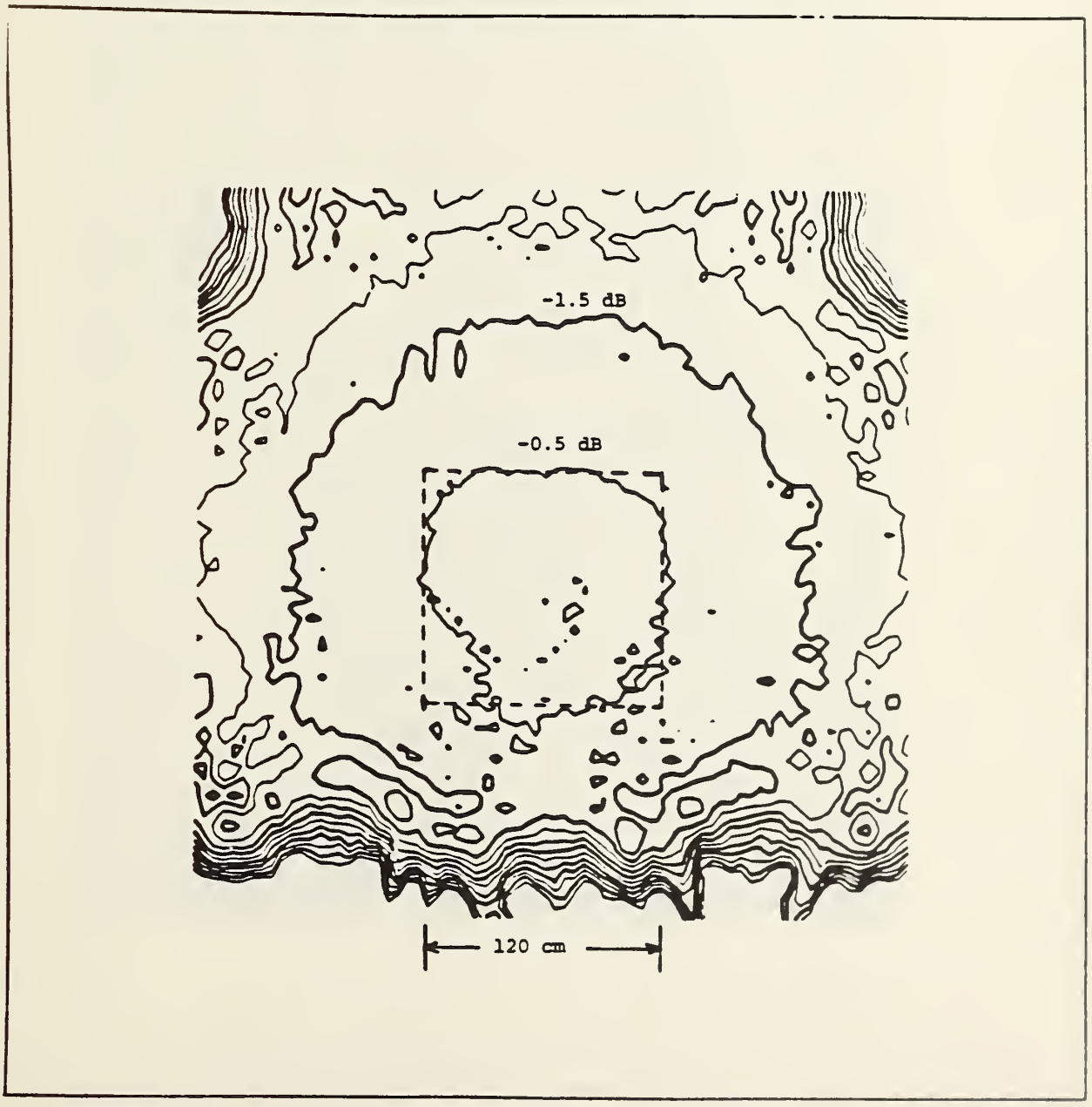

Figure 23. Compact range main component, 1 dB amplitude contours, f = 18 GHz, horn probe.

over ±10 degrees are required in azimuth and elevation, the spacecraft antennas must be positioned on a rotator capable of these motions (figure 22). For systems whose antennas are fragile and are meant to operate in a zero gravity environment, one must ensure that the "antenna configuration" does not change during the required rotations. This is a disadvantage for the compact range system, especially when compared to the planar near-field method which does not require antenna rotations. Second, the size of the test zone for the compact range must be sufficiently large not only to accommodate tipping the antennas in elevation and rotating them in azimuth, but also to house the entire satellite (not including perhaps the solar drum) if one is to measure the effects of antenna-antenna and antenna-structure interactions on the antenna parameters. To satisfy these requirements for the Intelsat VI satellite would require a test zone approximately 9.8 m wide, 6.1 m high, and 6.1 m deep! Since

Figure 24. Compact range main component, 10° phase contours, f = 18 GHz, horn probe.

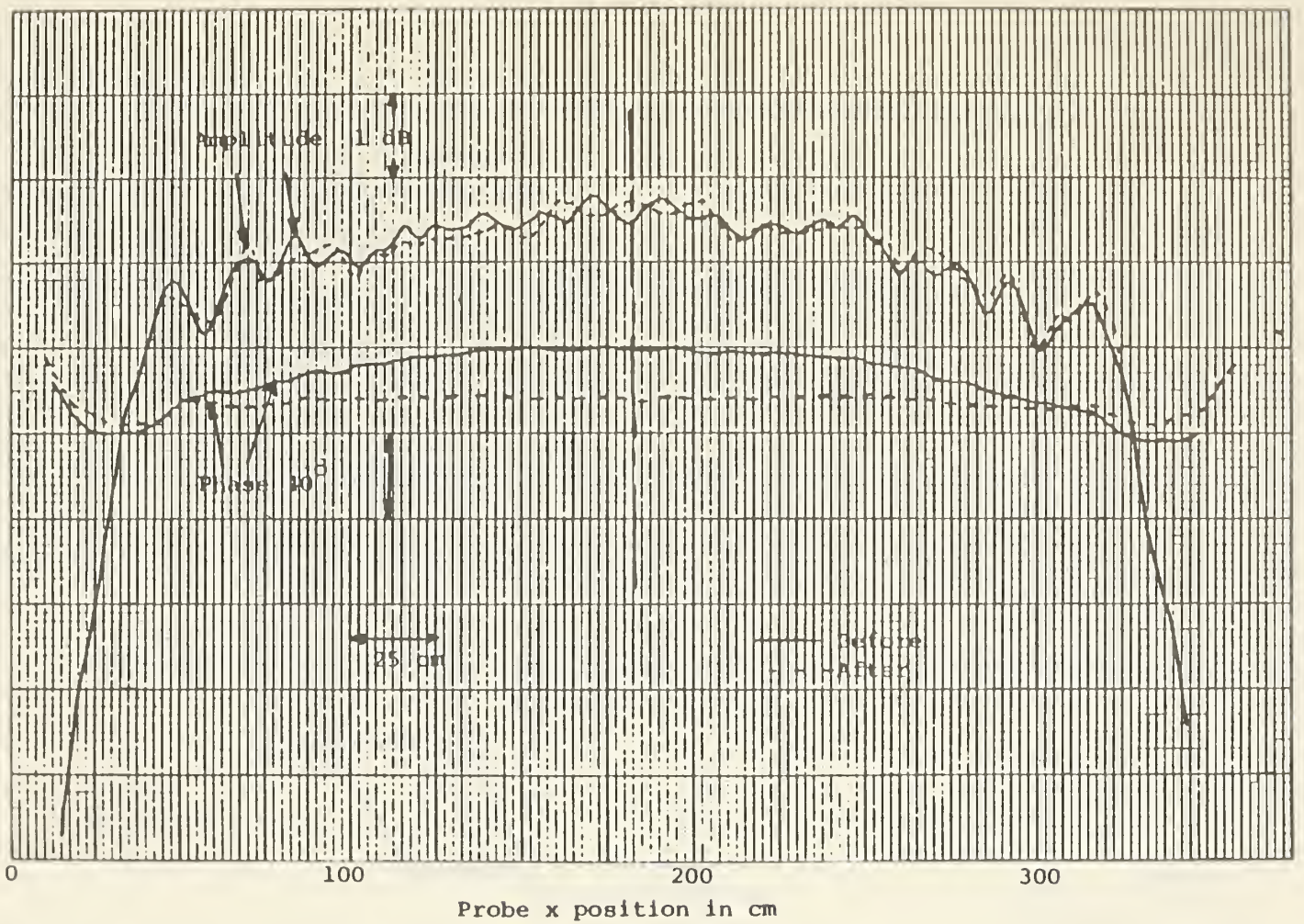

Figure 25. Compact range main component, amplitude and phase, before and after feed translation in -z, x scan, 7 = 335 cm (upper portion), f = 18.0 GHz.

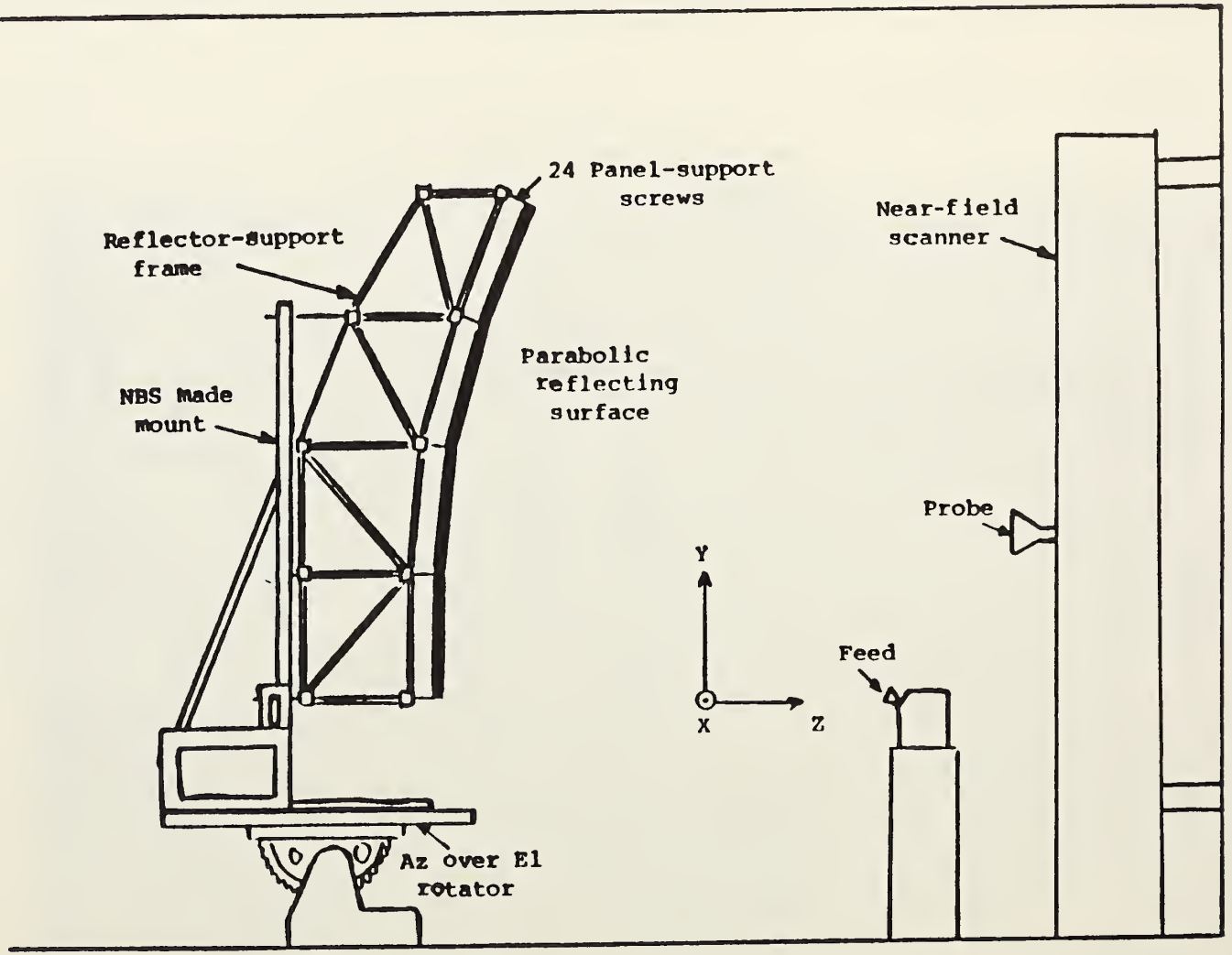

Figure 26. Measurement facility schematic and coordinate system, compact range, NBS, Boulder, Colorado.

single reflector compact ranges require reflector heights approximately two to four times the height of the test zone, a 6.1 m high quiet zone would require the reflector's radius to be in the order of 12 m or more, which is roughly twice the linear size of a compatible planar near-field scanner. Compact ranges of this size are neither available nor anticipated in the near future. Currently, compact ranges with quiet zones 7.3 m wide by 4.5 m high with no depth specified are available and are presently expected to cost between $1.5M and $3.0M dollars. This estimate does not include test equipment, and does not include the housing facility itself. For comparison, a compact range with a 1.5 m quiet zones cost in the order of $0.3M. Third, the measurement accuracies using a compact range need to be addressed. For the measurement of the main polarization component of test antennas, error bounds have been obtained for a compact zange whose quiet zone is 1.2 m wide by 1.2 m high with an amplitude taper of 0.5 dB and phase variations less than 10 degrees [14]. Typically, errors on the order of 0.05 dB and 1.0 dB occur respectively at the 0 dB and -40 dB power levels, as can be seen in figure 28. Such results are also comparable to those obtained on a far-field range with a 0.5 dB

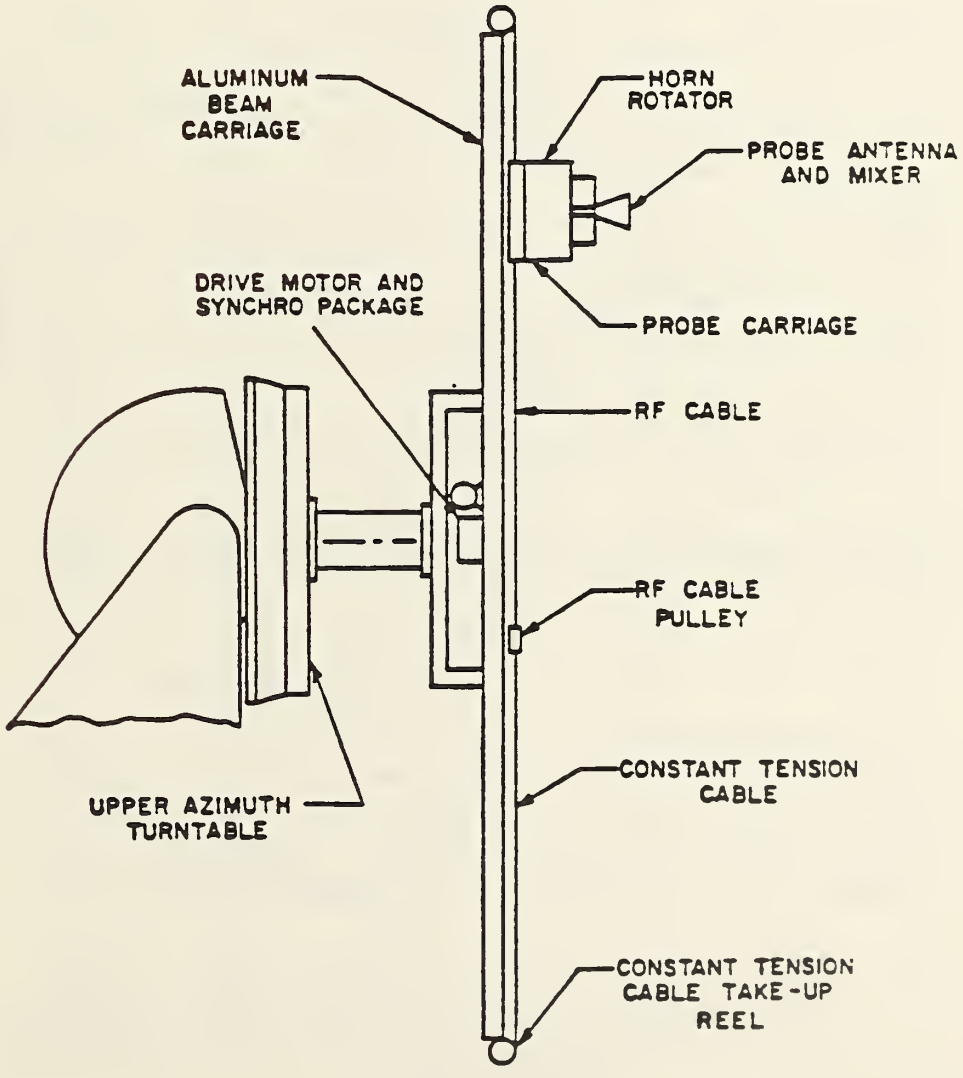

Figure 27. Schematic diagram of field probe mechanism (15).

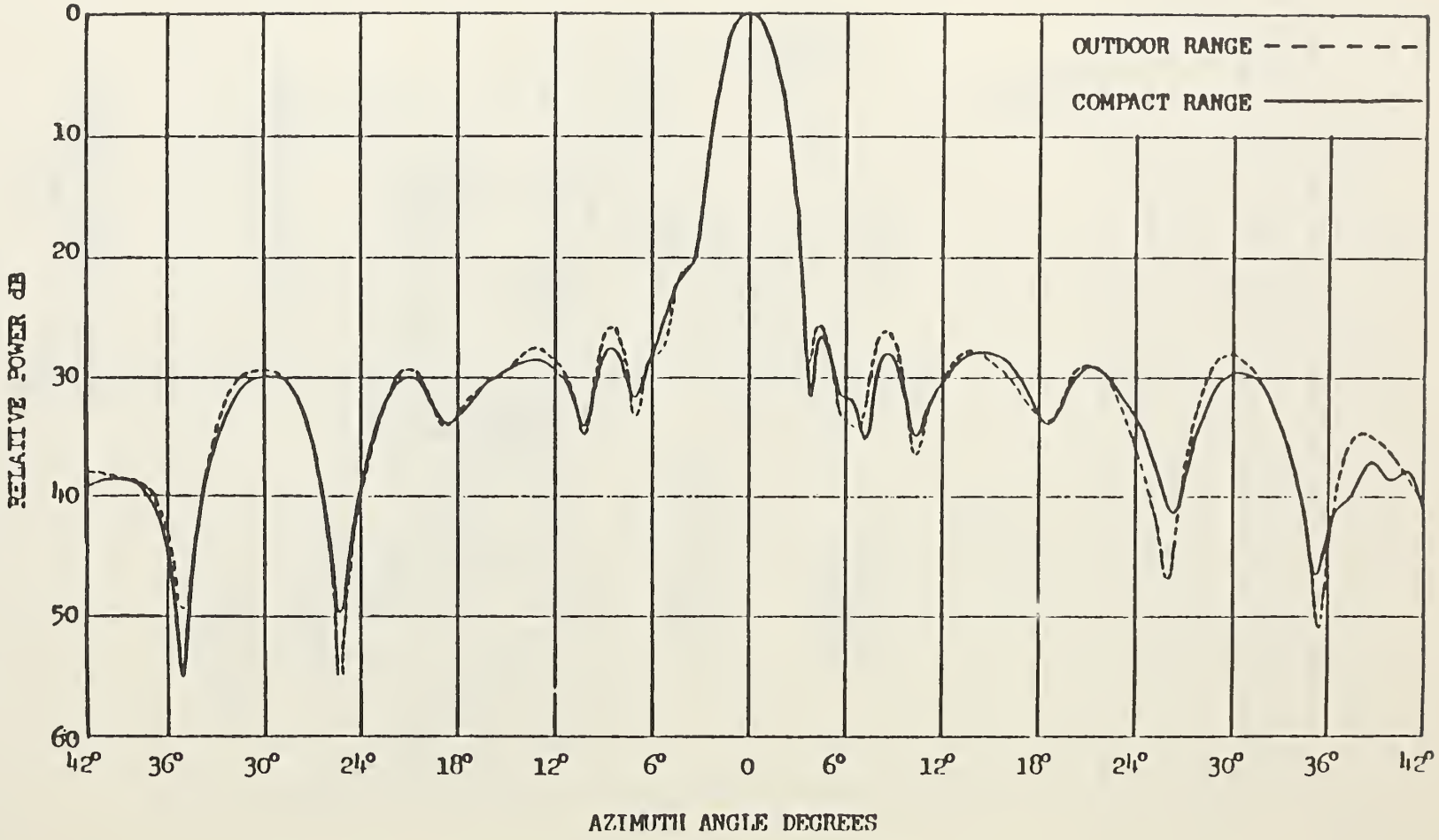

Figure 28. Comparison of the azimuth plane patterns on an outdoor range and on a point source compact range at 10 GHz (Courtesy Johnson and Poinsett [17]).

amplitude taper [15]. For the measurement of the cross polarized component, however, one must realize that the cross polarization of the field in the test zone is typically in the order of -30 dB. As a result, accurate measurements of the cross polarized component of the antenna under test below -30 dB is presently questionable using the compact range. This is a serious drawback where frequency reuse is utilized and polarization isolations need to be established.

As mentioned earlier, the certification of a compact range at each frequency band requires using either a planar near-field scanner or at least a field probe mechanism to assure that the specification in the quiet zone is attained. When changing frequency bands on the compact range, one must change the feed to accommodate the measurement. (Four feed changes would be required to cover the 4-14 GHz frequency range.) This necessitates realigning the compact range for each feed to ensure both acceptable amplitude taper and phase uniformity in the quiet zone. This can be quite time consuming but is very important for proper beam alignments, boresighting of the antenna under test, gain comparison measurements, effective isotropic radiated power (EIRP) measurements, and flux density measurements used for determining receiver saturation levels. These items are discussed in the next paragraph.

Of particular importance in antenna measurements using a compact range is the assumed uniformity of the plane wave field in the quiet zone. For example, when one utilizes a standard gain horn in the quiet zone as a reference standard, its receiving response should be independent of its location (not orientation, obviously) within the zone. This, of course, should also be true for the antenna under test, thereby assuring that accurate gain transfer measurements are made. This planarity of the field also is a factor in EIRP and flux density measurements. In the former case, the accuracy of the EIRP measurement is dependent on the accuracy of the gain transfer measurement. In the latter case, the accuracy of the flux density (to saturate the receiver) measurement depends on the uniformity of the flux density in the test zone. What is to be inferred here is that care should be taken, particularly in the use of a new compact range, to verify or establish the error bounds for antenna parameter measurements. In addition, with the compact range and for determining beam alignments or boresighting of the antenna under test, one is presently required to rotate the antenna 180 degrees about the range axis using a polarization positioner [16]. Since the size of the satellite antenna farm prohibits its placement on a polarization positioner, one must devise and evaluate alternate schemes to boresight these antennas using compact ranges. Where polarization positioners have been utilized for antennas under test, typical boresight alignment accuracies of 0.25 to 0.5 mrad (0.014 - 0.028 degrees) are cited [14].

Swept frequency measurement methods across a frequency band using compact ranges can result in the same advantages given by the far-field range. Specifically, the methods can provide diagnostic tools that are useful in identifying frequency sensitive beam squint, antenna resonances, and unwanted scattering sources of error. However, as in the far-field method, the compact range method does not yield the near-field data whose contour plots are often used to diagnose local anomalies in an antenna under test [13].

4.0 Choice of the Optimum Measurement Technique for Directive Communications Satellite Antenna Systems.

The basis for the choice of the best measurement technique has been established in the previous sections. Using this information, ratings were assigned to each evaluation factor for each measurement approach. The results are tabulated in table 7. The planar near-field measurement method has

the best score for both the critical factors and all the factors. In addition, it has the potential to improve its rating by further development of swept frequency and beam alignment techniques. Because of this, the planar technique will be the focus of the research effort for the remainder of this study.

Table 7 Comparative Rating of Measurement Techniques

Evaluation Factor	Weight	Ratings of Measurement Techniques: Planar	Cylindrical	Spherical	Compact Range
1. Characterize Interactions	1	10	10	10	2
2. Minimum Antenna Motion	2	10	5	2	2
3. Test Zone Size Acheivable					
a. Individual Antennas	2	10	10	10	10
b. Antennas and Interactions	1	10	10	10	2
4. Detailed Pattern Results	1.5	10	10	10	10
5. Accurate Results	2	10	8	8	8
6. Frequency Change Ease	0.5	8	8	8	8
7. Swept Frequency Results	2	4	2	2	10
8. Diagnostic Information	1.5	10	6	5	4
9. Bean Alignment Accuracy	1.5	8	7	7	8
10. System Parameter Results	1	10	7	7	7
11. Ease of or Need for Probe Correction	0.5	7	6	6	10
12. Software Complexity and Speed	0.5	8	7	6	10
13. Hardware Practical					
a. Antenna Size Test Zone	2	9	9	10	8
b. Interaction Size Test Zone	1	9	9	10	2
14. Hardware Commercially Available	0.5	8	9	10	10
15. Practical to Implement	2	10	5	5	5
16. Flexible to Antenna Size	1	8	8	8	8
17. Measurement Time	1.5	7	6	5	10
18. Demonstrated Results	1.5	10	7	5	10
19. Accuracy Demonstratable	1.5	10	7	6	8
Total Weighted Sum	280	251	201.5	191	199
		90%	72%	68%	71%
Critical Factors Weighted Sum (Those with Weight = 2)	120	106	78	74	86
		88%	65%	62%	72%

References

[1] DiFonso, D.F.; English, W.J. Far-field criteria for reflectors with phased array feeds. IEEE/AP-S International Symposium Digest; 1974. p. 54-56.

[2] Yaghjian, A.D. Upper-bound errors in far-field antenna parameters determined from planar near-field measurements, Part 1: Analysis. Nat. Bur. Stand. (U.S.) Tech. Note 667; 1975.

[3] Newell, A.C.; Crawford, M.L. Planar near-field measurements on high performance array antennas. Nat. Bur. Stand. (U.S.) NBSIR 74-380; 1974 July.

[4] Kerns. D.M. Plane-wave scattering-matrix theory of antennas and antenna-antenna interactions. Nat. Bur. Stand. (U.S.) Monograph 162; 1981 June.

[5] Rodrigue, G.P.; Joy, E.B.; Huddleston, G.K.; Burns, C.P.; Burdette, E.C. A study of phased array antenna patterns determined by measurements on a near-field range. U.S. Army Missile Command, Redstone Arsenal, Alabama, Internal Report; 1975 March.

[6] Rodrigue, G.P.; Joy, E.B.; Burns, C.P. An investigation of the accuracy of far-field radiation patterns determined from near-field measurements. U.S. Army Missile Command, Redstone Arsenal, Alabama, Internal Report; 1973 August.

[7] Newell, A.C. Upper bound errors in far-field antenna parameters determined from planar near-field measurements, Part 2: analysis and computer simulation. Lecture notes for NBS short course, Antenna parameter measurements by near-field techniques. 1975 July 7-11.

[8] Yaghjian, A.D. Near-field measurements on a cylindrical surface: A source scattering-matrix formulation. Nat. Bur. Stand. (U.S.) Tech. Note 696; 1977 June.

[9] Wacker, P.F. Non-planar near-field measurements: Spherical scanning. Nat. Bur. Stand. (U.S.) NBSIR 75-809; 1975 June.

[10] Hacker, P.S.; Schrank, H.E. Range distance requirements for measuring low and ultralow sidelobe antenna patterns. IEEE Trans. AP-S, AP-30(5); 1982 September.

[11] Vokurka, V.J. Seeing double improves indoor range. Design feature. Microwaves and RF. 24(2): 71-76; 1985 February.

[12] Johnson, R.C.; Ecker, H.A., Hollis, J.S. Determination of far-field antenna patterns from near-field measurements. Proc. IEEE 61(12); 1973 December.

[13] Repjar, A.G.; Kremer, D.P. Accurate evaluation of a millimeter wave compact range using planar near-field scanning. IEEE Trans. on Ant. and Prop. AP-30(3); 1982 May.

[14] Scientific Atlanta 1984/85 Instrumentation Products Catalog. Atlanta, GA: Scientific-Atlanta, Inc. 103-104.

[15] Hollis, J.S.; Lyon, T.J., Clayton, L., Jr. Microwave antenna measurements. Atlanta, GA: Scientific-Atlanta, Inc.: 1970 July. p. 14-14.

[16] Hess, P. Boresighting antennas. Atlanta, GA, Scientific-Atlanta Inc.: 1978 February.

[17] Johnson, R.C.; Poinsett, R.J. Compact antenna range techniques. Technical Report. RADC-TR-66-15; 1966 April.

APPENDIX A
Planar Near-Field Measurements Theory

A-1. Introduction

The planar near-field (PNF) measurement technique was the first of the near-field techniques to be developed, verified, and implemented as an operational method of obtaining antenna parameters. It represented a major departure from previous methods where the attempt had been to observe the far-field parameters of the antenna under test (AUT) directly and where very little mathematical theory or data processing was required between measured data and final results. A need for an alternative measurement technique, serious enough to justify the additional complexity, has been generated by the development of increasingly complex antennas such as phased-arrays and shaped-beam communication antennas. These antennas, and their associated electronic systems, have presented measurement problems which were impractical or impossible to meet with far-field ranges or anechoic chambers.

The success of this measurement technique has depended upon advances in three diverse areas. First, there has been the development of a rigorous, and yet easily applied, plane-wave scattering matrix theory which can be applied to arbitrary antennas and includes the mechanism to correct for the non-ideal characteristics of the probe. Secondly, the rapid growth of high-speed digital computers has made practical both the automatic control of the measurement process as well as accurate and efficient means of mathematical calculation. Finally, electronic receiving equipment is readily available which will accurately measure the amplitude and phase of microwave signals over large dynamic ranges.

The material which follows will be presented primarily from an experimental or applied point of view. It is oriented towards the engineer who must use the theory, computer programs, and instrumentation in the measurement of antennas.

A-2. Planar Near-Field Theory from a Measurement Point of View

The mathematical formulation used in this summary follows very closely, and is based entirely upon, the pioneering work of D. M. Kerns in his development of plane-wave scattering matrix theory. This work began in the late 1950's, was presented and used in various measurements during the 1960's, and has recently been published in a very complete and extensive monograph [A1] Although there have been other approaches to the theory and, as summarized both by Kerns and in a review paper [A2], there were a number of earlier developments; none have received the widespread acceptance and success that Kerns's work has. This is due to a combination of rigor, completeness, and practicality which has made the transition from mathematical theory to actual implementation much easier. In the present theory, it is not necessary to make simplifying assumptions related to the symmetry, separability of fields, polarization, or reciprocal nature of the AUT. Neither must the probe have similar or additional ideal properties. Yet in spite of, or perhaps because of, the rigorous nature of the theory, the final working equations and mathematical operations used in the implementations of the theory are surprisingly concise and easy to understand and use.

The following discussion of the theory will focus on these final working equations and their use. No attempt will be made to present a complete and rigorous derivation such as presented by Kerns, or to trace the development of near-field measurements as done by Johnson et al. in their review paper. We will, instead, present a development of the basic working equations from an intuitive or measurement point of view, then relate the near-field parameters and equations to more

conventional far-field quantities, finally pointing out some subtle aspects of the plane-wave scattering matrix theory which may be overlooked and can lead to confusion if not handled correctly.

A-3. Definition of Antenna Coordinate System, Vector Components, and Direction Parameters

The results of either near- or far-field measurements are generally given in terms of the vector components of the radiated electric field as a function of direction or position. Both the vector components and the direction parameters must be defined with respect to some coordinate system and, for maximum utility, the coordinate system should be fixed to the antenna. With such a coordinate system, the measured parameters are independent of the mounting or orientation of the antenna and, if required, can be easily transformed from the antenna coordinate system to another measurement or operation system if their relative orientation and position are given.

The antenna coordinate system used throughout this discussion will be one with the plus or minus z-axis in the nominal boresight direction and the major polarization axis in the x- or y-direction for linearly polarized antennas. For other polarizations, the locations of the x- and y-axes are defined by either the geometrical structure of the antenna or the location of fiducial marks.

One example of an array antenna with its coordinate system defined as above is shown in figure A1. In this case, the beam may be electronically steered in many directions, so the z-axis is defined as normal to the plane of the array with the y-axis parallel to the narrow walls of the radiating horns and, therefore, in the direction of the main component of the aperture electric field.

Once the coordinate system is defined, we must also define vectors and/or angles to specify directions relative to the antenna, as well as unit vectors to be used in describing the vector components of the field. There are a number of possible choices for these direction and component parameters. As each of the possible choices is used at some point in the analysis, they will now be discussed.

The components of the electric field, $\underline{V}$, can be described in terms of rectangular components and as functions of a position vector $\underline{r}$.

$$\underline{V}(\underline{r}) = V_x(\underline{r})\,\underline{e}_x + V_y(\underline{r})\,\underline{e}_y + V_z(\underline{r})\,\underline{e}_z \tag{A1}$$

where

$$\underline{r} = x\underline{e}_x + y\underline{e}_y + z\underline{e}_z \ , \tag{A2}$$

and the $\underline{e}$'s are unit vectors along the three axes. An alternative position or direction vector used extensively in the planar analysis is the propagation vector $\underline{k}$ which specifies the direction of propagation and phase constant of a plane wave. The three rectangular components are denoted k_x, k_y, and $k_z = \pm\gamma$. Since the magnitude of $\underline{k}$ is fixed by the relation $\underline{k} \cdot \underline{k} \equiv k^2 = \omega^2\mu\varepsilon$, only two of the components are required to specify the complete vector and, therefore, a given direction in space. Generally, the two components used are those transverse to the z-direction and the transverse vector is denoted by the symbol $\underline{K}$.

$$\underline{K} = k_x\underline{e}_x + k_y\underline{e}_y \ , \tag{A3}$$

$$\gamma = \sqrt{k^2 - k_x^2 - k_y^2} = \sqrt{k^2 - K^2} \tag{A4}$$

Since k_x and k_y vary independently between $-\infty$ and $+\infty$ and are chosen as real quantities, γ is taken as positive for $K < k$ and positive imaginary for $K > k$. Real values of γ correspond to real space, real angles, and propagating plane waves. Imaginary values of γ correspond to imaginary space and evanescent waves.

While the above parameters are useful in many applications, spherical angles and spherical vector components are more widely used for describing far-field parameters where the field is perpendicular to the radial direction, and, therefore, to $\underline{k}$. Figure A1 shows the spherical angles θ, ϕ, and the unit vectors $\underline{e}_\theta$, $\underline{e}_\phi$ which are widely used and very appropriate in many cases. If the main beam of the antenna is along the z-axis, as specified in the definition of the coordinates, and the antenna is linearly polarized, the θ- and ϕ-components are not the most appropriate for specifying the field vectors. In the region of the main beam, the unit vectors $\underline{e}_\theta$ and $\underline{e}_\phi$ change direction relative to the antenna as a function of ϕ. We could change the definition of the antenna coordinates so that the polar axis (the z-axis) was not in the vicinity of the main beam; however, this would make the reference to existing planar analysis more difficult, and there are times when the θ-ϕ-coordinates and components are required. For these, and other reasons which will become apparent, the defined antenna coordinates and θ-ϕ definitions should be retained.

To obtain an alternate set of spherical angles and components, the x-, y-, z-axes are left fixed in the same position relative to the antenna, and the y-axis is chosen as a new polar axis for the definition of the angles E, A, and the unit vectors $\underline{e}_E$, $\underline{e}_A$, shown in figure A2. These components have the advantage that, for a linearly polarized antenna appropriately rotated about the z-axis, the field is primarily either E- or A-polarized.

A third set of spherical angles is shown in figure A3 where the x-axis is the polar axis and the angles and unit vectors are denoted respectively by α, ε, $\underline{e}_\alpha$, $\underline{e}_\varepsilon$. This set is useful for specifying a linearly polarized field, as is the A-E set.

All three of the spherical angle sets are useful in certain instances, and are each closely associated with one of the three types of rotator mounts used in measuring antenna patterns. Figures A4, A5, and A6 show how the θ-ϕ, A-E, and α-ε angles and components are respectively appropriate for the model, az over el, and el over az mounts. In each case, the upper rotator of the mount produces a rotation about an axis fixed to the antenna and is, therefore, the polar axis of the rotator. The spheres shown in the figures are fixed to the antennas and represent their spherical coordinates. When the mount rotates, the sphere moves with the antenna, and the source antenna, or probe, traces out the longitude and latitude lines on the sphere. The relative motion between the AUT and the source, or probe, is equivalent to their moving on the surface of the sphere and measuring the field along lines of longitude or latitude.

One of the primary motivations in maintaining a coordinate system fixed to the antenna, and in defining three different sets of spherical angles, is to facilitate the reference to each different set and to avoid confusion in the transformation equations between different sets. If all three were referred to as θ-ϕ sets with the coordinate system reoriented relative to the antenna each time, the notation, references, and transformations would be quite confusing.

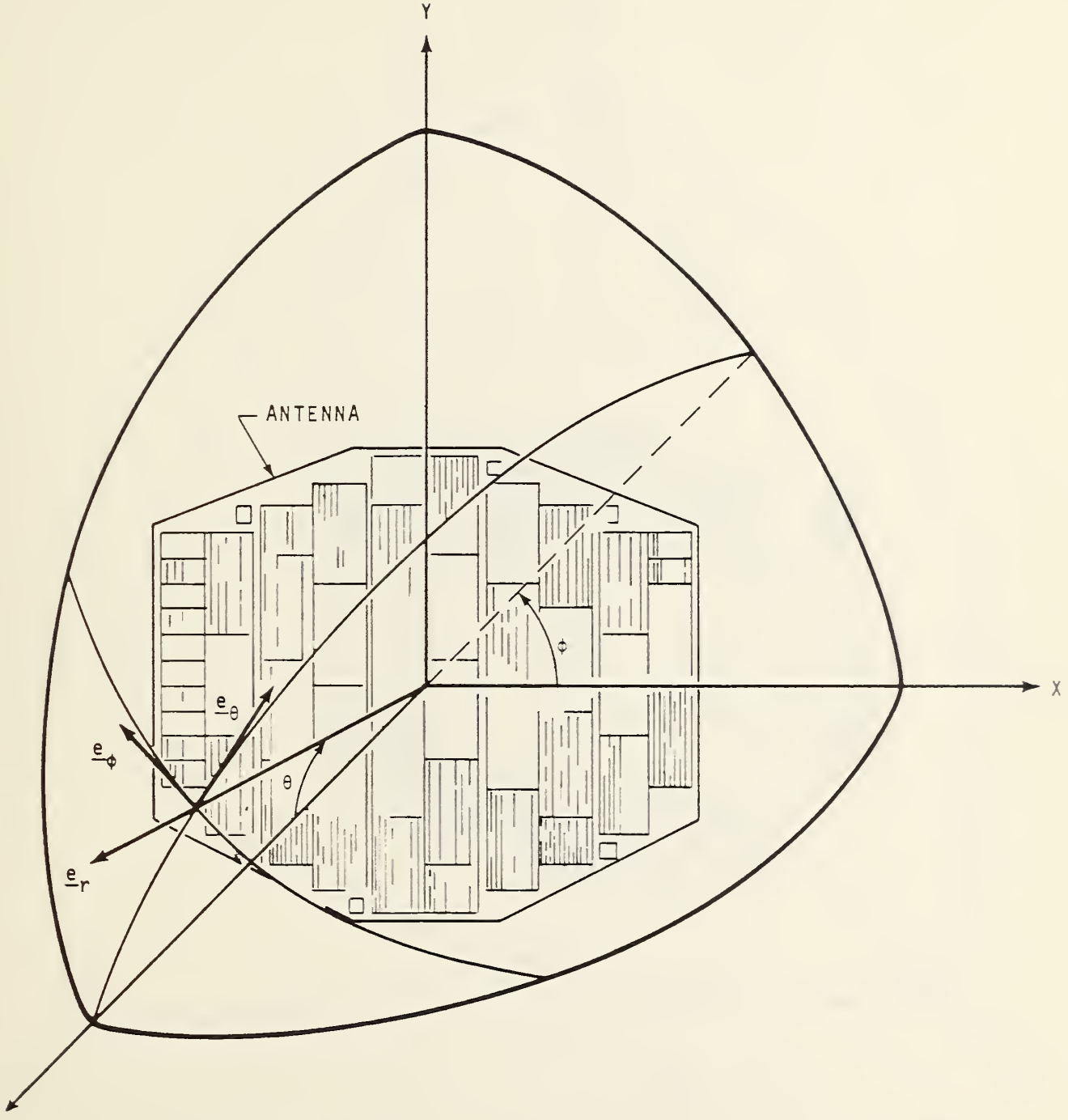

Figure A-1. Antenna coordinate system using θ and ϕ spherical angles with z as the polar axis.

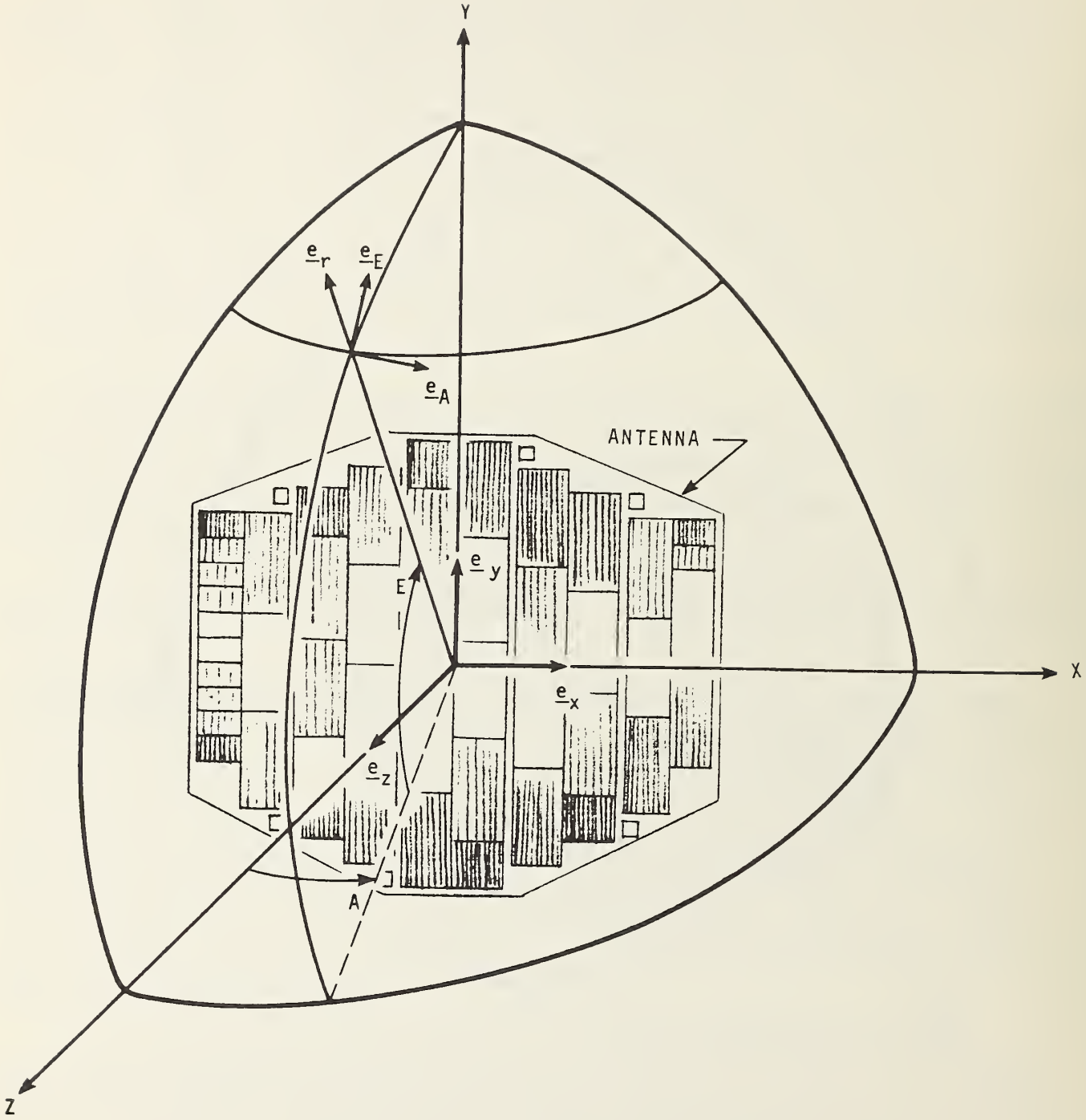

Figure A-2. Antenna coordinate system using A and E spherical angles with y as the polar axis.

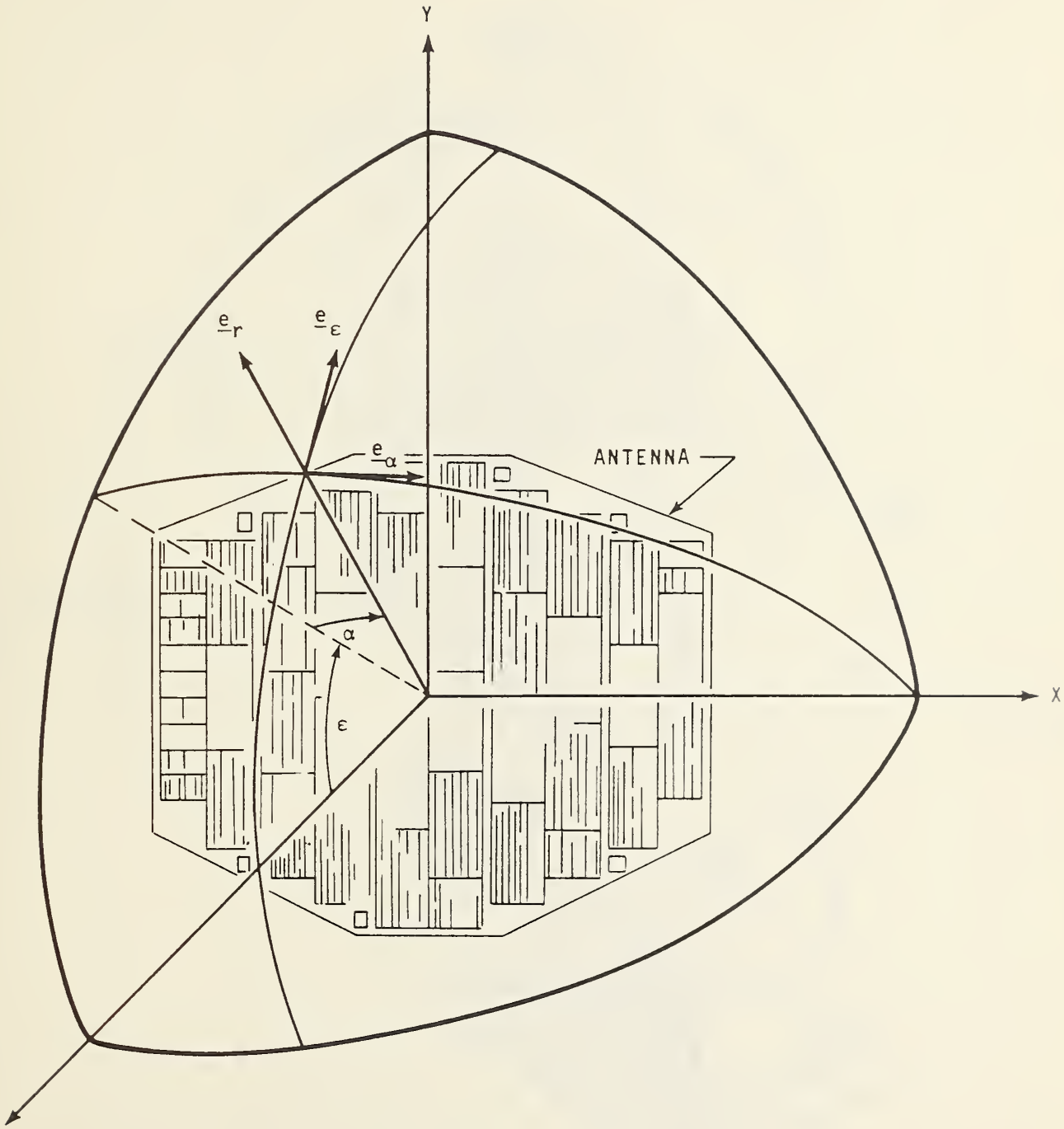

Figure A-3. Antenna coordinate system using α and ε spherical angles with x as the polar axis.

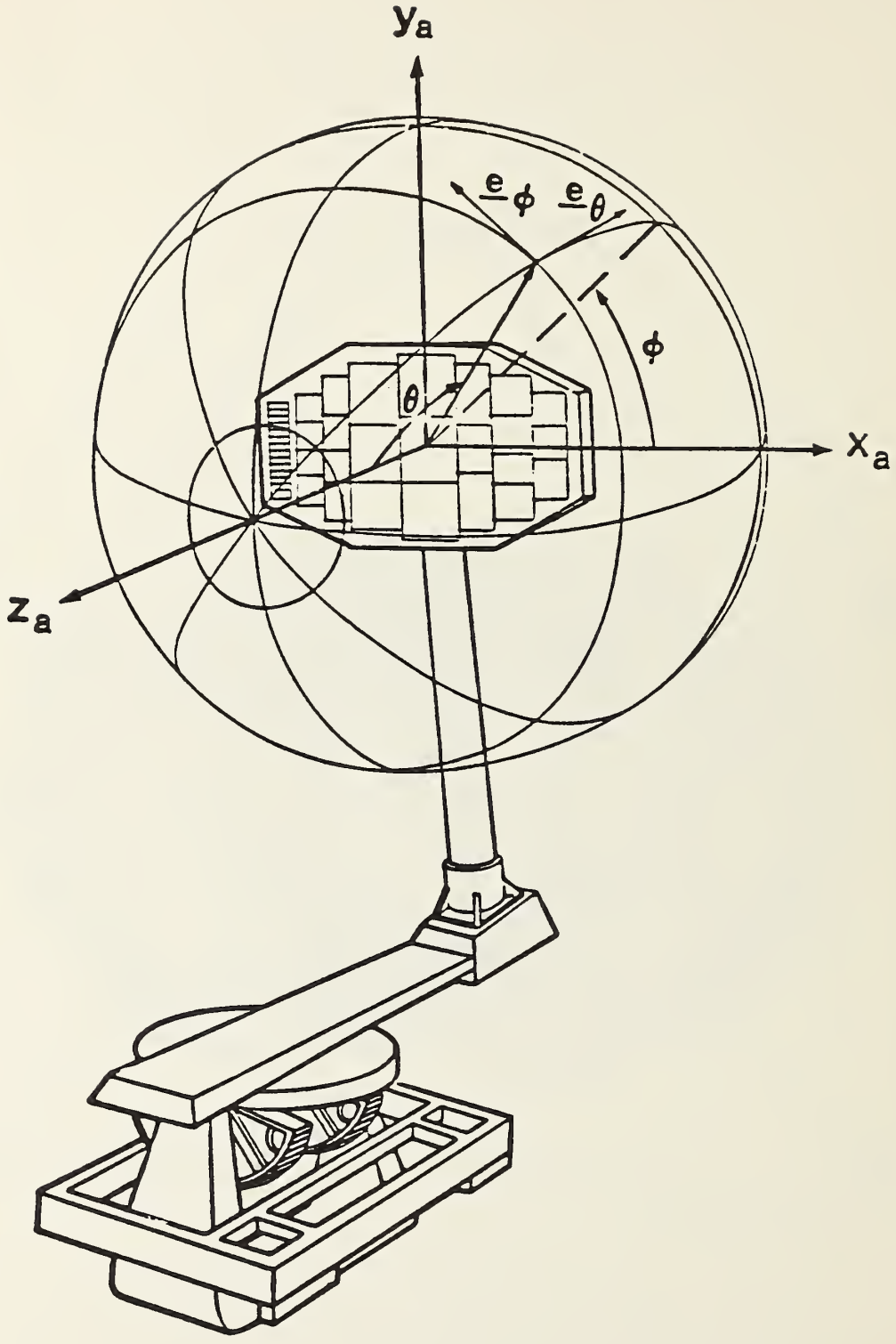

Figure A-4. Model tower used to measure θ-ϕ and h-v vector components.

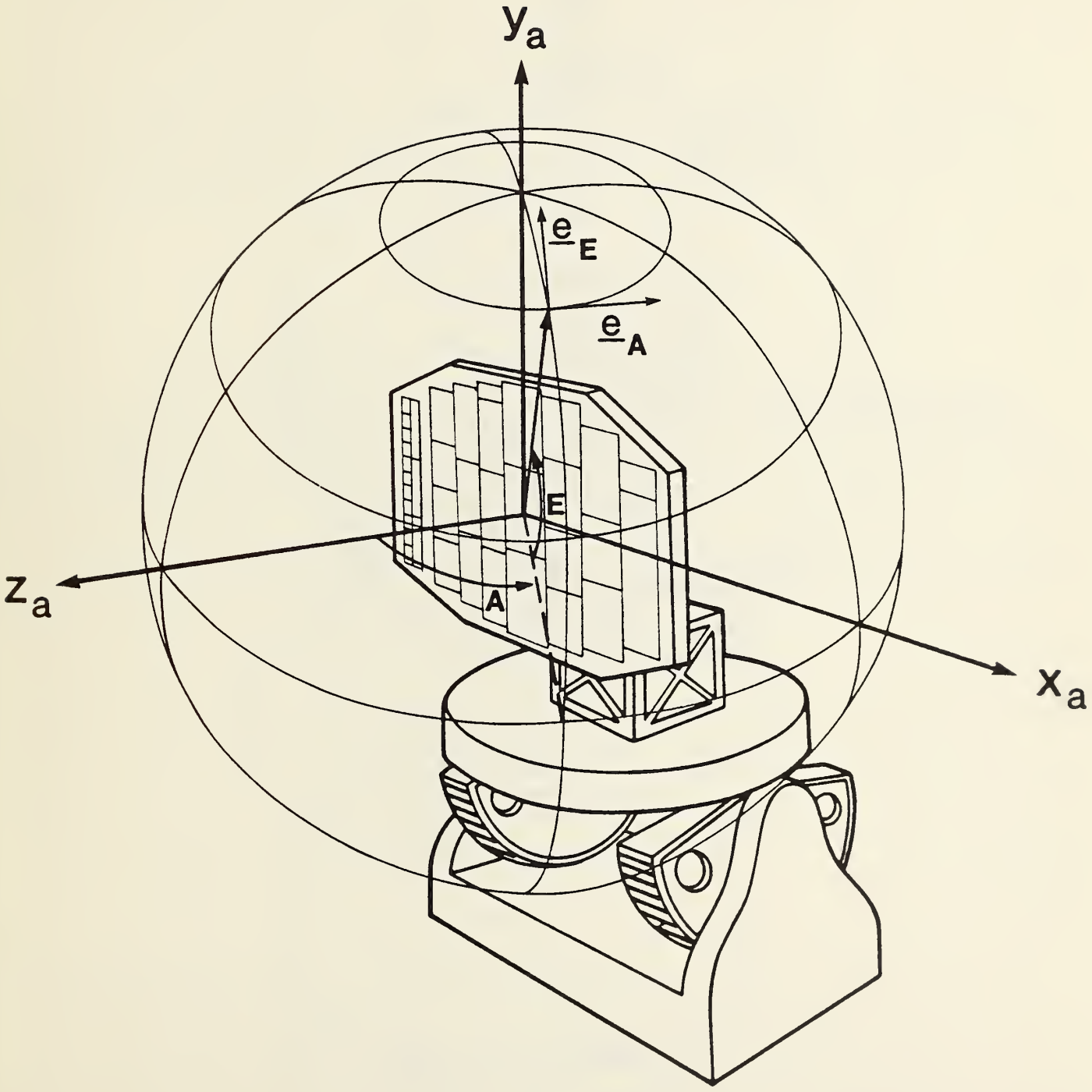

Figure A-5. Azimuth over elevation rotator used to measure A-E vector components.

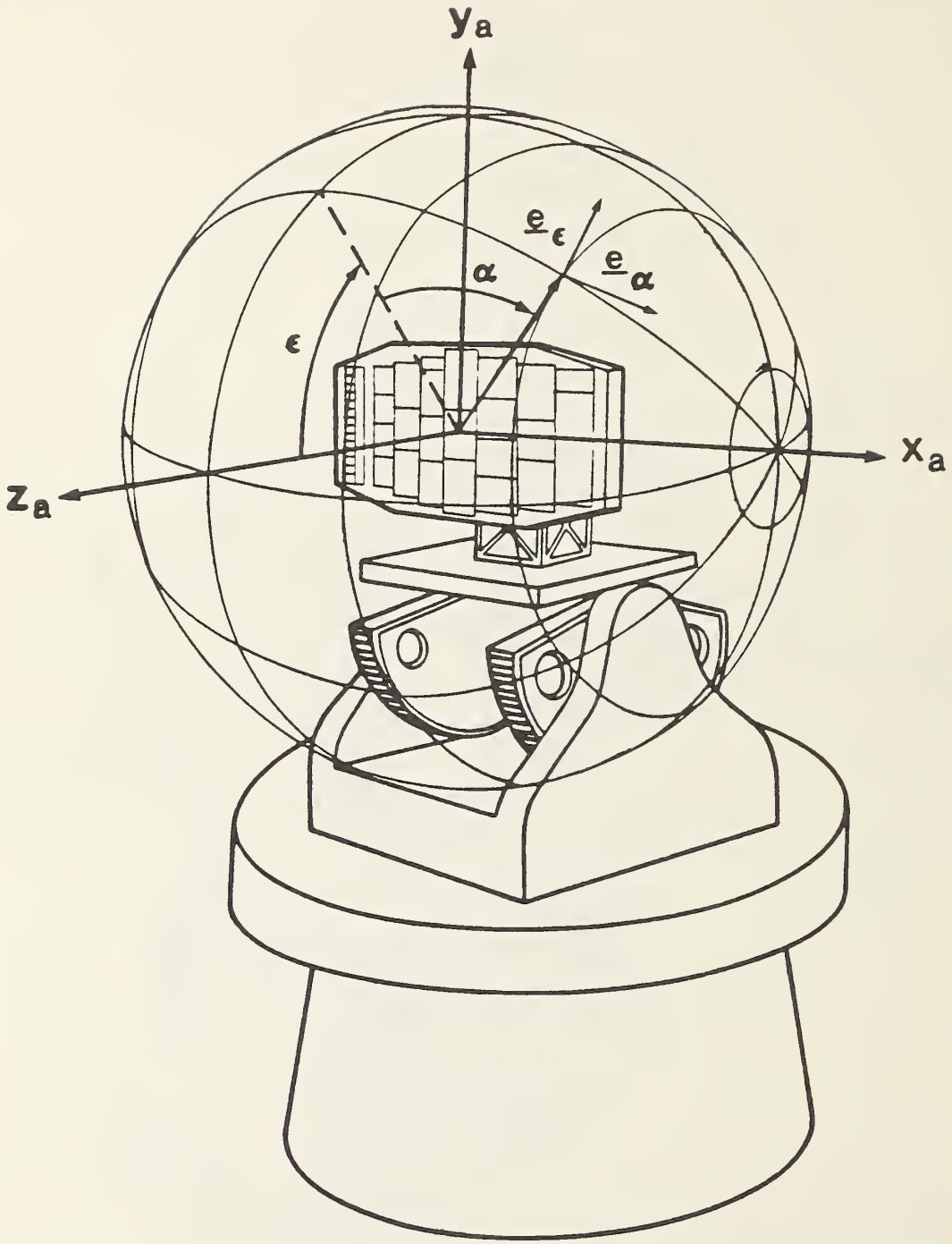

Figure A-6. Elevation over azimuth rotator used to measure α-ε vector components.

As already noted, a direction in real space can be defined by specifying either the components of the propagation vector or one of the sets of spherical angles. Transformation between different parameters is accomplished by the following equations:

$$\frac{k_x}{k} = \sin\theta \cos\phi = \cos E \sin A = \sin\alpha \ , \tag{A5}$$

$$\frac{k_y}{k} = \sin\theta \sin\phi = \sin E = \cos\alpha \sin\varepsilon \ , \tag{A6}$$

$$\frac{k_z}{k} = \cos\theta = \cos E \cos A = \cos\alpha \cos\varepsilon \ . \tag{A7}$$

The transformations are one-to-one for all directions except at the poles of each set where ambiguities do exist. The problem is in determining the azimuthal angles (those which are a rotation about the polar axes, namely ϕ, A, and ε) at the poles of the corresponding coordinate system. For example, from eqs (A5), (A6), and (A7), the transformation equations from the (A, E) to (θ, ϕ) coordinates are

$$\cos\theta = \cos A \cos E, \tag{A8}$$

$$\tan\phi = \tan E / \sin A \ , \tag{A9}$$

and when A=E=0, ϕ is indeterminate. In such cases, it is necessary to choose a specific value for ϕ, and, depending upon the application, it is usually set to either $\pi/2$ or zero. Similar situations arise in determining A and ε when at the poles of those coordinates, but values can be assigned which will give consistent and correct results.

The transformations between the vector components are also required and are derived from expressions for the spherical unit vectors in terms of the rectangular unit vectors.

$$\underline{e}_\theta = \cos\theta \cos\phi \ \underline{e}_x + \cos\theta \sin\phi \ \underline{e}_y - \sin\theta \ \underline{e}_z \tag{A10a}$$

$$\underline{e}_\phi = - \sin\phi \ \underline{e}_x + \cos\phi \ \underline{e}_y \tag{A10b}$$

$$\underline{e}_A = \cos A \ \underline{e}_x - \sin A \ \underline{e}_z \tag{A11a}$$

$$\underline{e}_E = -\sin A \sin E \ \underline{e}_x + \cos E \ \underline{e}_y - \cos A \sin E \ \underline{e}_z \tag{A11b}$$

$$\underline{e}_\alpha = \cos\alpha \ \underline{e}_x - \sin\alpha \sin\varepsilon \ \underline{e}_y - \sin\alpha \cos\varepsilon \ \underline{e}_z \tag{A12a}$$

$$\underline{e}_\varepsilon = \cos\varepsilon \ \underline{e}_y - \sin\varepsilon \ \underline{e}_z \tag{A12b}$$

From these expressions, the vector component transformations are:

$$V_A(A, E) = \frac{\cos\phi}{\cos E} V_\theta(\theta, \phi) - \frac{\cos\theta \sin\phi}{\cos E} V_\phi(\theta, \phi) \ , \text{ and} \tag{A13a}$$

$$V_E(A, E) = \frac{\cos\theta \sin\phi}{\cos E} V_\theta(\theta, \phi) + \frac{\cos\phi}{\cos E} V_\phi(\theta, \phi) \ , \tag{A13b}$$

where $\cos E = \sqrt{1 - (\sin\theta \sin\phi)^2}$, and the angles θ and ϕ are given by eq (A8);

$$V_\alpha(\alpha, \varepsilon) = \frac{\cos\theta \cos\phi}{\cos\alpha} V_\theta(\theta, \phi) - \frac{\sin\phi}{\cos\alpha} V_\phi(\theta, \phi) \quad \text{(A14a)}$$

$$V_\varepsilon(\alpha, \varepsilon) = \frac{\sin\phi}{\cos\alpha} V_\theta(\theta, \phi) + \frac{\cos\theta \cos\phi}{\cos\alpha} V_\phi(\theta, \phi) \quad \text{(A14b)}$$

where

$$\cos\alpha = \sqrt{1 - (\sin\theta \cos\phi)^2} \text{ , and} \quad \text{(A15)}$$

$$\cos\theta = \cos\alpha \cos\varepsilon \text{ ,} \quad \text{(A16)}$$

$$\tan\phi = \cos\alpha \sin\varepsilon \text{ ;} \quad \text{(A17)}$$

$$V_\alpha(\alpha, \varepsilon) = \frac{\cos A}{\cos\alpha} V_A(A, E) - \frac{\sin A \sin E}{\cos\alpha} V_E(A, E) \quad \text{(A18a)}$$

$$V_\varepsilon(\alpha, \varepsilon) = \frac{\sin A \sin E}{\cos\alpha} V_A(A, E) + \frac{\cos A}{\cos\alpha} V_E(A, E) \quad \text{(A18b)}$$

$$\cos\alpha = \sqrt{1 - (\sin A \cos E)^2} \quad \text{(A19)}$$

$$\sin E = \cos\alpha \sin\varepsilon \text{ ,} \qquad \tan A = \tan\alpha/\cos\varepsilon \quad \text{(A20)}$$

There is a fourth set of linear components which are sometimes measured, and arise from a different use of the model mount shown in figure A4. If the source antenna is linearly polarized and stays fixed as the antenna is rotated on the mount, the θ-ϕ components are obtained. In some cases, the source antenna is rotated about its axis by the same ϕ-angle as the AUT. The vector components obtained and denoted $\underline{e}_h$ and $\underline{e}_v$ are those shown in figure A7, which is a projection of the θ-ϕ coordinates on the x-y plane. The transformation between these components and the θ-ϕ components are:

$$\underline{e}_h = \cos\phi\, \underline{e}_\theta - \sin\phi\, \underline{e}_\phi \quad \text{(A21a)}$$

$$\underline{e}_v = \sin\phi\, \underline{e}_\theta + \cos\phi\, \underline{e}_\phi \quad \text{(A21b)}$$

$$V_h(\theta,\phi) = V_\theta(\theta,\phi) \cos\phi - V_\phi(\theta,\phi) \sin\phi \quad \text{(A22a)}$$

$$V_v(\theta,\phi) = V_\theta(\theta,\phi) \sin\phi + V_\phi(\theta,\phi) \cos\phi \quad \text{(A22b)}$$

It should be noted that with the above definition of components and angles and along the x-z plane where k_y=0

$$V_A(A,0) = V_\alpha(\alpha,0) = V_h(\theta,0 \text{ or } \pi) = \pm V_\theta(\theta, 0 \text{ or } \pi) \quad \text{(A23a)}$$

$$V_E(A,0) = V_\varepsilon(\alpha,0) = V_v(\theta, 0 \text{ or } \pi) = \pm V_\phi(\theta, 0 \text{ or } \pi). \quad \text{(A23b)}$$

Similarly, along the y-z plane where k_x=0

$$V_A(0,E) = V_\alpha(0,\varepsilon) = V_h(\theta, \pm\pi/2) = \mp V_\phi(\theta, \pm\pi/2) \quad \text{(A24a)}$$

$$V_E(0,E) = V_\varepsilon(0,\varepsilon) = V_v(\theta, \pm\pi/2) = \pm V_\theta(\theta, \pm\pi/2). \quad \text{(A24b)}$$

With the aid of the above transformations and their inverses, any of the vector components can be obtained from any other set.

A-4. The Transmission Integral and Associated Parameters

Consider now the two-antenna system shown schematically in figure A8. The antenna on the left, referred to as the antenna under test (AUT), is oriented with its coordinate system coincident with what may be called the reference coordinate system OXYZ. The generator connected to this antenna produces an incident wave amplitude a_0 at the terminal surface S_0. As a starting point, assume that the antenna radiates a single y-polarized, plane wave propagating along the z-axis which is proportional to the input amplitude. The complex proportionality constant, $T_{10}(\underline{K} = 0)$ is referred to as the plane wave transmitting coefficient and the subscript "10" denotes that it applies to the transmission from

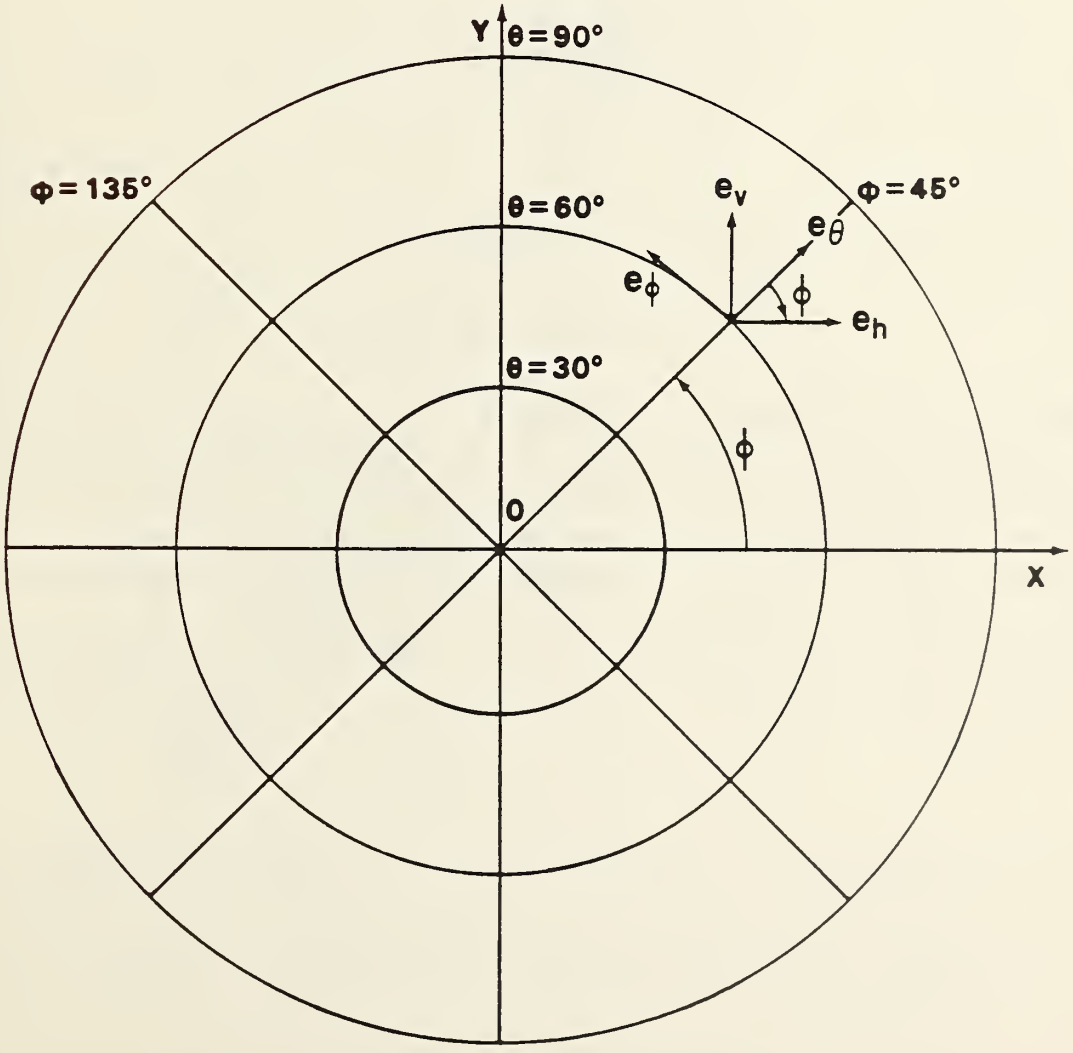

Figure A-7. Relationship between h-v and θ=ϕ vector components.

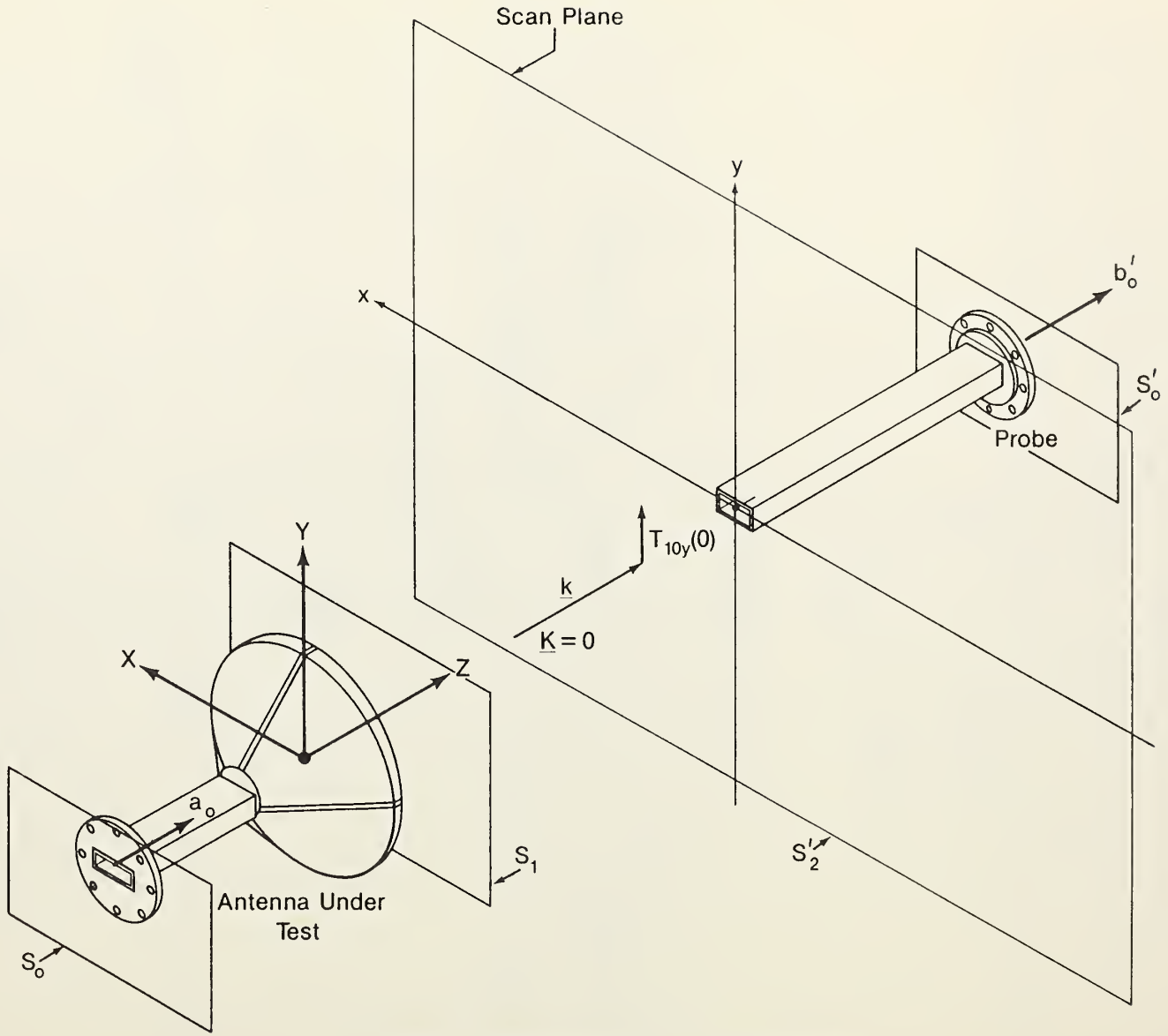

Figure A-8. Schematic of antenna with ideal linearly polarized plane wave.

terminal surface S_0 to S_1 at the origin of the coordinate system. The independent variable $\underline{K}$ defines the direction of propagation of the plane wave and is zero along the z-axis. The plane wave propagating from S_1 to S_2' will be modified by the phase factor e^{ikd} and received by the "probe" antenna on the right. It will produce an output wave amplitude at the terminal surface S_0' denoted by b_0'. The probe's receiving coefficient for this incident plane wave is denoted by $S_{02}'(\underline{K} = 0)$. If we assume that multiple reflections are negligible, the transmission equation for this highly simplified condition is then

$$b_0' = F' a_0 T_{10}(\underline{K} = 0)\, e^{ikd} S_{02}'(\underline{K} = 0), \tag{A25}$$

where $F' = 1/(1 - \Gamma_\ell \Gamma_p)$, and Γ_ℓ and Γ_p are reflection coefficients for the load and probe respectively. (It should be noted that the time factor assumed here is $e^{-i\omega t}$. While this is the opposite of most electrical engineering formulations, it is consistent with the original derivation of the plane wave theory and will be used herein.) In general, a plane wave will have some cross component, as shown in figure A9, and the transmitting and receiving coefficients are generalized from complex scalars to complex two-component vectors, namely,

$$\underline{T}_{10}(\underline{K} = 0) = T_{10x}(\underline{K} = 0)\, \underline{e}_x + T_{10y}(\underline{K} = 0)\, \underline{e}_y , \tag{A26}$$

$$\underline{S}_{02}'(\underline{K} = 0) = S_{02x}'(\underline{K} = 0)\, \underline{e}_x + S_{02y}'(\underline{K} = 0)\, \underline{e}_y , \tag{A27}$$

and the transmission equation becomes

$$\begin{aligned} b_0' &= F' a_0 \left(T_{10x}(\underline{K} = 0)\, S_{02x}'(\underline{K} = 0) + T_{10y}(\underline{K} = 0)\, S_{02y}'(\underline{K} = 0)\right) e^{ikd} \\ &= F' a_0 \left(\underline{T}_{10}(\underline{K} = 0) \cdot \underline{S}_{02}'(\underline{K} = 0)\right) e^{ikd} . \end{aligned} \tag{A28}$$

To further generalize the equation, the transmitting coefficient is extended from a complex vector describing a single plane wave to a complex vector function describing a continuous spectrum of plane waves, as shown in figure A10, and will hereafter be referred to as the plane wave transmitting characteristic (PWTC). For each value of $\underline{K}$, $a_0 \underline{T}_{10}(\underline{K})$ completely specifies the amplitude, phase, and polarization of the plane wave propagating in that direction. In a similar way, $\underline{S}_{02}'(\underline{K})$ defines the probe's response to incident plane waves and this parameter will be referred to as the plane wave receiving characteristic (PWRC). The total output signal is now the combination of responses to each plane wave and is expressed mathematically by integrating over all values of k_x and k_y. Hence,

$$b_0' = F' a_0 \iint \underline{T}_{10}(\underline{K}) \cdot \underline{S}_{02}'(\underline{K}) e^{i\gamma d} dk_x dk_y . \tag{A29}$$

Note that the exponential now contains the factor γ rather than k since the phase change will vary with $\underline{K}$ and, although not generally noted explicitly, γ is a function of $\underline{K}$ (see eq A4). If the probe is now translated in the plane z = d to the position $\underline{P} = x\underline{e}_x + y\underline{e}_y$, as shown in figure A11, an additional phase factor $e^{i\underline{K}\cdot\underline{P}}$ will result and the final form for the transmission integral is

$$b_0'(\underline{P}) = F' a_0 \iint \underline{T}_{10}(\underline{K}) \cdot \underline{S}_{02}'(\underline{K}) e^{i\gamma d} e^{i\underline{K}\cdot\underline{P}} dk_x dk_y ; \tag{A30}$$

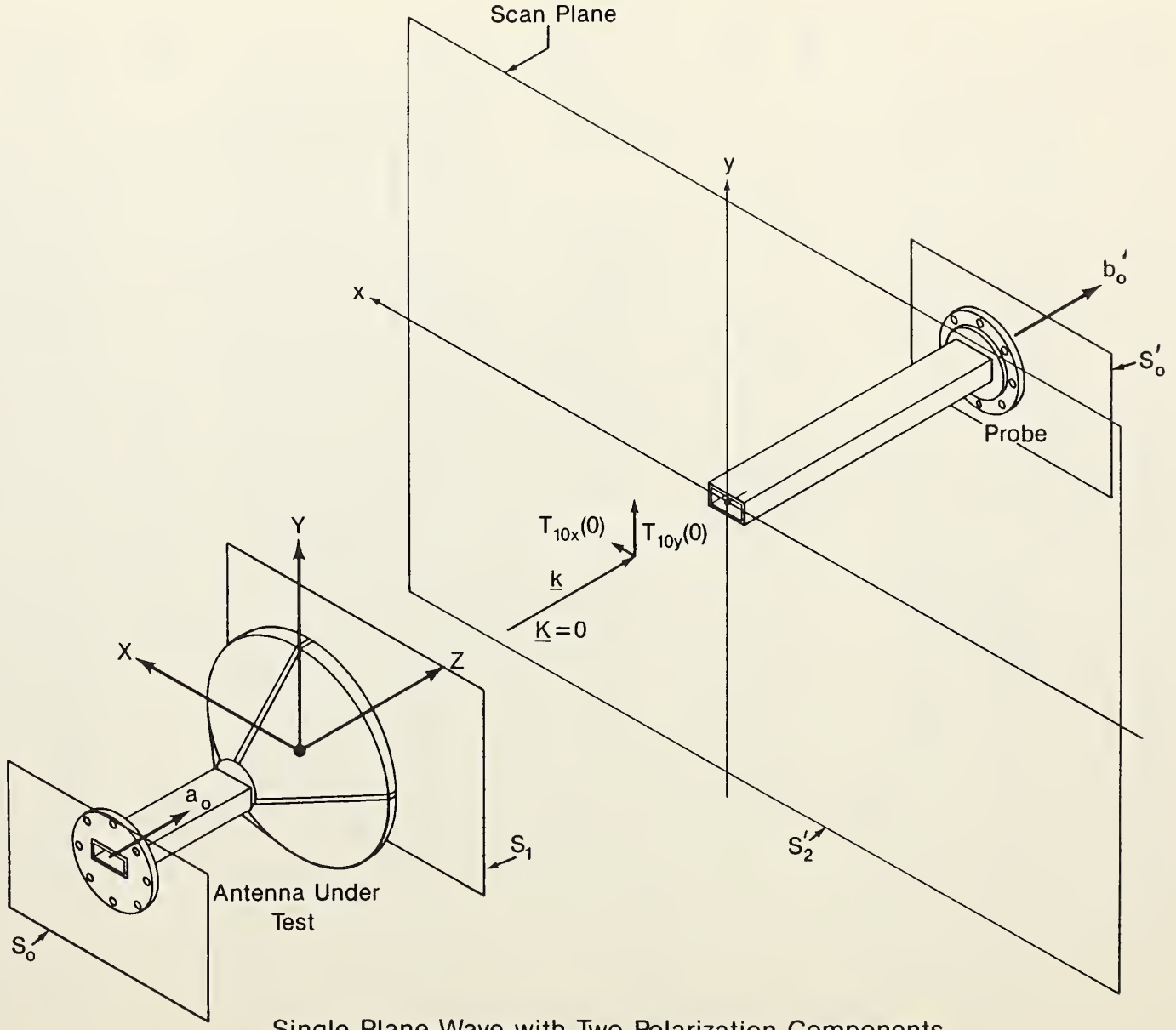

Figure A-9. Plane wave with both main and cross polarization.

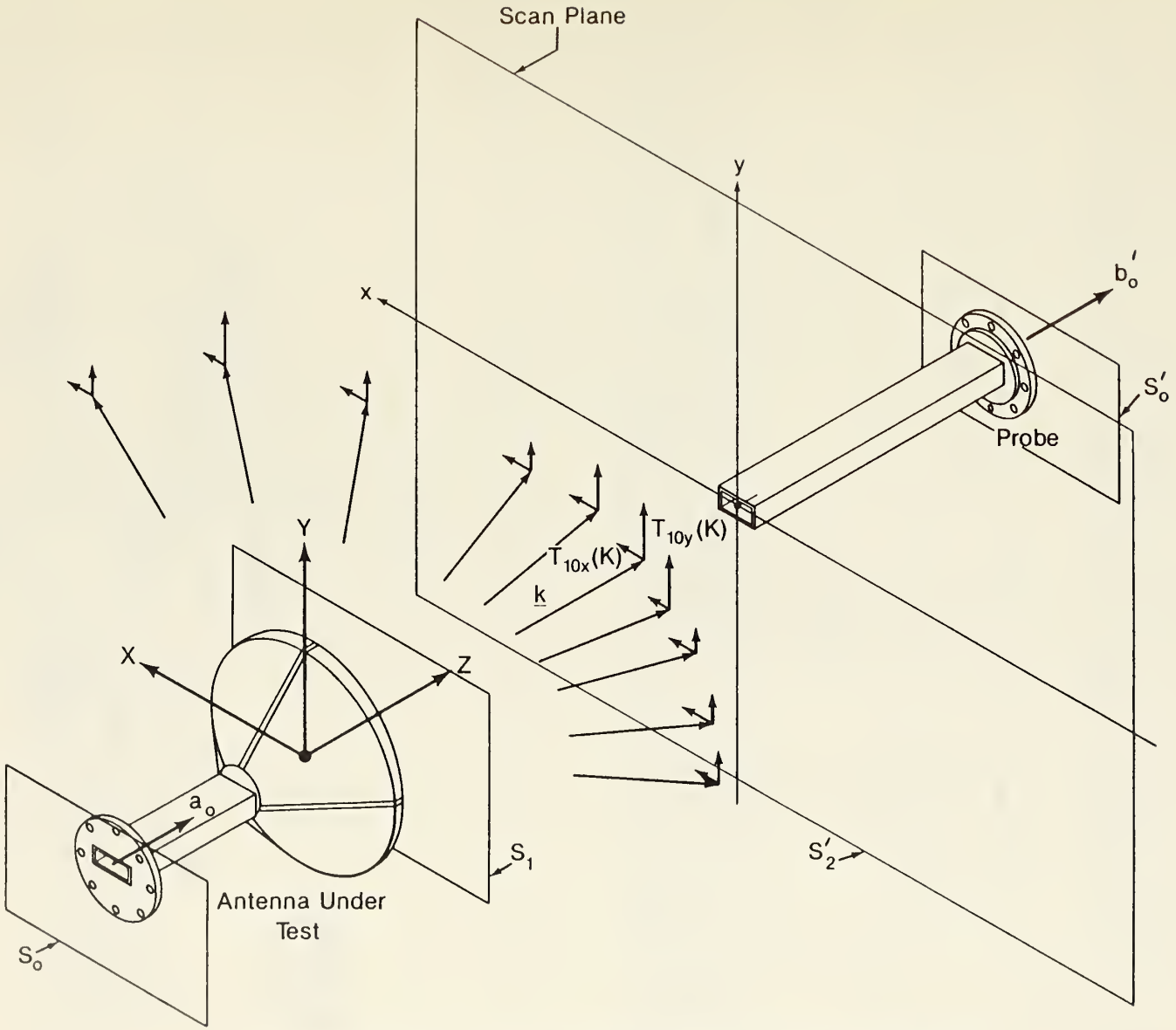

Figure A-10. Angular spectrum of plane waves with varying main and cross polarized components.

or, written in the shorthand notation,

$$b_0'(\underline{P}) = F' a_0 \int \underline{T}_{10}(\underline{K}) \cdot \underline{S}_{02}'(\underline{K}) e^{i\gamma d} e^{i\underline{K}\cdot\underline{P}} d\underline{K} \ . \tag{A31}$$

Although this equation has been developed here by using a specific highly idealized situation, the results are much more general. The only approximation actually required in the derivation is the assumption that multiple reflections between the two antennas are negligible. When this assumption is satisfied, the transmission integral is valid for any antennas with arbitrary pattern and polarization properties and for arbitrary separation distance. It is the basic equation upon which the PNF measurements are based.

In keeping with the development by Kerns, the transmitting and receiving functions $\underline{T}_{10}(\underline{K})$ and $\underline{S}_{02}'(\underline{K})$ used here are the "transverse" vectors; they include only the components transverse to the z-axis. The z-component of the complete transmitting vector, $\underline{t}_{10}(\underline{K})$, can be found from the requirement that the complete vector must be orthogonal to the direction of propagation

$$\underline{t}_{10}(\underline{K}) \cdot \underline{k} = 0 \ . \tag{A32}$$

Since the z-component is redundant, and the theory is used to analyze measurements made in the x-y plane, there is a logical justification, and in some cases a convenience and economy, in developing the theory in terms of the transverse rather than the complete vectors. Kerns uses the transverse vectors almost exclusively in his work and when individual components are specified, they are the x-

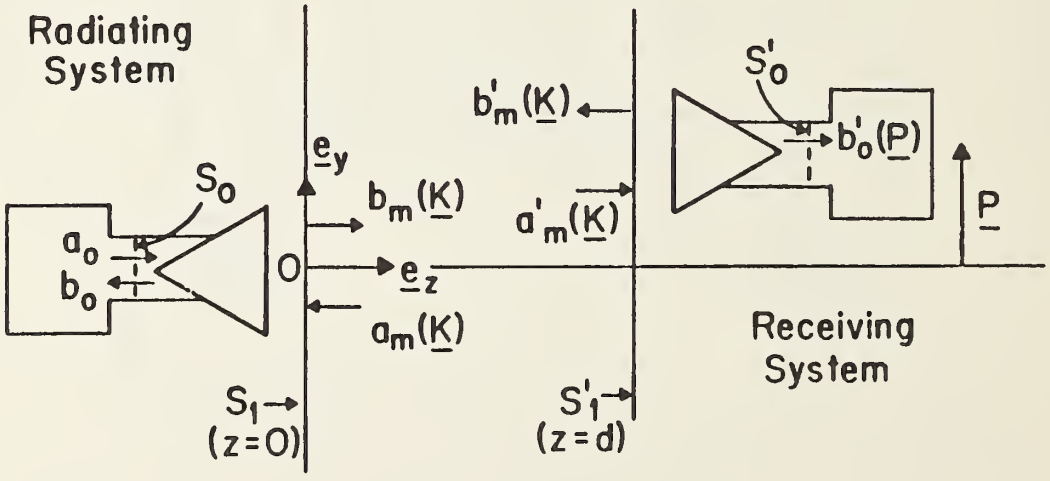

Figure A-11. Translation of probe in measurement plane.

and y-components or $\underline{\kappa}_1$- and $\underline{\kappa}_2$- components. The latter unit vectors are, respectively, in and perpendicular to the plane of $\underline{k}$ and $\underline{e}_z$ where

$$\underline{\kappa}_1 = \underline{K}/K \ , \tag{A33}$$

$$\underline{\kappa}_2 = \underline{e}_z \times \underline{\kappa}_1, \tag{A34}$$

and the notations for the $\underline{\kappa}_1$ and $\underline{\kappa}_2$ components of $\underline{T}_{10}(\underline{K})$ are, respectively, $T_{10}(1,\underline{K})$, $T_{10}(2,\underline{K})$. Where necessary or convenient, Kerns does introduce the complete vectors and uses a notation, also employed here, for denoting the transverse vectors by capital letters and the complete vectors by lower case letters. The use of the transverse vectors has continued in other analyses, but the convention to differentiate between the two has not always been followed; therefore, care must be taken to determine which one is actually being used.

While the transverse vectors are convenient in the development of the theory, it is often preferable to use the complete vectors for practical implementation of the theory, and the latter approach will be used almost exclusively in the following presentation. This choice is made because the desired final result of either near- or far-field measurements is generally the complete electric (or magnetic) field vector or the components orthogonal to $\underline{k}$ rather than the components orthogonal to $\underline{e}_z$. If $\underline{T}_{10}(\underline{K})$ is determined from the near-field measurements and calculations, additional steps are required to calculate its z-component and then obtain either circular or linear components corresponding to main and cross polarizations. These extra steps can be eliminated by employing the complete vectors in the working equations. In addition, there is occasionally a simplification and clarity in the equations which improves understanding.

In order to define the relationship between the complete and transverse vectors we define the unit vectors

$$\underline{e}_k \equiv \underline{k}/k \ , \tag{A35}$$

$$\underline{e}_{||} \equiv \underline{\kappa}_2 \times \underline{e}_k \ , \tag{A36}$$

$$\underline{e}_{\perp} \equiv \underline{\kappa}_2 \ , \tag{A37}$$

and note, that for the propagating region where $K < k$,

$$\underline{e}_{||} = \underline{e}_\theta \qquad \underline{e}_{\perp} = \underline{e}_\phi . \tag{A38}$$

For the propagating region, the relationships between the complete vectors and the transverse components are

$$\underline{t}_{10}(\underline{K}) = \frac{k}{\gamma} T_{10}(1,\underline{K})\ \underline{e}_\theta + T_{10}(2,\underline{K})\ \underline{e}_\phi \ , \tag{A39a}$$

$$\underline{t}_{20}(\underline{K}) = -\frac{k}{\gamma} T_{20}(1,\underline{K})\ \underline{e}_\theta + T_{20}(2,\underline{K})\ \underline{e}_\phi \ , \tag{A39b}$$

$$\underline{s}_{01}(\underline{K}) = -\frac{\gamma}{k} S_{01}(1,\underline{K})\ \underline{e}_\theta + S_{02}(2,\underline{K})\ \underline{e}_\phi \ , \tag{A40a}$$

$$\underline{s}_{02}(\underline{K}) = \frac{\gamma}{k} S_{02}(1,\underline{K})\ \underline{e}_{\theta} + S_{02}(2,\underline{K})\ \underline{e}_{\phi} \ . \tag{A40b}$$

(The subscripts "10" and "20" are discussed following eq (A48).) For the evanescent region where $\underline{e}_{\theta}$ and $\underline{e}_{\phi}$ are not defined, the unit vectors $\underline{e}_{||}$ and $\underline{e}_{\perp}$ should be substituted, respectively, in eqs (A39) - (A40) for $\underline{e}_{\theta}$ and $\underline{e}_{\phi}$.

A number of interesting and important facts related to eqs (A39) and (A40) should be noted. For the transmitting characteristics, the complete vector is transverse to $\underline{k}$,

$$\underline{k} \cdot \underline{t}_{10}(\underline{K}) = 0, \tag{A41}$$

$$\underline{k} \cdot \underline{t}_{20}(\underline{K}) = 0, \tag{A42}$$

the on-axis values of complete and transverse vectors are equal

$$\underline{t}_{10}(0) = \underline{T}_{10}(0), \tag{A43}$$

$$\underline{t}_{20}(0) = \underline{T}_{20}(0),$$

and $\underline{T}_{10}(\underline{K})$ is the projection of $\underline{t}_{10}(\underline{K})$ on the x-y plane.

The complete and transverse receiving characteristics are related in a much different way which, at first, may seem unreasonable. Due to the factor γ/k in eq (A40), the magnitude of the complete vector is less than the magnitude of the transverse vector, i.e.,

$$|\underline{s}_{01}(\underline{K})| \leq |\underline{S}_{01}(\underline{K})| \ , \tag{A45}$$

or, equivalently,

$$\underline{s}_{01}(\underline{K}) \cdot \underline{s}^{*}_{01}(\underline{K}) \leq \underline{S}_{01}(\underline{K}) \cdot \underline{S}^{*}_{01}(\underline{K}) \tag{A46}$$

(the asterisk denotes the complex conjugate).

This is due to the fact that the receiving characteristic does not represent an actual vector field quantity. It represents the antenna's response to two orthogonal polarizations of incident plane waves. The two components of that response, corresponding to the two polarizations, are combined into a "vector" for convenience and conciseness in writing equations. But, as illustrated by eq (A45), it has this non-vector property which must be noted in the transformation between complete and transverse vectors. And, although the terms "complete" and "transverse" are used, $\underline{S}_{01}(\underline{K})$ is not the projection of $\underline{s}_{01}(\underline{K})$ on the x-y plane. However, the relations

$$\underline{s}_{01}(0) = \underline{S}_{01}(0), \tag{A47}$$

$$\underline{k} \cdot \underline{s}_{01}(0) = 0, \tag{A48}$$

do hold and the same is true for $\underline{s}_{02}$.

Some comments are advisable at this point to explain the reason for the use of both "1" and "2" in the subscripts for the spectral coefficients, such as $\underline{t}_{10}$, $\underline{t}_{20}$, $\underline{s}_{01}$, and $\underline{s}_{02}$. This notation is used to distinguish between the plane wave characteristics of the antenna in the right (subscripts 01, 10) and left (subscripts 02, 20) half spaces corresponding respectively to plane waves with $k_z = +\gamma$ and $k_z = -\gamma$. For instance, in the configuration shown in figure A11, the characteristic of the AUT being measured and appearing in eqs (A25) - (A31) is $\underline{T}_{10}(\underline{K})$, and, correspondingly, the pertinent probe receiving characteristic is $\underline{S}'_{02}(\underline{K})$. This is also the case in almost all planar measurements. We are generally not concerned with the back lobes of the AUT, described by $\underline{T}_{20}(\underline{K})$. The right-side receiving characteristic of the probe, $\underline{S}'_{01}(\underline{K})$, does not appear in the transmission integral and, therefore, cannot affect the measurement. In cases where the back lobes are of interest, the AUT can be reoriented and the transmission equation written in terms of $\underline{T}_{20}(\underline{K})$. A concise notation, to be used at appropriate times hereafter, is the subscript "q" in place of the "1" or "2" where equations apply to either value. Table A1 contains a summary of the notation denoting the meaning of the various symbols and subscripts.

Table A1 Notation Summary

Subscripts denote

Transmitting	→ 10,20
Receiving	→ 01,02
Right Side	→ 10,01
Left Side	→ 20,02

Vector Component

$T_{10x}(\underline{K})$ = x-component

$t_{10R}(\underline{K})$ = right circular component

$t_{10A}(\underline{K})$ = azimuthal-component

Capital letters denote transverse vector (x- and y-components or χ_1 and χ_2)

$$\underline{T}_{10}(K) = T_{10x}(\underline{K})\underline{e}_x + T_{10y}(\underline{K})\underline{e}_y$$
$$= T_{10}(1,\underline{K})\underline{\chi}_1 + T_{10}(2,\underline{K})\underline{\chi}_2$$

Small letters denote complete vectors (linear spherical such as θ and ϕ-components, A and E-components or circular R and L-components)

$$\underline{t}_{10}(\underline{K}) = t_{10\theta}(\underline{K})\underline{e}_\theta + t_{10\phi}(\underline{K})\underline{e}_\phi$$
$$= t_{10A}(\underline{K})\underline{e}_A + t_{10E}(\underline{K})\underline{e}_E$$
$$= t_{10R}(\underline{K})\underline{e}_R + t_{10L}(\underline{K})\underline{e}_L$$

Different letters or primes are used to denote plane-wave parameters for different antennas

$\underline{s}'_{02}(K)$, $\underline{s}''_{02}(K)$

"t" is typically used for the antenna under test, and "s" for the probe

Returning to the transmission integral, and noting from eqs (A39) and (A40) that

$$\underline{t}_{10}(\underline{K}) \cdot \underline{s}'_{02}(\underline{K}) = \underline{T}_{10}(\underline{K}) \cdot \underline{S}'_{02}(\underline{K}), \tag{A49}$$

we see that eq (A31) can be written in terms of the complete vectors as

$$b'_0(\underline{P}) = F' a_0 \int \underline{t}_{10}(\underline{K}) \cdot \underline{s}'_{02}(\underline{K})\, e^{i\gamma d}\, e^{i\underline{K}\cdot\underline{P}}\, d\underline{K}\,, \tag{A50}$$

and this becomes the final form for the transmission integral. Since the object of the measurements is the properties of the AUT, a solution of eq (A50) is required in terms of the measured data $b'_0(\underline{P})$ and the probe's PWRC $\underline{s}'_{02}(\underline{K})$. The first step in this solution uses the fact that eq (A50) is a Fourier transform relation. If we denote the coupling product as

$$D'(\underline{K}) = \underline{t}_{10}(\underline{K}) \cdot \underline{s}'_{02}(\underline{K})\,, \tag{A51}$$

the Fourier inverse is

$$D'(\underline{K}) = \frac{e^{-i\gamma d}}{4\pi^2 F'} \int \frac{b'_0(\underline{P})}{a_0}\, e^{-i\underline{K}\cdot\underline{P}}\, d\underline{P}\,. \tag{A52}$$

In actual measurements, the ratio $b'_0(\underline{P})/a_0$ is generally obtained in two steps. First, a reference point $\underline{P}_0$ is chosen which is at or near the maximum amplitude of $b'_0(\underline{P})$. Relative near-field data are then obtained with respect to the probe output at this point and denoted by

$$B'_0(\underline{P}) = \frac{b'_0(\underline{P})}{b'_0(\underline{P})}. \tag{A53}$$

A normalization constant A' is then measured, which is the ratio of the AUT input to the probe output with the probe at $\underline{P}_0$. In terms of these parameters eq (A52) becomes

$$D'(\underline{K}) = \frac{e^{-i\gamma d}}{4\pi^2 F' A'} \int B'_0(\underline{P})\, e^{-i\underline{K}\cdot\underline{P}}\, d\underline{P}\,, \tag{A54}$$

where

$$A' = \frac{a_0}{b'_0(\underline{P})}\,. \tag{A55}$$

Equation (A51) provides one equation for the two unknown components of $\underline{t}_{10}(\underline{K})$. A second equation is obtained by using another probe with a suitable PWRC $\underline{s}''_{02}(\underline{K})$ which produces measured data $B''_0(\underline{P})$, normalization constant A", and calculated plane wave spectrum

$$D''(\underline{K}) = \frac{e^{-i\gamma d}}{4\pi^2 F' A''} \int B''_0(\underline{P})\, e^{-i\underline{K}\cdot\underline{P}}\, d\underline{P}. \tag{A56}$$

The two equations to be solved for $\underline{t}_{10}(\underline{K})$ are, therefore,

$$D'(\underline{K}) = \underline{t}_{10}(\underline{K}) \cdot \underline{s}'_{02}(\underline{K})\,, \tag{A57a}$$

$$D''(\underline{K}) = \underline{t}_{10}(\underline{K}) \cdot \underline{s}''_{02}(\underline{K})\,. \tag{A57b}$$

An explicit solution of eq (A57) requires a choice of orthogonal unit vectors such as $\underline{e}_A$, $\underline{e}_E$; $\underline{e}_\theta$, $\underline{e}_\phi$; etc. to be used in the expansion of the dot product in eq (A57). Rather than choose a specific set at

this time, let us denote two general orthogonal unit vectors by $\underline{e}_m$ and $\underline{e}_c$, which have the connotation of representing the main and cross-component fields of the AUT. Expanding eq (A57) in terms of these components, and solving for $t_{10m}(\underline{K})$ and $t_{10c}(\underline{K})$, gives

$$t_m = \frac{D's_c'' - D''s_c'}{s_m's_c'' - s_c's_m''} , \tag{A58a}$$

$$t_c = \frac{D''s_m' - D's_m''}{s_m's_c'' - s_c's_m''} , \tag{A58b}$$

where the abbreviations $t_m = t_{10m}(\underline{K})$, $t_c = t_{10c}(\underline{K})$, $s_m' = s_{02m}'(\underline{K})$, $s_m'' = s_{02m}''(\underline{K})$, etc. have been employed for brevity. As a general rule the probes are chosen such that the first one couples primarily to the main component and the second couples primarily to the cross component. An exception to this is when linear probes are used to measure a circularly polarized antenna, or vice versa. However, in either case,

$$|s_m'| > |s_c'| , \qquad |s_c''| > |s_m''| , \tag{A59}$$

and the solution is then written

$$t_m = \frac{\frac{D'}{s_m'} - \frac{D''}{s_c''}\rho_s'}{1 - \rho_s'/\rho_s''} \tag{A60}$$

$$t_c = \frac{\frac{D''}{s_c''} - \frac{D'}{s_m'}\rho_s''}{1 - \rho_s'/\rho_s''} . \tag{A61}$$

where the receiving polarization ratios are

$$\rho_s'(\underline{K}) = s_{02c}'(\underline{K})/s_{02m}'(K) , \tag{A62}$$

$$\rho_s''(\underline{K}) = s_{02c}''(\underline{K})/s_{02m}''(\underline{K}) . \tag{A63}$$

It is apparent that the PWRC's of the two probes must be linearly independent to give independent equations in (A57). From eqs (A60) and (A61), the essential requirement is that

$$\rho_s'(\underline{K}) \neq \rho_s''(\underline{K}) , \tag{A64}$$

where the dependence upon $\underline{K}$ has been made explicit to emphasize that this condition must hold for every direction where $\underline{t}_{10}(\underline{K})$ is desired. The linear independence requirement does not demand that the probes be orthogonally polarized in every direction, although this would be the best arrangement. Nor does it prohibit the use of circularly polarized probes; for if the first probe is nominally right-hand circular, and the second nominally left-hand circular, or vise versa, eq (A64) is satisfied.

In many cases, instead of using two distinct probes, a single probe with nominal linear polarization is used. The "second" one is obtained by rotating the probe about its z-axis by 90°. This approach has the advantages that only one probe measurement is required; $\underline{s}_{02}'(\underline{K})$ and $\underline{s}_{02}''(\underline{K})$ are obtained from the same measured data, and certain normalizations and phase measurements are simplified.

The transmission equation and probe correction have been obtained for the case of a transmitting test antenna and receiving probe. The inverse arrangement is also possible where the probe is

transmitting and the receiving characteristics of the AUT are obtained. In this case, the transmission equation becomes

$$b_0(\underline{P}) = F\, a_0' \int \underline{t}_{01}(\underline{K}) \cdot \underline{s}_{20}'(\underline{K})\, e^{-i\gamma d} e^{-i\underline{K}\cdot\underline{P}}\, d\underline{K} \tag{A65}$$

where

$$F = 1/(1 - \Gamma_1\Gamma_a), \tag{A66}$$

Γ_a is the reflection coefficient of the AUT and a_0' is the input amplitude to the probe. The measurements and calculations follow in a parallel way to the case of a transmitting test antenna.

Now that the PWTC has been obtained, equations are desirable to relate it both to receiving properties and to more conventional antenna parameters. If the antenna is reciprocal, $\underline{t}_{qo}$ and $\underline{t}_{oq}$ are related by the reciprocity equation

$$\underline{t}_{oq}(\underline{K}) = \frac{y_0\gamma\, \underline{t}_{qo}(-\underline{K})}{n_0 k} . \tag{A67}$$

The total power gain, receiving effective area, and asymptotic far-electric field are, respectively,

$$G_q(\underline{K}) = \frac{4\pi y_0 \gamma^2 \left|\underline{t}_{q0}(\underline{K})\right|^2}{n_0(1 - |\Gamma_a|^2)} \tag{A68}$$

$$\sigma_q(\underline{K}) = \frac{4\pi^2 n_0 \left|\underline{t}_{oq}(\underline{K})\right|^2}{y_0(1 - |\Gamma_a|^2)} \tag{A69}$$

$$\underline{E}_q(\underline{r}) \sim i\gamma\, \underline{t}_{qo}(\underline{R}k/r) a_0 e^{ikr}/r . \tag{A70}$$

In the above relations, $y_0 = \sqrt{\varepsilon/\mu}$ is the plane wave admittance in the transmission medium, n_0 is the characteristic admittance for propagated waves in the transmission line connected to the antennas, Γ_a is the antennas' reflection coefficient, and $\underline{r}$ is the position vector with transverse part $\underline{R}$,

$$\underline{r} = \underline{R} + z\underline{e}_z . \tag{A71}$$

In measurement-related calculations, it is seldom, if ever, necessary to utilize the admittance factors n_0 and y_0, explicitly. They generally cancel out in final results; and, since a flexible normalization is employed (Kerns, 1981, p. 52), it is also possible to arbitrarily choose $n_0 = y_0$. The only situation where explicit values must be used is when the transmission lines on the AUT and probe are different.

The above relations in eqs (A67) - (A70) are written for the test antennas coefficients $\underline{t}_{10}(\underline{K})$, but the same equations are true for the probe and are valid if "t" is replaced by "s". When writing general relations such as eqs (A67) - (A70) and (A78) - (A92) that are true for any antenna, the "t" will be used but the equations are valid for any antenna and the symbol denoting that antenna can be substituted for the "t" where appropriate.

We conclude this section with a discussion of circularly-polarized parameters, which are often useful alternatives to the linear components. The circular basis vectors are defined in terms of the general linear unit vectors ($\underline{e}_1$, $\underline{e}_2$). In this use, ($\underline{e}_1$, $\underline{e}_2$) are any pair of unit vectors orthogonal to $\underline{k}$ such that ($\underline{e}_1$, $\underline{e}_2$, $\underline{e}_k$) are a right-handed triad. In particular,

$$\underline{e}_1 = \underline{e}_\theta, \underline{e}_\alpha, \underline{e}_A, \underline{e}_h; \tag{A72}$$

$$\underline{e}_2 = \underline{e}_\phi, \underline{e}_\varepsilon, \underline{e}_E, e_v; \tag{A73}$$

and the circular basis vectors are

$$\underline{e}_R = (\underline{e}_1 + i\underline{e}_2)/\sqrt{2}\ , \tag{A74}$$

$$\underline{e}_L = (\underline{e}_1 + \underline{e}_2)/\sqrt{2}\ , \tag{A75}$$

Then

$$\underline{V}_R = \underline{e}_R\, e^{i(kr - \omega t)} \tag{A76}$$

and

$$\underline{V}_L = \underline{e}_L\, e^{i(kr - \omega t)} \tag{A77}$$

represent, respectively, right and left circularly-polarized plane waves traveling in the outward radial direction and the complete PWTC in terms of circular components is

$$\underline{t}_{qo}(\underline{K}) = t_{qoR}(\underline{K})\ \underline{e}_R + t_{qoL}(\underline{K})\ \underline{e}_L\ . \tag{A78}$$

The transformations between linear and circular components are then,

$$t_{qoR}(\underline{K}) = (t_{q01}(\underline{K}) - it_{q02}(\underline{K}))/\sqrt{2} \tag{A79}$$

$$t_{qoL}(\underline{K}) = (t_{q01}(\underline{K}) + it_{q02}(\underline{K}))/\sqrt{2}, \tag{A80}$$

$$t_{q01}(\underline{K}) = (t_{qoR}(\underline{K}) + t_{qoL}(\underline{K}))/\sqrt{2}, \tag{A81}$$

$$t_{q02}(\underline{K}) = i(t_{qoR}(\underline{K}) - t_{qoL}(\underline{K}))/\sqrt{2}, \tag{A82}$$

where the third subscript denotes the component. Transmitting polarization ratios are defined for linear and circular components, respectively, as

$$p_{t\ell}(\underline{K}) = t_{q01}(\underline{K})/t_{q02}(\underline{K}) = -i\left(\frac{1 + p_{tc}(\underline{K})}{1 - p_{tc}(\underline{K})}\right), \tag{A83}$$

$$p_{tc}(\underline{K}) = \frac{t_{qoL}(\underline{K})}{t_{qoR}(\underline{K})} = \frac{p_{t\ell}(\underline{K}) + i}{p_{t\ell}(\underline{K}) - i}. \tag{A84}$$

While these complex polarization ratios are very useful in calculations involving polarization mismatch, more conventional parameters, such as axial ratio and tilt angle, are also required. In terms of the polarization ratios, these are

$$AR\ (\underline{K}) \equiv \frac{|t_{qoR}(\underline{K})| + |t_{qoL}(\underline{K})|}{|t_{qoR}(\underline{K})| - |t_{qoL}(\underline{K})|} = \frac{1 + |p_{tc}(\underline{K})|}{1 - |p_{tc}(\underline{K})|}\ , \tag{A85}$$

$$\tau(\underline{K}) = 1/2\ \arg\ (P_{tc}(\underline{K})). \tag{A86}$$

The circular polarization components of the PWTC are defined to correspond to the polarization of the transmitted waves, in accordance with the IEEE definitions [A3]. The receiving parameters, $\underline{s}'_{oq}$, however, are defined in terms of the antennas response to incident plane waves. s'_{oqR} should, therefore, couple only to an incident right circularly-polarized wave and, similarly, s'_{oqL} should couple only to one of left circular polarization. This implies that the coupling product, eq (A51), should be written

$$D'(\underline{K}) = t_{10R}(\underline{K})s'_{02R}(\underline{K}) + t_{10L}(\underline{K})s'_{02L}(\underline{K}) \ . \tag{A87}$$

This consistent choice for the coupling product requires that

$$s'_{oqR}(\underline{K}) = (s'_{oq1}(\underline{K}) + is'_{oq2}(\underline{K}))/2, \tag{A88}$$

$$s'_{oqL}(\underline{K}) = (s'_{oq1}(\underline{K}) - is'_{oq2}(\underline{K}))/\sqrt{2} \ , \tag{A89}$$

$$s'_{oq1}(\underline{K}) = (s'_{oqR}(\underline{K}) + s'_{oqL}(\underline{K}))/\sqrt{2} \ , \tag{A90}$$

$$s'_{oq2}(\underline{K}) = -i(s'_{oqR}(\underline{K}) - s'_{oqL}(\underline{K}))/\sqrt{2} \ . \tag{A91}$$

The resulting differences between eqs (A79) - (A82) and eqs (A88) - (A91) imply that the receiving basis vectors are complex conjugates of the transmitting ones, i.e.,

$$\underline{s}'_{oq}(\underline{K}) = s_{oqR}(\underline{K})\ \underline{e}^{*}_{R} + s_{oqL}(\underline{K})\ \underline{e}^{*}_{L} \ . \tag{A92}$$

The only assumptions involved in the development of the equations in this section other than the usual ones of linearity, superposition, etc., are:

1. There is no scattering from the probe, the scanner, or the room to produce extraneous signals at the probe.
2. Measurements extend over an infinite area.
3. The measured spectrum is band limited and data are measured at increments equal to or smaller than specified by the sampling theorem.

Since each of the above three assumptions are evaluated and considered in the error analysis, the working equations can be considered to be exact and the sources of error are then due to uncertainties in measured data.

References

[A1] Kerns, D.M. Plane-wave scattering-matrix theory of antennas and antenna-antenna interactions. Nat. Bur. Stand. (U.S.) Monograph 162; 1981 June.

[A2] Johnson, R.C.; Ecker, H.A.; Hollis, J.S. Determination of far-field antenna patterns from near-field measurements. Proc., IEEE 61; 1973 December. p. 1668-1694.

[A3] IEEE Standard 145-1983 Definitions of Terms for Antennas. The Institute of Electrical and Electronics Engineers, Inc. New York.

APPENDIX B
Cylindrical Near-Field Theory Summary

Just as in the planar theory, we begin here by defining reference and probe coordinates. In this case, there are actually three coordinate systems, as shown in figure B1. The reference system C_o is fixed relative to the test antenna, with its origin at the center of the measurement cylinder [B1] and the coordinates and components of the results will be defined with respect to this coordinate system. The probe cylindrical system C_1 is fixed to the probe with its origin at the end of the probe and the z_1-axis parallel to z_o. The auxiliary probe coordinates are also fixed to the probe, but the origin of the C_o' system is along the z_o-axis, as shown in figure B1, displaced a distance z_o along this axis and rotated by the angle ϕ_o about the z_o-axis. The transmitting properties of the test antenna, relative to C_o, for the given orientation, is denoted by $T_n^s(\gamma)$. The polarization index "s" takes on the values 1 and 2 which corresponds respectively to ϕ_o- and θ_o-components. For each component, the complex value of $T_n(\gamma)$ defines the amplitude and phase of the cylindrical wave with z-component of $\underline{k}$ equal to γ and mode index n. Once $T_n^s(\gamma)$ has been determined, the far-field parameters are easily obtained from the relations,

$$\underline{V}_{r\to\infty}(r_o, \phi_o, \theta_o) = -2k \sin\theta \frac{a_o e^{ikr}}{r} \sum_{n=-\infty}^{\infty} (-i)^n \left[T_n^1(\gamma)\, \underline{e}_{\phi_o} - iT_n^2(\gamma)\, \underline{e}_{\theta_o}\right] e^{in\phi} \tag{B1}$$

$$G(\theta_o, \phi_o) = \frac{16\pi k^2 \sin^2\theta}{Z_o \eta_o \left(1 - |\Gamma_a|^2\right)} \left| \sum_{-\infty}^{\infty} (-i)^n\, T_n^1(\gamma)\, e^{in\phi} \right|^2 + \left| \sum_{-\infty}^{\infty} (-i)^n\, T_n^2(\gamma)\, e^{in\phi} \right|^2 \tag{B2}$$

$$\rho(\theta_o, \phi_o) = \frac{V_\phi(\theta_o, \phi_o)}{V_\theta(\theta_o, \phi_o)} = \frac{i \sum_{-\infty}^{\infty} (-i)^n T_n^1(\gamma)\, e^{in\phi}}{\sum_{-\infty}^{\infty} (-i)^n T_n^2(\gamma)\, e^{in\phi}} \tag{B3}$$

respectively for electric field, power gain, and polarization ratio, when $\gamma = k\cos\theta$.

In a similar way, the cylindrical-mode receiving coefficients of the probe relative to C_o' are denoted by $R_n'^s(\gamma)$, where s, n, and γ are the same as for the test antenna transmitting coefficients $T_n^s(\gamma)$. The prime on the R denotes that these are coefficients with respect to the auxiliary probe coordinates. The transmission formula is then given by the equation,

$$B_o'(\phi_o, z_o) = \frac{b_o'(\phi_o, z_o)}{b_o'(\phi_m, z_m)} =$$

$$\frac{a_o}{b_o'(\phi_m, z_m)\left(1 - \Gamma_\ell \Gamma_p\right)} = \sum_{n=-\infty}^{\infty} \int_{-\infty}^{\infty} \left[\sum_{s=1}^{2} R_n'^s(\gamma)\, T_n^s(\gamma)\right] e^{in\phi_o} e^{i\gamma z_o}\, d\gamma \,. \tag{B4}$$

As in the planar case, two independent measurements with different probes are, in general, required to obtain the two polarization components of $T_n(\gamma)$. The second probe's coefficients are denoted by $R_n''^s(\gamma)$ and the second transmission equation is

$$B_o''(\phi_o, z_o) = \frac{b_o''(\phi_o, z_o)}{b_o''(\phi_n, z_n)} = \tag{B5}$$

$$\frac{a_o}{b_o''(\phi_n, z_n)\left(1 - \Gamma_\ell \Gamma_p\right)} \sum_{n=-\infty}^{\infty} \int_{-\infty}^{\infty} \left[\sum_{s=1}^{2} R_n''^s(\gamma)\, T_n^s(\gamma)\right] e^{in\phi_o} e^{i\gamma z_o}\, d\gamma \,.$$

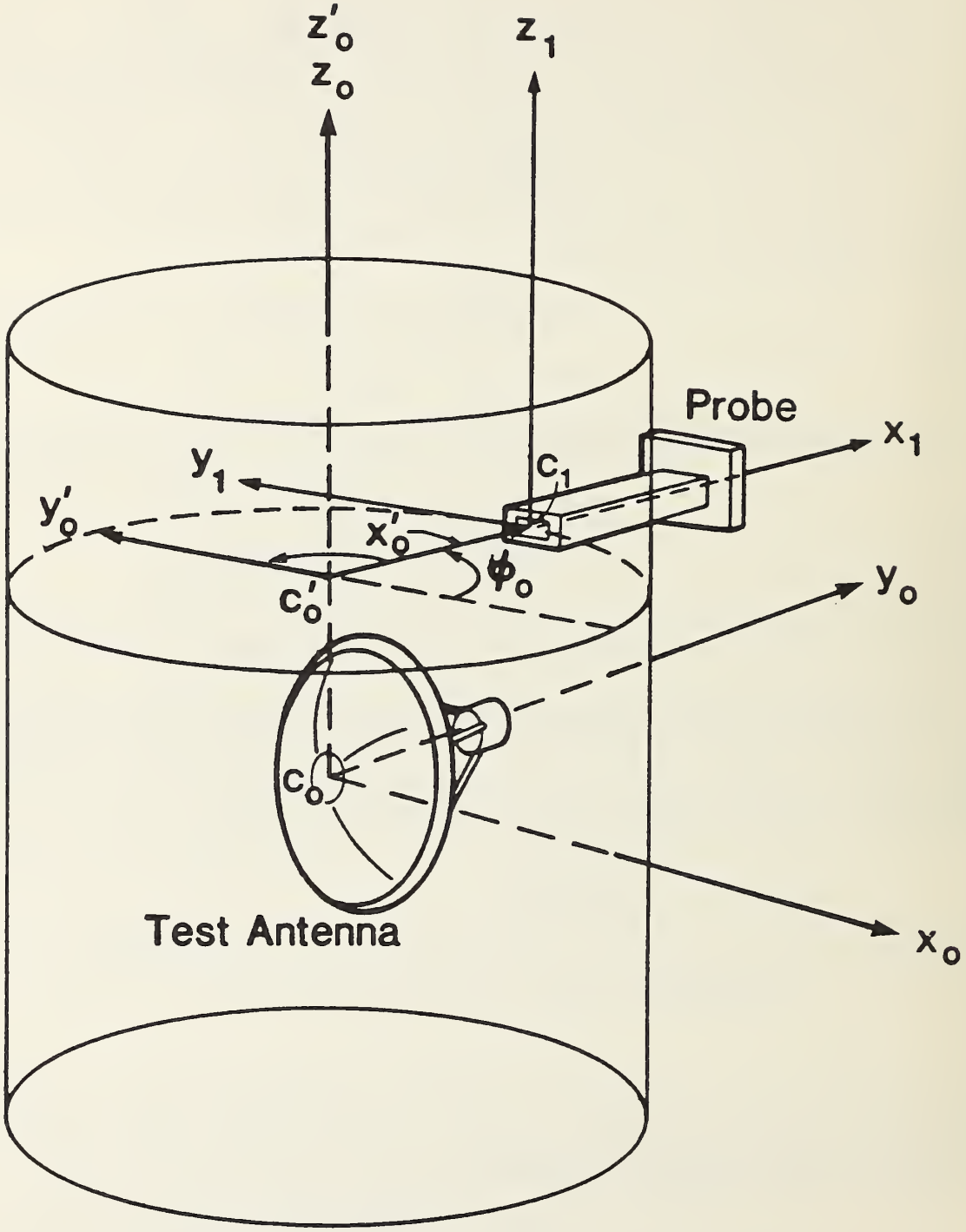

Figure B-1. Three coordinate systems referred to in cylindrical measurements.

In eqs (40) and (41) the two normalization points are (ϕ_m, z_m) and (ϕ_n, z_n) and the measurements include the relative data B'_o, B''_o, and the normalization constants

$$A_m = \frac{b'_o(\phi_m, z_m)}{a_o}, \qquad A_n = \frac{b''_o(\phi_n, z_n)}{a_o}$$

The first step in the solution for the T's is to invert the transmission equations by noting that eqs (40) and (41) involve a Fourier series in ϕ_o and Fourier integral in z_o. The inverse is easily obtained to give the coupling products within the brackets

$$I'_n(\gamma) = \sum_{s=1}^{2} R_n'^s(\gamma)\, T_n^s(\gamma)$$

$$= \frac{(1 - \Gamma_\ell \Gamma_\rho)\, A_m}{4\pi^2} \int_{-\infty}^{\infty} \int_{o}^{2\pi} B'_o(\phi_o, z_o)\, e^{-in\phi_o}\, e^{-i\gamma z_o}\, d\phi_o dz_o, \tag{B6}$$

$$I''_n(\gamma) = \sum_{s=1}^{2} R_n''^s(\gamma)\, T_n^s(\gamma)$$

$$= \frac{(1 - \Gamma_\ell \Gamma_\rho)\, A_n}{4\pi^2} \int_{-\infty}^{\infty} \int_{o}^{2\pi} B''_o(\phi_o, z_o)\, e^{-in d_o}\, e^{-i\gamma z_o}\, d\phi_o\, dz_o. \tag{B7}$$

Assuming that the receiving parameters $(R_n'^s, R_n''^s)$ are known, eqs (42) and (43) can be solved from the transmitting functions $T_n^s(\gamma)$ of the test antenna:

$$T_n^1(\gamma) = [R_n''^2(\gamma)\, I'_n(\gamma) - R_n'^2(\gamma)\, I''_n(\gamma)]/\Delta_n(\gamma) \tag{B8a}$$

$$T_n^2(\gamma) = [R_n'^1(\gamma)\, I''_n(\gamma) - R_n''^1(\gamma)\, I'_n(\gamma)]/\Delta_n(\gamma), \tag{B8b}$$

where

$$\Delta_n(\gamma) = R_n''^2(\gamma)\, R_n'^1(\gamma) - R_n'^2(\gamma)\, R_n''^1(\gamma). \tag{B9}$$

Dividing numerators and denominators of eq (B7) by the product $(-R_n'^2(\gamma)\, R_n''^1(\gamma))$ puts the above probe correction equations in a form more parallel to those for planar measurements (see eqs (A60) and (A61).

$$T_n^1(\gamma) = \frac{\dfrac{I''_n(\gamma)}{R_n''^1(\gamma)} - \dfrac{I'_n(\gamma)}{R_n'^2(\gamma)\, \rho''_n(\gamma)}}{1 - \rho'_n(\gamma)/\rho''_n(\gamma)} \tag{B10a}$$

$$T_n^2(\gamma) = \frac{\dfrac{I'_n(\gamma)}{R_n'^2(\gamma)} - \dfrac{I_n(\gamma)}{R_n''^1(\gamma)}\, \rho'_n(\gamma)}{1 - \rho'_n(\gamma)/\rho''_n(\gamma)} \tag{B10b}$$

In the above equations, the ρ's are cylindrical mode polarization ratios,

$$\rho'_n(\gamma) = \frac{R'^1_n(\gamma)}{R'^2_n(\gamma)} \tag{B11}$$

$$\rho''_n(\gamma) = \frac{R''^1_n(\gamma)}{R''^2_n(\gamma)} . \tag{B12}$$

The steps in the cylindrical near-field measurements and calculations are then:

1. Measure the far-field pattern, polarization and gain of the probe relative to its own coordinate system.
2. For the specified orientation in the coordinate system calculate the probe parameters $R'^s_n(\gamma)$ and $R''^s_n(\gamma)$.
3. Place the antenna in a known orientation in the reference coordinate system C_o.
4. Measure the relative near-field data and normalization constants $B'_o(\phi_o, z_o)$, $B''_o(\phi_o, z_o)$, $A_n(\phi_n, z_n)$, $A_m(\phi_m, z_m)$ with two independent probes or two orientations of a linearly polarized probe.
5. Calculate the coupling product coefficients for the measured data, $I'_n(\gamma)$ and $I''_n(\gamma)$ and apply the probe correction to obtain the cylindrical mode coefficients for both polarizations, $T^1_n(\gamma)$ and $T^2_n(\gamma)$.
6. From the cylindrical modes, calculate the far-field parameters.

References

[B1] Yaghjian, A.D. Near-field measurements on a cylindrical surface: A source scattering-matrix formulation. Nat. Bur. Stand. (U.S.) Tech. Note 696; 1977 September.

APPENDIX C
Spherical Near-Field Theory Summary

For spherical near-field measurements, a probe is used whose pattern is symmetrical about its axis (z-axis). Far-field pattern measurements are obtained for the probe, and the data are fitted with a spherical mode expansion.

$$\underline{W}(\theta,\phi) = \sum_{\sigma,\mu,\nu} Q^{\sigma\mu\nu}\, \underline{F}^{\sigma\mu\nu}(\theta,\phi) \tag{C1}$$

where $\underline{W}(\theta,\phi)$ is the complex vector far-field pattern, $\underline{F}^{\sigma\mu\nu}(\theta,\phi)$ are vector spherical wave functions, and $Q^{\sigma\mu\nu}$ is the spherical mode expansion for the probe. The polarization index σ assumes the values 1 and 2 corresponding to TE and TM modes; the μ index expresses the dependence on the azimuthal angle Q; and the ν index refers to the θ or polar angle dependence. When the Q's for the probe have been obtained, reciprocity is generally employed to find the spherical mode receiving coefficients denoted as $\underline{p}^{\sigma\mu\nu}$. Both the $\underline{p}$'s and Q's for the probe at this point are defined with respect to the coordinate system of the probe. For probes with the assumed ϕ-symmetry, only those modes for which $\mu = \pm 1$ are nonzero. Furthermore, when the probe is small it will have relatively few ν values that are nonzero. An ideal dipole, for instance, would have only $\nu = 1$ as a nonzero $\underline{p}$ or Q.

The next step in the data processing is referred to as the translation of centers. In this procedure, the probe coefficients are determined with respect to the coordinate system of the AUT at a radius A from the origin by the relation

$$p^{s\mu nA} = \sum_{\sigma,\nu} C^{sn}_{\sigma\mu\nu}(A)\, \underline{p}^{\sigma\mu\nu}. \tag{C2}$$

In the above, $p^{s\mu nA}$ denotes the translated coefficients; s and n relate respectively for polarization and θ just as σ and ν did; and the translation coefficients $C^{sn}_{\sigma\mu\nu}(A)$ are obtained by complex involved recursion relations [1].

The spherical coupling equation for the measurement shown schematically in figure C1 and corresponding to similar expressions for planar and cylindrical methods (see eqs (A50) and (B4)) is then given by [C2,C3]

$$B^{A}(\chi_0,\theta_0,\phi_0) = \sum_{s,m,n} Q^{smn} \sum_{\mu} p^{s\mu nA} e^{-im\phi_0}\, d^{(n)}_{\mu m}(\theta_0)\, e^{i\mu\chi_0} \tag{C3}$$

The Q's in eq (C3) are the spherical mode coefficients for the AUT and correspond to the planar $\underline{t}_{10}(\underline{K})$ and cylindrical $T^{s}_{n}(\nu)$ coefficients. The Q's are similarly the objective of the measurement process.

Equation (3) can be inverted by using the orthogonality relation

$$\frac{1}{8\pi^2} \int_0^{2\pi}\int_0^{\pi}\int_0^{2\pi} B^{A}(\phi_0,\theta_0,\chi_0)\, D^{(n')}_{m'\mu'}(\phi_0,\theta_0,\chi_0)\, \sin\theta_0 \phi_0 \theta_0 \chi_0$$

$$= (Q^{1m'n} p^{1\mu'n'A} + Q^{2m'n'} p^{2\mu'n'A})/(2n+1). \tag{C4}$$

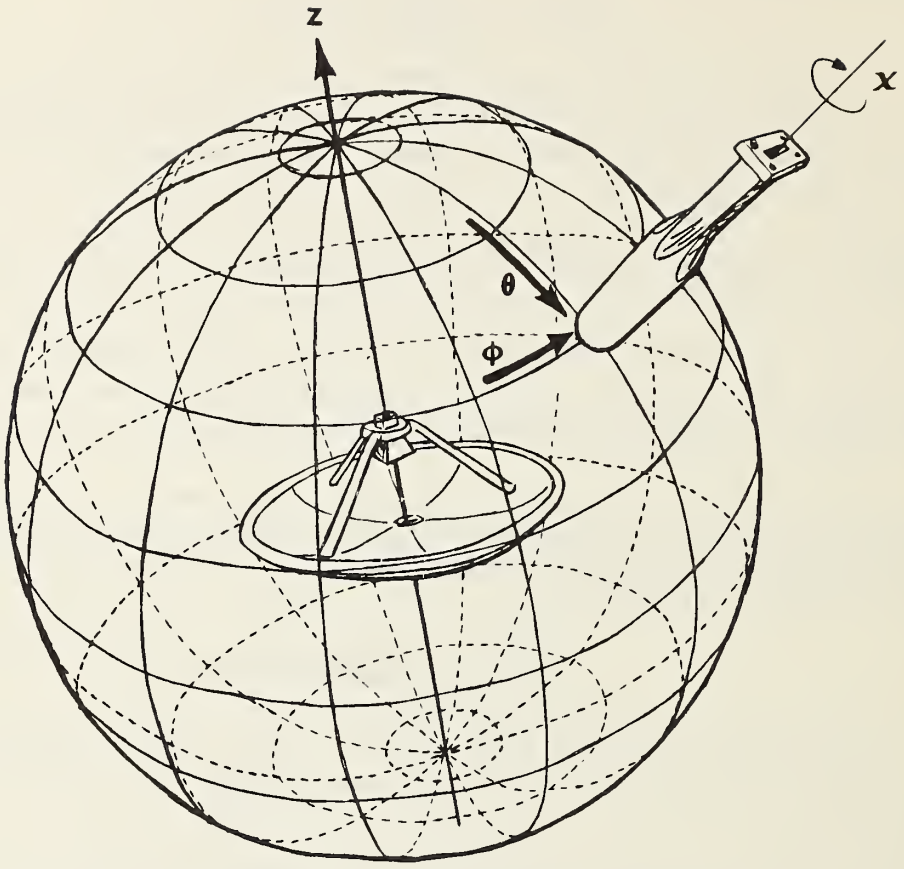

$$W^{A}(\chi,\theta,\phi) = \sum_{m,n,\mu,s} (P^{s\mu nA}\ Q^{smn})\ \underbrace{e^{im\phi} d^{(n)}_{m\mu}(\theta)\ e^{i\mu\chi}}$$

PROBE RECEIVING COEFFICIENTS WITH RESPECT TO oxyz

FACTORS DUE TO PROBE MOTION ON SURFACE OF SPHERE

ANT TRANSMITTING COEFFICIENTS WITH RESPECT TO oxyz

A = RADIUS OF SPHERE

s = POLARIZATION INDEX

Figure C-1. Spherical scanning schematic.

Equation (C4) implies the need for numerical integration of the measured data in χ_0, ϕ_0, and θ_0. The integration in χ_0 is reduced to a sum of two data sets by the properties of the symmetrical probe. Since all of the p's are zero except for those with $\mu = \pm 1$, data are obtained for $\chi_0 = 0$ denoted $B^A(0,\theta_0,\phi_0)$ and $\chi = \pi/2$ denoted $B^A(\pi/2,\theta_0\phi_0)$. Combining these data sets accomplishes the integration in χ_0. Integration in ϕ_0 is accomplished with the FFT making that process accurate and efficient.

Numerical integration in θ would be time consuming and possibly subject to errors. Wacker, who also proposed the use of the symmetric probe to accomplish the χ integration, developed an efficient algorithm for accomplishing the θ-integration as well. This involves a combination of FFTs and matrix multiplication which give accurate results and good efficiency [C3]. This algorithm was further implemented, developed and improved [C4,C5], and is the basis for all spherical near-field data processing.

Once the model coefficients are determined, the far-field pattern is computed by using eq (C3) in a novel way that takes advantage of the above algorithm and eliminates the need for evaluating any of the vector basis function, the F's of eq (C1). It uses the concept that an ideal dipole at infinity would measure the electric field. So the ideal dipole coefficient is used in eq (C2) to obtain the translated coefficients for an ideal dipole at $A = \infty$. These coefficients are then used in eq (C3) along with the Q's of the AUT obtained from the near-field measurement and calculations. The calculated $B^{\infty}(\chi_0 = 0,\theta_0,\phi_0)$ and $B^{\infty}(\chi_0 = \pi/2,\theta_0,\phi_0)$ are the far electric field components. The evaluation of the summation in eq (C3) employs the efficient Wacker algorithm process for speed and accuracy. Once the far-field has been obtained, gain, pattern, and polarization parameters are easily obtained.

References

[C1] Bruning, J.H.; Lo, Y.T. Multiple scattering of EM waves by spheres. IEEE Trans. Ant. Propagat. AP-19; 1971 May. p. 378-390.

[C2] Jensen, F. Electromagnetic near-field far-field correlations. LD-15. Technical University of Denmark, Lyngby; 1970.

[C3] Wacker, P.F. Non-planar near-field measurements: Spherical scanning. Nat. Bur. Stand. (U.S.) NBSIR 75-809; 1975 June. 69 p.

[C4] Lewis, R.L. The use of three-term recursion relations for numerical computations as applied to near-field spherical scanning. URSI Symposium on Electromagnetic Wave Theory, Stanford, California; 1977. p. 224-226.

[C5] Holm Larsen, F. Improved algorithm for probe-corrected spherical near field far field transformation. Electronic Letters. 15; 1979 September 13. p. 588-589.

NBS-114A (REV. 2-8C)

U.S. DEPT. OF COMM. BIBLIOGRAPHIC DATA SHEET (See instructions)	1. PUBLICATION OR REPORT NO. NBSIR 85-3031	2. Performing Organ. Report No.	3. Publication Date September 1985

4. TITLE AND SUBTITLE

Development of Near-Field Test Procedures for Communication Satellite Antennas Phase I, Part 1

5. AUTHOR(S)

Allen C. Newell and Andrew G. Repjar

6. PERFORMING ORGANIZATION (If joint or other than NBS, see instructions)

NATIONAL BUREAU OF STANDARDS
DEPARTMENT OF COMMERCE
WASHINGTON, D.C. 20234

7. Contract/Grant No.

8. Type of Report & Period Covered

9. SPONSORING ORGANIZATION NAME AND COMPLETE ADDRESS (Street, City, State, ZIP)

10. SUPPLEMENTARY NOTES

☐ Document describes a computer program; SF-185, FIPS Software Summary, is attached.

11. ABSTRACT (A 200-word or less factual summary of most significant information. If document includes a significant bibliography or literature survey, mention it here)

The purpose of this program is to define and further develop the capabilities of near-field antenna test techniques, specifically for the requirements associated with the development and verification testing of reconfigurable, multibeam, frequency reuse, commercial satellite antennas. Phase I, Part 1 gives a general survey, definition, and description of near-field and compact range measurement methods as they apply to satellite antenna systems testing. Each of these methods is evaluated to determine how well they meet the measurement requirements. Included for each technique is a summary of the measurement method, discussions on probe correction and data processing, measurement hardware considerations, a results available section, and measurement accuracy and range certification considerations. The basis for the choice of the best measurement technique is established with the planar near-field measurement method receiving the best score for the directive antennas considered. As a result, further study will focus on this technique and will be reported on subsequently. A detailed presentation of planar near-field measurements theory is presented in Appendix A.

12. KEY WORDS (Six to twelve entries; alphabetical order; capitalize only proper names; and separate key words by semicolons)

antennas; antenna measurements; compact range; cylindrical near-field scanning; near-field measurements; near-field testing; planar near-field scanning; satellite antennas; spherical near-field scanning.

13. AVAILABILITY

☐ Unlimited
☐ For Official Distribution. Do Not Release to NTIS
☐ Order From Superintendent of Documents, U.S. Government Printing Office, Washington, D.C. 20402.
☒ Order From National Technical Information Service (NTIS), Springfield, VA. 22161

14. NO. OF PRINTED PAGES 84

15. Price

☆ U.S. GOVERNMENT PRINTING OFFICE:1985—676-384 / 45009

USCOMM-DC 6043-P80